



Estimating Total Suspended Matter in Turbid River Surface Waters using a WISP-3 Hyperspectral Radiometer and Sentinel-2 Optical Imagery

J.C. Wiggins

Estimating Total Suspended Matter in Turbid River Surface Waters using a WISP-3 Hyperspectral Radiometer and Sentinel-2 Optical Imagery

As part of:

Fostering inclusive growth, health and equity by mainstreaming water quality in River Basin Management in the Brantas River Basin, Indonesia

by

J.C. Wiggins

to obtain the degree of Master of Science
at Delft University of Technology,

To be publicly defended Monday August 17, 2020 at 10 am UTC +2.

Student number: 4262433
Project duration: September 23, 2019 – August 17, 2020

Thesis committee:	Dr. ir. M.W. (Maurits) Ertsen (Chair)	Water Resources Management (TU)
	Dr. ir. W. (Wahyudi) Citrosiswoyo, M.Sc	Ocean Engineering (ITS)
	Dr. ir. T. (Teguh) Hariyanto, M.Sc	Geomatics Engineering (ITS)
	Dr. ir. O. (Olivier) Hoes	Water Resources Management (TU)
	Dr. ir. M. (Marnix) Laanen	Water Insight B.V.
	Dr. S.L.M. (Stef) Lhermitte	Geoscience and Remote Sensing (TU)

An electronic version of this thesis is available at <http://repository.tudelft.nl/>.

Abstract

This research focuses on using Sentinel-2 optical imagery to provide a means of high-resolution monitoring and evaluation of changes in Total Suspended Matter (TSM) concentration in the Brantas river basin. In situ spectral measurements as well as laboratory results show an extremely turbid nature of the Brantas River surface water. Current monitoring of the river water quality, is done by point measurements representing point estimations of the water quality in time and space. Interactions within the system are mostly unknown. Having accurate knowledge of near real time water quality information will greatly enhance the effectiveness of the monitoring organizations, especially if this comes in a high spatial and temporal resolution. The Sentinel- 2 remote sensing platform delivers information which can be used to derive such data with a 10m resolution and revisit time of 5 days. To estimate TSM concentrations a multi-conditional algorithm is developed. It uses linear regression for low to medium TSM concentrations based on the green and red band reflectance values and polynomial regression for high to extremely high TSM concentrations based on the red edge NIR band. Testing the multi-conditional algorithm on the WISP-3 in situ spectral data shows the model's performance is good with $r^2 = 0.79$, RMSE = 66.5 mg/L and NRMSE = 9.7%. Performance of the multi-conditional algorithm is found to be poor when based on Sentinel-2 (S2) bottom of atmosphere data from bands green, red and red edge NIR. However, when recalibrating the polynomial model on Sentinel-2 atmospherically uncorrected top of atmosphere data, results are more promising: $r^2 = 0.75$, RMSE = 64.2 mg/L and NRMSE = 11.3%. Also, TSM estimates from remote sensing reflectances atmospherically corrected by different processors are compared, from which ACOLITE (RMSE = 5.0 mg/L, NRMSE = 25.3%) performs significantly better than C2RCC (RMSE = 11.3 mg/L, NRMSE = 57.5%) and Sen2Cor (RMSE = 42.8 mg/L, NRMSE = 217%). This study shows that 1) high-resolution spatial and temporal variation of TSM concentration estimation can be made visible within the Brantas river basin, 2) an overview of TSM concentration estimation of the entire basin at one moment in time can be achieved and visualised, 3) an extensive historical record of TSM concentration estimations can be accessed, and 4) information is provided to prioritize sampling locations and field surveying times.

Keywords: remote sensing, Total Suspended Matter, WISP-3, Sentinel-2, Brantas river, multi-conditional algorithm, atmospheric correction

This project has received funding from Delft University Fund (grant agreement 2019-060), Sustainable Water Fund (FDW, grand agreement NL-KVK-27378529-FDW16046RI) as well as from the Lamminga Fonds (grant agreement Lamm-19-41-PV).

Table of contents

1 Introduction	7
2 Theoretical background	10
2.1 Surface water quality assessment by optical remote sensing in general	10
2.2 Using optical remote sensing to estimate TSM concentrations	10
2.3 Remote sensing on river corridors	11
2.4 Remote sensing measuring techniques: on site and from space	11
2.4.1 Hyperspectral handheld in situ data	11
2.4.2 Sentinel-2 satellite mission	13
2.4.2.1 Atmospheric correction procedures	13
2.4.2.2 Cloud masking	14
2.4.2.3 Errors introduced in spectral data from satellites	15
2.4.2.4 Google Earth Engine as a remote sensing analysis platform	15
2.5 In situ laboratory TSM measuring techniques	15
2.6 Statistical parameters for performance assessment	15
3 Materials and methods	17
3.1 Study area	17
3.2 Data collection	19
3.2.1 Results overview from fieldwork missions	19
3.2.2 On site historical measurements from external datasets	20
3.2.3 On site and laboratory surface water sampling	20
3.2.3.1 Quality assessment of Standard Laboratory Operating Procedure	20
3.2.4 WISP-3 reflectance data	20
3.2.4.1 Quality assessment of methods with WISP-3 in-situ measurements	21
3.2.5 Hyperspectral satellite images	21
3.2.5.1 Image acquisition	21
3.2.5.2 Quality assessment of Sentinel-2 optical satellite imagery	22
3.2.5.3 Sentinel-2 bands simulated from WISP-3 data	22
3.3 Data processing WISP-3	22
3.3.1 Calibration	22
3.3.2 Stefan Sims' fingerprinting algorithm	22
3.4 Data processing hyperspectral satellite images	22
3.4.1 Atmospheric correction models	22
3.4.1.1 Sen2Cor	23
3.4.1.2 C2RCC	23
3.4.1.3 ACOLITE	23
3.4.1.4 Forcing atmospheric correction	23
3.4.2 Cloud masking of L1C and L2A products	23
3.5 Development of multi-conditional TSM algorithm	23
3.5.1 Basic TSM models tested	24

3.5.2 Algorithm bounds selection	24
3.5.3 Multi-conditional TSM algorithm validation	24
3.5.4 Model and algorithm performance	24
3.6 Development of model based on linear regression of S2 match-ups with historical in situ measurements	25
3.7 Summary of workflow from first idea to end product	26
4 Results	27
4.1 Typical water reflectance spectra	27
4.2 Bio-optical properties of the Brantas River surface water	28
4.3 Relationship between WISP-3 and TSM concentration	31
4.4 Multi-conditional TSM algorithm based on WISP-3 data	34
4.4.1 Switching bounds selection	34
4.4.2 Performance of multi-conditional algorithm	35
4.5 Exploring Sentinel-2 data	37
4.5.1 Atmospheric correction of S2 data	37
4.5.1.1 Match-ups from recent fieldwork missions for atmospheric correction	38
4.5.1.2 Comparing uncorrected and AC model results and performances	38
4.5.1.3 TSM concentration estimates based on AC corrected Rrs values	39
4.5.2 Using uncorrected S2 data for TSM estimations	41
4.5.2.1 Time series spectral information Sentinel-2 bands	41
4.5.2.2 Match-ups between uncorrected S2 data and TSM measurements from historical data in situ measurements	43
4.5.2.3 Algorithm based on S2 atmospherically uncorrected L1C data and historical in situ dataset	47
4.5.2.4 Time series of modelled TSM concentrations using the model based on S2 L1C data	49
4.6 Snapshot of TSM concentration in time for entire river basin	51
4.6.1 Using algorithm based on uncorrected S2 L1C data	52
4.6.2 Using MCA and atmospherically corrected image by ACOLITE	52
4.7 Summary of results	55
5 Discussion	58
6 Conclusions	62
7 Perspectives	64
References	65
Appendix A: Effect of fingerprinting algorithm on WISP-3 in situ spectra	70
Appendix B: Built-in algorithms WISP-3 compared to laboratory results TSM concentrations	71
Appendix C: Comparing results of single and multiple band algorithms based on WISP data and laboratory results	73
Appendix D: Comparing results of single and multiple band algorithms based on Sentinel-2 simulated data and laboratory results	77
Appendix E: Inter-comparison of TSM algorithms based on single and multiple WISP-3 and Sentinel-2 bands	81
Appendix F: Time series spectral information band 7 Sentinel-2 L1C and L2A compared for 59 locations	84

Appendix G: Match-ups S2 B7 data with historical TSM values, investigating reason for noise	87
Appendix H: Whole spectra (all bands) L2A from S2 satellite imagery from all are measurements for all locations	88
Appendix I: Overview of sampling days, region and sampling stations	91
Appendix J: Comparing results of AC models including forced-by-WISP-3 for 24 locations along the Brantas River (S2 image 28-02-2020)	92
Appendix K: Comparing results of AC models including above water spectral measurements by WISP-3 for 9 locations on Waduk Sutami (S2 image 24-03-2020)	94
Appendix L: Overview of 59 investigated locations with water / land pixel indication	95
Appendix M: Comparing TSM in situ measurements with modelled values based on S2 L1C B7 for all 59 locations	98
Appendix N: Data management plan	101

Abbreviations and Definitions

<i>Abbreviation</i>	<i>Explanation</i>
ACOLITE	Atmospheric correction for OLI 'lite'
APHA	American Public Health Association
B3	Sentinel Band 3 (green)
B4	Sentinel Band 4 (red)
B7	Sentinel Band 7 (red edge 3)
BBWS	Brantas Water Resources Management
BOA	Bottom of Atmosphere
BOD	Biochemical oxygen demand
C2RCC	Case 2 Regional Coast Colour
CDOM	Colored dissolved organic matter
Chl-a	Chlorophyll a
COD	Chemical oxygen demand
DO	Dissolved oxygen
EC	Electrical conductivity
Ecoton	Non governmental organization working on biodiversity and sustainability
EPA	Environmental Provincial Agency East Java
ESA	European Space Agency
GEE	Google Earth Engine
GIS	Geographic Information System
iCOR	Image correction for atmospheric effects
ISO	International Organization for Standardization
ITS	Sepuluh Nopember Institute of Technology
kd	Light attenuation
MCA	Multi-conditional algorithm
MSG	Monosodium glutamate
MSI	Multi Spectral Imager
NIR	Near infrared
OLI	Operational Land Imager, satellite by the Ball Aerospace & Technologies Corporation
PJT-I	Perum Jasa Tirta I, Agency for Brantas and Bengawan Solo River Basins
Polymer	Polynomial-based algorithm applied to MERIS
RBINS	Royal Belgian Institute of Natural Sciences
S2	Sentinel-2 satellite mission
S2A	Sentinel-2 satellite A
S2B	Sentinel-2 satellite B
Sen2Cor	Sentinel 2 Correction
SNAP	Sentinel Application Platform
SNI	Indonesian National Standard
SWIR	Shortwave infrared
SWQP	Surface water quality parameter
SWT	Surface water temperature
TOA	Top of Atmosphere
TSM	Total Suspended Matter
TSS	Total Suspended Solids
TU	Turbidity
TU	Delft University of Technology
WISP-3	Water Insight handheld spectrometer
WQ	Water quality

1

Introduction

Immediate action is needed to improve - or at least stop further degradation of - the water quality of the Brantas river. It has deteriorated over the past decades (Roosmini et al. 2018; Fulazzaky 2009), as it has in several other river basins in Indonesia. This research focuses on using Sentinel-2 optical imagery to provide a means of high-resolution monitoring of changes in Total Suspended Matter concentration. It is a way of evaluating optical surface water quality parameters within the Brantas project. This project is titled “Fostering inclusive growth, health and equity by mainstreaming water quality in River Basin Management” and has started in 2018. Its aim is to make water quality an integral part of water management in the Brantas catchment. The overall goal is to significantly improve water quality, in such a way that chances of exposure to water-borne diseases are reduced and the river can function as a sustainable source of water again (Ertsen et al. 2018). Pollution comes from multiple sources (e.g. industry such as sugar cane, food seasoning MSG, textile and paper factories, urban raw sewage, domestic waste, agriculture). This increased export of inorganic nutrients can cause several negative environmental impacts, such as loss of habitat and biodiversity (Rabalais 2002). Also, an increase of phytoplankton blooms can result in hypoxia and increased fish mortality (Diaz and Rosenberg 2008; Turner et al. 2003). Problems with dumping of waste in the Brantas River have been reported too, ranging from household waste, such as diapers (Suhanti, n.d.), to industrial waste such as bags full of aluminium ash (Bruijns 2018).

Monitoring of the river water quality is currently done by point measurements representing point estimations of the water quality in time and space. Sampling of the whole river takes several days to weeks. Therefore, no accurate image can be obtained of the river system as a whole, and obtaining spatial and temporal variations of river water quality is almost impossible (Jerry C. Ritchie, Zimba, and Everitt 2003). How do tributaries influence the main river? How do water quality parameters influence each other? Interactions within the system are basically unknown. Also, stakeholders need to be able to identify polluters, especially when tasked with enforcing the law. Having accurate knowledge of near real time water quality information would greatly enhance the effectiveness of the organizations, especially if this comes in a high spatial and temporal resolution. Information derived from satellite missions can provide this information. It is a potentially advantageous method for cheaper, continuous measurements, with an ability to estimate SWQPs without being physically present.

Since the early 1970s, it has been successfully proven that optical remote sensing can be used to derive concentrations from water quality parameters by measuring the light reflected by the water. This makes the technique suitable for estimating optical surface water quality parameters (SWQPs). However, these techniques are mostly applied on considerably large water bodies like oceans, large, inland lakes and broad rivers. The current status of the use of optical remote sensing shows that water quality estimates from remote sensing are well established in estuarine and coastal zones (Brando and Dekker 2003; Chen, Hu, and Muller-Karger 2007; Hellweger et al. 2004), but less well developed in river systems (Tomsett and Leyland 2019). This research will study if these methods can also be applied on a river system like the Brantas. However, using optical remote sensing data in river corridors, introduces specific problems due to their optical complexity. Generally speaking, the use of optical remote sensing for small water bodies

comes down to a trade-off between high-resolution data and availability of (narrow) hyperspectral bands. The widths of rivers examined in this study vary from 20 - 160 meters (with exception of the Waduk Sutami reservoir, which gets as wide as up to 800 m). Therefore, the Sentinel- 2 platform is chosen as a data source, delivering data with 10m resolution (only pixels consisting of pure water can be used).

The ultimate goal of this study is to find out if continuous water quality monitoring of a narrow river flowing through a large area (e.g. the whole Brantas River basin) at once is possible by remote sensing, and if so, if it can reveal spatial and temporal information at high resolution. If water quality changes over time can then be mapped continuously, as to fill the gaps from point measurements as they are conducted now, valuable information is added in a higher temporal and spatial resolution than is possible at present.

For the Brantas river system, the most important water quality parameters are DO, BOD₅ and COD. These water quality parameters, however, are lacking a distinctive optical signal. Nonetheless, concentrations of non-optical variables may be correlated with optical variables such as Chl-a concentrations, TU, TSM, CDOM and SWT, which do affect the reflected radiation (Kallio 2000; Abayazid, El-Adawy, and Others 2019; El Din and Zhang 2017). To limit the scope of this study as to make it actually feasible, it will only look at TSM concentrations. So, in other words, at first the water quality parameter variable with the easiest detectable optical signature is investigated. Since a range of low to extremely high turbidity levels can be expected to be found in the Brantas river system, a multi-conditional algorithm is developed, able to incorporate different TSM models, combining each model's sensitivity characteristics and which can be individually tuned for specific ranges.

To estimate TSM concentrations, this study will focus on:

1. Developing a reliable multi-conditional algorithm based on single and multiple band models, using linear and polynomial relationships, or a combination of both;
2. Validating results from satellite imagery by data from a hyperspectral handheld radiometer, which in turn is validated by in situ laboratory measurements, all together resulting in a spectral fingerprint of the Brantas river;
3. Creating and analyzing modelled time series (2015-2020) of TSM concentrations for nearly 60 locations along the Brantas River.

The algorithm developed during this study finds its usability in accurately estimating TSM concentrations in river systems, which is important for ecosystem studies and sediment transport monitoring. The method used can be adopted to also derive algorithms for other water quality parameters. Summarizing, the main topic is estimating TSM concentrations by means of optical remote sensed satellite imagery. This report shows how a regionally calibrated multi-conditional algorithm can be developed, which uses data and methods publicly available.

Following this introduction, this thesis continues with a theoretical background providing information to understand methods and instruments used. It is divided in two main parts: remote sensing and in situ measuring techniques. This chapter focuses on the relation between surface water quality and remote sensed images, and the use of optical imagery and the need of atmospheric corrections. The part on in situ measuring techniques explains the theory of the equipment used.

The materials and methods chapter shows and explains the by this study followed procedures. Also, data processing techniques and steps are explained. How are objectives fulfilled and how will the research questions be answered? The chapter is finalized with a workflow diagram. For developing TSM models, the specific steps are explained showing how to get to a multi-conditional algorithm. Also, the boundary selection method is shown.

The results chapter shows the results of applying the described methods on both own in situ data, collected during fieldwork missions in Indonesia, and historical data from project stakeholders. Results are discussed, after a brief introduction on typical water reflectance spectra observed in the Brantas river system. This chapter, in combination with the discussion chapter, forms the heart of the report, since all results are visualised, reviewed, compared and discussed. The report ends with conclusions and perspectives on further research on optical and non-optical SWQPs. Also, perspectives for stakeholders and the Brantas project as a whole are shown.

2

Theoretical background

This chapter will provide a brief overview of the theoretical knowledge needed to be able to understand the relations and models used. Principles are explained of remote sensing technologies for water quality assessment, how this works for TSM concentration estimation and how spectral data is derived for in situ reflectance measurements. Also, how measurements are performed from space, including atmospheric correction procedures, are briefly discussed.

2.1 Surface water quality assessment by optical remote sensing in general

Water quality assessment is the process of measuring chemical, physical and biological characteristics of surface water and identifying the possible contamination sources affecting the water quality (Usali and Ismail 2010). Development of remote sensing techniques for monitoring water quality began in the early 1970s and are now widely used to monitor water quality parameters such as suspended sediments, chlorophyll, temperature, which all have a distinct optical signal, changing the energy spectra of reflected solar or thermal radiation (Jerry C. Ritchie, Zimba, and Everitt 2003). Most other chemicals and bio-physical constituents do not directly affect or change the spectral or thermal properties of surface waters. They can only be inferred indirectly from measurements of other water quality parameters, which are affected by these constituents.

Sensors mounted on satellites can measure the radiation reflected from the water surface, at various wavelengths. Absorption and backscattering characteristics of surface water can be significantly influenced by substances in the water (Jerlov 1976; Kirk 1983). Thereby, remote sensing has the ability to measure changes in spectral signals backscattered from water. Measured changes are expressed in water quality parameters by means of empirical or analytical models. The optimal wavelength to be used depends on the substance measured, as well as on the concentration of the substance measured. Furthermore, the optimal wavelength to be used also depends on sensor characteristics.

2.2 Using optical remote sensing to estimate TSM concentrations

Early techniques measured spectral and thermal differences in emitted energy from water surfaces. First empirical approaches to estimate suspended sediments were developed by Ritchie et al. (1975). Many researchers now use the visible and near infrared bands in their investigations to obtain robust models between water leaving reflectances and TSM concentrations (Jerry C. Ritchie, Zimba, and Everitt 2003; Shafique et al. 2003; Jerry C. Ritchie, Cooper, and Schiebe 1990; J. C. Ritchie and Cooper 1991; F. Wang et al. 2006). Nowadays, TSM is among the most commonly measured water quality parameters which are estimated by use of remote sensing (Onderka 2008; Sudheer, Chaubey, and Garg 2006; Wu 2003; Bhatti et al. 2008).

TSM concentrations are best estimated using wavelengths between 700 and 800 nm (Oxford 1976). However, optimum wavelength to be used differs depending on the TSM concentration itself (Curran and E. M. M. Novo 1988). Early research (Jerry C. Ritchie, Cooper, and Schiebe 1990; J. C. Ritchie and Cooper 1991) already shows that if the range of suspended sediment is roughly between 0 and 50 mg/L

reflectance from almost every wavelength will be linearly related to suspended sediment concentrations. For higher concentrations, saturation effects have been observed when computing the TSM concentration, especially for lower wavelengths. That is why a multi-conditional approach is found best to derive an algorithm being able to estimate concentrations from low to high concentrations. Approach followed is demonstrated by Novoa et al (2017). It uses a switching method that automatically selects the most sensitive TSM vs. water leaving reflectance relationship to always use the most sensitive wavelength information with the strongest relationship, avoiding the earlier mentioned saturation effect.

2.3 Remote sensing on river corridors

Using optical remote sensing data in river corridors, introduces specific problems due to their optical complexity. Optical absorption and backscattering results in high optical variability. The effect of the atmosphere on the signal received by satellite sensors is significant, especially in the lower (blue/green) wavelengths. In order to retrieve useful water leaving reflectances, accurate modelling of atmospheric absorption and scattering effects as well as specular water surface reflection effects is required (Gao et al. 2009). Further challenges in estimating water leaving reflectances at the surface are indicated as follows, and in accordance with Moses et al. (2017):

1. The proximity to terrestrial sources of atmospheric pollution will result in an optically heterogeneous atmosphere that is difficult to model;
2. The adjacency effects from neighbouring land pixels around the water body adds unwanted signal; and
3. The significantly large reflectance of water in the near-infrared region due to high sediment concentrations, as often is seen in inland turbid waters, prevents the use of atmospheric correction models which are widely available but adopted for either land surfaces or oceans.

2.4 Remote sensing measuring techniques: on site and from space

This study uses two types of remotely sensed data: 1) in situ spectral measurements from the handheld radiometer WISP-3 and 2) from the Sentinel-2 satellite mission platform. This section briefly explains how each type of data is obtained.

2.4.1 Hyperspectral handheld in situ data

The handheld hyperspectral radiometer WISP3 is used for collecting subsurface irradiance reflectance values $R(0-)$ to assess the water colour and derive water quality parameters. To derive $R(0-)$ values, information of three measurements is combined. Light penetrates the water surface. A part is absorbed and a part is reflected by particles in the water, which in the end define the water colour. The water colour is determined by measuring three channels:

- a. Downwelling irradiance E_d ($\text{mW}/(\text{m}^2 * \text{nm})$)
- b. Downwelling radiance L_d ($\text{mW}/(\text{m}^2 * \text{nm} * \text{sr})$)
- c. Upwelling radiance L_u ($\text{mW}/(\text{m}^2 * \text{nm} * \text{sr})$)

Spectral irradiance is the irradiance of a surface per unit wavelength, and is measured in (milli)watts per square metre per nanometre. Spectral radiance is the radiance of a surface per unit wavelength. These are directional quantities measured in (milli)watt per steradian per square metre per nanometre.

L_u includes all light leaving the water (water leaving radiance L_w) as well as sky light reflected at the water surface. L_d is the downwelling radiance and E_d consists of the downwelling irradiance that is incident on the water surface. The WISP-3 is equipped with three single radiometers, measuring E_d , L_d and L_u at 401 bands (400 – 800 nm), shown in detail in figure 1. From measuring E_d , L_d and L_w , the reflectance $R(0-)$ and Remote sensing reflectance values R_{rs} can be calculated. The reflectance is a ratio between downwelling and upwelling light. It therefore shows how much of the incoming sunlight is left after travelling through the water. R_{rs} is calculated as follows:

$$R_{rs} = \frac{L_u - \rho * L_d}{E_d}$$

With:

ρ = sky correction, the radiance of skylight at zenith angle of 42°
 $\rho \approx 0.028$ (Mobley 1999)

The reflectance $R(0-)$ is calculated as follows:

$$R(0-) = R_{rs} * Q * \frac{n^2}{1-r_0}$$

With:

$Q = \text{PI}$

r_0 = the Fresnel coefficient for 0-degree angle of incidence

$r_0 = 0.021$

n = the index of refraction

$n = 1.341$ for ocean waters and 1.333 for freshwaters (Dekker and Peters 1993)

This study deals with fresh water so: $\frac{n^2}{1-r_0} = 1.81$

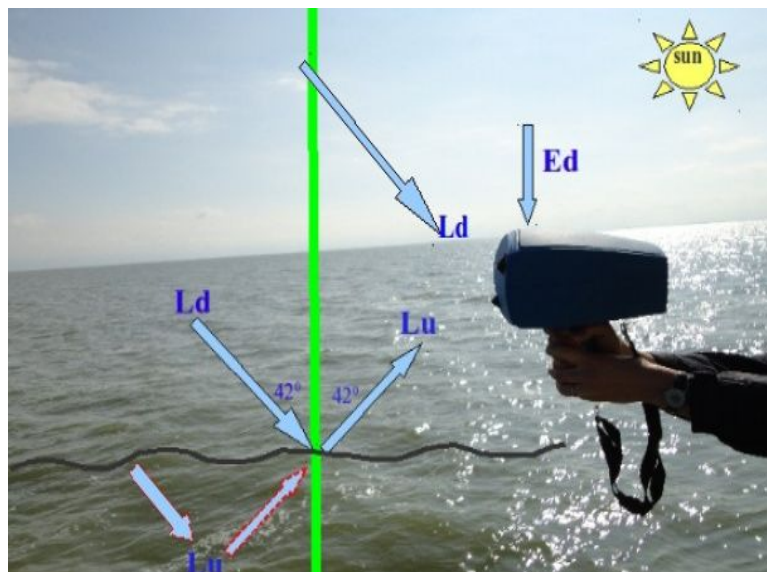


Figure 1: Schematic overview of three separate above surface spectra of sky and water used to derive $R(0-)$ water leaving reflectance (Peters and Laanen, n.d.).

When comparing the spectra for quality checking, the irradiance (E_d) should always have the highest values of the three separate spectra. The downwelling radiance (L_d) is a fraction of E_d and should therefore be significantly lower (approximately a factor 10). However, both E_d and L_d measure the sky, and therefore the spectral shapes should be following the same pattern. The downwelling radiance L_u should be much lower than L_d . If there is a high sediment load, factors with a negative influence on the measurement may be at play. This can be bottom visibility, macrophytes, floating plants, garbage or

inappropriate measuring angles. The prominent dip near 765 nm results from atmospheric conditions: this dip is caused by oxygen in the atmosphere. The peak at 763 nm is caused by absorption of O₂. In general, the region around 760 - 770 nm is highly influenced by interference from the atmosphere, there is a lot happening at the same time. Therefore, I will focus on the section beyond the atmospheric absorption dip of 770 nm. At all times absorption dips which can be seen on all channels should be avoided.

2.4.2 Sentinel-2 satellite mission

The European Space Agency introduces its Sentinel-2 mission as follows (European Space Agency n.d.): “The Copernicus Sentinel-2 mission comprises a constellation of two polar-orbiting satellites placed in the same sun-synchronous orbit, phased at 180° to each other. It aims at monitoring variability in land surface conditions, and its wide swath width (290 km) and high revisit time (10 days at the equator with one satellite, and 5 days with 2 satellites under cloud-free conditions) will support monitoring of Earth's surface changes.” Though originally developed for monitoring land surfaces, it has proven its usability for analysing water surfaces, too. Table 1 shows an overview over spatial resolutions, band number, central wavelengths and band widths.

Table 1: *Wavelengths and bandwidths of the 3 spatial resolutions of the MSI instruments*

Spatial Resolution (m)	Band Number	S2A		S2B	
		Central Wavelength (nm)	Bandwidth (nm)	Central Wavelength (nm)	Bandwidth (nm)
10	2	492.4	66	442.2	21
	3	559.8	36	559.0	36
	4	664.6	31	664.9	31
	8	832.8	106	832.9	106
20	5	704.1	15	703.8	16
	6	740.5	15	739.1	15
	7	782.8	20	779.7	20
	8a	864.7	21	864.0	22
	11	1613.7	91	1610.4	94
	12	2202.4	175	2185.7	185
60	1	442.7	21	442.2	21
	9	945.1	20	943.2	21
	10	1373.5	31	1376.9	30

The majority of studies on TSM concentrations tends to use relatively coarse (250 m) MODIS data focussing on large, well-gauged rivers such as the Yangtze (J-J Wang and Lu 2010), the Amazon (Mangiarotti et al. 2013; Santos et al. 2018), the Changjiang (Liu et al. 2006) and the Solimoes (Espinoza-Villar et al. 2018). Medium resolution images (20–30 m) are used to investigate TSM concentrations e.g. where the Mississippi and Missouri rivers meet (Umar, Rhoads, and Greenberg 2018) and in the Yangtze (Jian-Jun Wang et al. 2009). Because of the very nature of the Brantas river system with typical river widths of only 30 - 100 m the use of Sentinel-2 answers the need of high-resolution data with resolution in the visible light and NIR bands of 10 m and red edge NIR band of 20 m.

2.4.2.1 Atmospheric correction procedures

Atmospheric interference is significantly large over water bodies. From the signal measured by satellites over inland water, about 90 percent stems from atmospheric contribution (Pereira-Sandoval et al. 2019). This is caused by atmospheric haze which scatters light, especially in the lower (blue, green) wavelengths. Interferences increase as reflected radiance from water decreases, meaning water with high clarity or high

algae concentrations are most affected (Gholizadeh, Melesse, and Reddi 2016). Proper atmospheric correction procedures play an important role when estimating water quality from water leaving reflectance values, especially if they are based on single or multiple relations using bands from the visible light spectrum (Filipponi 2018). Over an open ocean, atmospheric interference can be fairly easily corrected by assuming that the water leaving radiance in the NIR is equal to zero. When this assumption holds, an algorithm based on a relatively simple dark-pixel correction can be performed. Over inland and coastal waters, this assumption does not hold due to the fact that the water-leaving radiance in the NIR is greater than zero. Presence of water components like sediments and dissolved organic particles are mostly responsible for this signal.

AC of S2 data can be done by the Sentinel-2 Level-2A Prototype Processor, which is labelled Sen2Cor for Sentinel 2 (atmospheric) Correction. From the Sen2Cor Configuration and User Manual ("Sen2Cor Configuration and User Manual" 2017):

"Sen2Cor performs a pre-processing of Level-1C (L1C) Top of Atmosphere (TOA) image data, and applies a scene classification and atmospheric correction and a subsequent conversion into an ortho-image Level-2A Bottom-Of-Atmosphere (BOA) reflectance product. Outputs are an Aerosol Optical Thickness (AOT) map, a Water Vapour (WV) map and a Scene Classification map together with Quality Indicators data."

The S2 MSI mission was not designed for aquatic remote sensing, therefore also the Sen2Cor is not designed for water bodies. Sen2Cor is based on the dark dense vegetation approach (Kaufman and Sendra 1988). This approach assumes that vegetation is sufficiently dark. Also, it is assumed that the ratio between BOA at different wavelengths is constant. To be used successfully, this algorithm requires some pixels to correspond to dense dark vegetation (Ouaidrari and Vermote 1999).

Another available AC model is provided by the ACOLITE algorithm, initially developed to perform AC over water from Landsat-8 OLI optical multispectral data. It has been extended for the use on S2 data. ACOLITE bundles the atmospheric correction algorithms and processing software developed at RBINS for aquatic applications of Landsat (5/7/8) and Sentinel-2 (A/B) satellite data and several other metre scale satellites such as Pléiades-1 A/B, SPOT 6/7, RapidEye, PlanetScope, and WorldView-2 imagery. ACOLITE performs both the atmospheric correction and can output several parameters derived from water reflectances. ACOLITE is based upon the Dark Spectrum Fitting (DSF) atmospheric correction algorithms for aquatic applications. The method is based on the fact that meter scale satellites have a relatively narrow swath, therefore assuming the atmosphere is homogeneous over a (sub)scene. By this assumption, the atmospheric path reflectance can be estimated from multiple targets in the same scene. These targets are selected based upon the lowest TOA reflectances in all bands. This is a fundamentally different approach compared to other water-focused AC models, which use predefined "dark" bands (oftentimes being the NIR and SWIR). The ACOLITE algorithm automatically finds the best band, yielding in the lowest atmospheric path (Vanhellemont and Ruddick 2018).

Also, the Case-2 Regions CoastColour (C2RCC) algorithm (Brockmann et al. 2016) can be used for AC. It relies on a large database derived from in situ measurements of radiative transfer simulations inverted by neural networks. Besides the aforementioned atmospheric correction algorithms for the Sentinel-2A MSI also iCOR, l2gen and Polymer are publicly available. Research shows that most AC models show high uncertainties, in many cases >100% and sometimes up to >1000% (Warren et al. 2019). In this study, the uncorrected images (L1C) will be compared between the S2 standard Sen2Cor (L2A) and the most promising AC models for aquatic applications, being ACOLITE and C2RCC (Pereira-Sandoval et al. 2019).

2.4.2.2 Cloud masking

Classification of clouds, cirrus, snow, shadows and clear sky areas is an important step in the pre-processing of optical remote sensing images (Hollstein et al. 2016) and crucial when using remote sensed images for retrieval of surface reflectance values (Hagolle et al. 2010; Muller-Wilm et al. 2013)

The correct retrieval of surface reflection values becomes impossible for optically thick clouds and pixels affected by cirrus. Shadows of clouds must be treated as individual cases for a physically correct retrieval of surface reflectance values (Hollstein et al. 2016).

2.4.2.3 Errors introduced in spectral data from satellites

Sun-glint can significantly affect S2 MSI data at specific viewing azimuth angles, especially when approaching the summer solstice (Filipponi 2018). Another effect which might introduce errors can be caused by the adjacency effect: influence on measured pixel reflectance values by the reflectance of adjacent pixels. Literature shows that target pixels which are darker than the background, become brighter but also cases are observed where it is the other way around: target pixels, which are brighter than the background, become darker. Adjacency effects start playing a role within high spectral resolutions with resolutions higher than 1000 m (Ma Jianwen et al. 2006).

2.4.2.4 Google Earth Engine as a remote sensing analysis platform

When using the vast amount of data provided by satellite missions one can choose one out of two options: either bring the data to your algorithm (i.e. manipulating data locally, offline) or bring the algorithm to the data (i.e. data processing in the cloud, and by doing so making use of the joint processing speed of the available servers). The Google Earth Engine (GEE) will be used for S2 data processing of this study, in conjunction with ESA's Sentinel Application Platform (SNAP) software. GEE contains servers with petabytes of satellite imagery available at high performance computation speed (Gorelick et al. 2017). SNAP will be used for processing and evaluating results from 3 types of atmospheric correction procedures: 1) forced atmospheric correction, 2) ACOLITE and C2RCC. ArcMap 10.7.1 will be used for building maps showing spatial distribution of model estimated TSM concentrations in the Brantas river basin.

2.5 In situ laboratory TSM measuring techniques

The determination of laboratory values for Total Suspended Matter is done by taking a well-mixed, measured volume of a water sample and filtering it through a pre-weighed glass fiber filter. The filter is heated to constant mass at $104 \pm 1^\circ \text{C}$ and then weighed. The mass increase divided by the water volume filtered is equal to the TSM in mg/L. This method is suitable for the determination of solids in potable and surface waters as well as wastewaters with TSM concentrations of up to 20,000 mg/L.

2.6 Statistical parameters for performance assessment

The performance of each model is assessed using the coefficient of determination r^2 , the root mean square error (RMSE in mg/L) and the normalized root mean square percentage error (NRMSPE also in %). The NRMSPE is added to intercompare performance of different models, or models based on a different dataset.

R^2 is the proportion of the variance in the dependent variable (TSM concentration) that is predictable from the independent variable (Rrs). R^2 provides a measure of how well the observed outcomes are mimicked by the model, based on the proportion of total variation of outcomes explained by the model.

RMSE is a widely used standard way to measure the error of a model in predicting quantitative data. The error is expressed in measured units and by this it is a suitable way of evaluating the usefulness and accuracy of a model. It can be used to compare errors of different models for the same dataset and not between datasets, since it is scale-dependent. RMSE is the square root of the average of the squared errors. By this, the effect of each error on the RMSE is proportional to the size of the squared error. This means larger errors have a disproportionately large effect on RMSE, so it is sensitive to outliers. RMSE is calculated as follows:

$$RMSE [mg/L] = \sqrt{\frac{\sum_{i=1}^n (\hat{y}_i - y_i)^2}{n}}$$

$\hat{y}_1, \hat{y}_2, \dots, \hat{y}_n$ are predicted values

y_1, y_2, \dots, y_n are observed values

n is the number of observations

As the last statistical parameter used in this study, NRMSE is added for assessment of model performance. NRMSE also expresses the magnitude of the error in relation to the actual values, but since it's normalized for the dataset, values can be compared between models, based on different datasets. NRMSE is calculated as follows:

$$NRMSE [\%] = \frac{\sqrt{\frac{\sum_{i=1}^n (y_i - y_j)^2}{n}}}{y_{max} - y_{min}} * 100$$

y_{max} is the maximum observed value

y_{min} is the minimum observed value

3

Materials and methods

The goal of this chapter is to show the methodology used, starting with taking initial measurements until finishing with a multi-conditional algorithm to derive TSM concentrations from optical remote sensed data. The chapter starts with defining the study area, followed by how data is collected and processed. Quality assessment of collected data is explained along the way. Then, model development is explained. The chapter ends with showing a workflow diagram summarizing all of the above.

3.1 Study area

Choosing the Brantas basin as a case follows from its importance: the Brantas River is East Java's longest river. It flows 260 km from its spring at Mt. Arjuno to the point where it branches into two rivers, the Surabaya River and the Porong River. The Surabaya River (40 km) splits into the Mas River and Jagir River, just before it enters the inner part of Surabaya City. Porong (53 km), Mas and Jagir River (both approximately 14 km long) all drain into the Madura Strait. Approximately 30 million people live in the Brantas River watershed (PJT-I Public Corporation 2005).

The Brantas River basin is subdivided in an upper, middle and lower part. The upper part flows through a reservoir, named Waduk Sutami. WISP-3 measurements and water samples for lab analysis are taken along the whole stretch of the river, from source to sea, although most measurements are taken downstream of Waduk Sutami. See figure 2 on the next page for an overview of the Brantas Basin.

Through 35 organizations (PJT-I Public Corporation 2003) that play a role in water resources development and management of the Brantas River, a long time series with a vast amount of data is available on approximately 8 different rivers in or near the Brantas river basin. This study will focus on the Brantas river, Surabaya River and Porong River, as depicted in figure 2.

To increase the chances of finding significant differences in measured water leaving reflectances, sample sites are identified where the most extreme possible differences in DO, BOD, COD and TSM are known to be measured in the past or at least are expected to occur on a very short distance from one another. Also, sampling sites are chosen to represent the whole river stretch with associated distinctive water quality: fairly clean water upstream, more contaminated water at the start of the industrial area and severely contaminated water downstream in the heavily populated metropolitan area just before discharging into the Madura Strait. These sampling sites are shown in figure 3 below. More detailed information on locations is given in the next section on data collection.

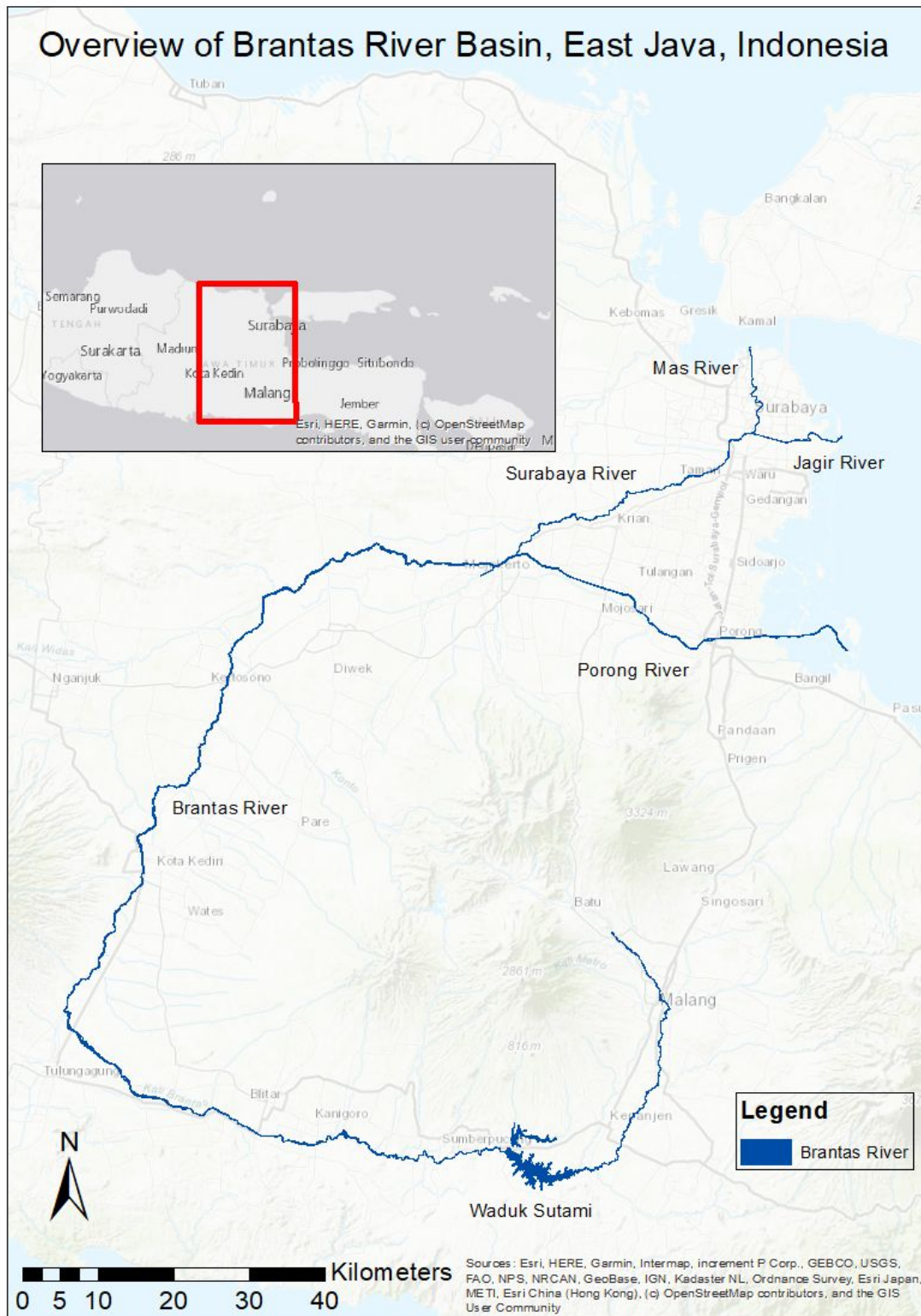


Figure 2: Overview of Brantas River and all its branches. Fieldwork sample sites are located along all branches, from source to sea. Individual sampling sites are shown in figure 3.

3.2 Data collection

This section first shows a general overview of fieldwork missions and their data production. After, explanations can be found about databases encompassing on site historical measurements, in situ laboratory and spectral measurements and an explanation about retrieval of hyperspectral satellite data.

3.2.1 Results overview from fieldwork missions

1. In total 14 sampling campaigns have been carried out between December 2019 and March 2020, with a duration of 1 or 2 days each.
2. In total 285 WISP-3 measurements are taken. In most cases, 3-5 measurements are taken at the same sampling site, within one minute. Sometimes the measuring angle to the sun was slightly altered. This was done to be able to later select the best measurements with the least noise.
3. In total a combination of 27 WISP-3 measurements and results from laboratory analysis passed the quality check and can be used for regression analysis (match-ups WISP-3 and laboratory data).
4. Satellite images of only 2 days during the sampling period have a cloud percentage < 20 %. Because of the high percentage of small cloud patches, for every image all locations are examined separately, instead of choosing images on total cloud cover percentage.

During the course of this study, and especially during fieldwork campaigns, close cooperation with PJT-1, EPA and BBWS resulted in successfully collecting and analysing water samples. I joined them on their regular sampling campaigns, and in between I organised my own. Figure 3 shows an overview of all locations with match-ups of WISP-3 and laboratory measurements. From these 12 locations, a total of 27 measurements can be used for linear and logarithmic regression.

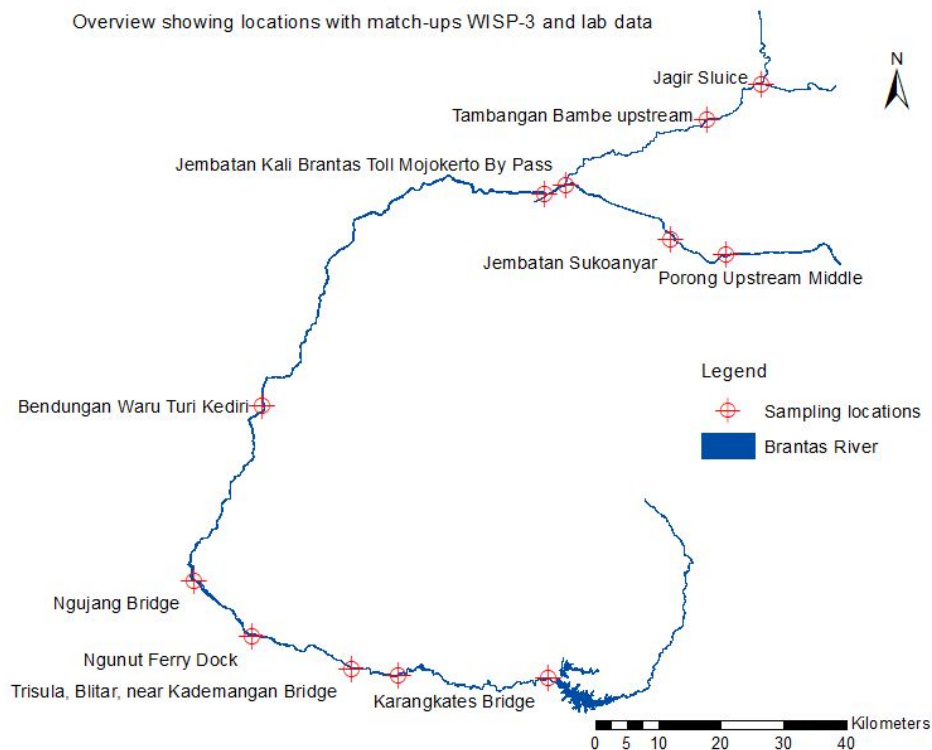


Figure 3: Overview showing locations with match-ups of WISP-3 and laboratory measurements

3.2.2 On site historical measurements from external datasets

Regular water quality monitoring activities in the Brantas basin are performed by 3 organizations:

1. Brantas Water Resources Management Organization (BBWS),
2. Environmental Provincial Agency East Java (EPA) and
3. Perum Jasa Tirta-1, Agency for Brantas and Bengawan Solo River Basins (PJT-1).

Generally speaking, BBWS, EPA and PJT-1 measure pH, DO, TDS, temperature and conductivity on-site while all other variables (approximately 35 more) are measured in the laboratory. Databases were provided for use in this study by PJT-1 (2019), EPA (2015-2018) and BBWS (2016-2020). Unfortunately, the BBWS data came without exact measuring dates and therefore are excluded from further analysis.

3.2.3 On site and laboratory surface water sampling

Since the initial set-up of this study was broader, also investigating other water quality parameters, during all fieldwork campaigns DO and temperature measurements were done by myself on site with an AZ 8403 Portable Digital Dissolved Oxygen DO Tester. Samples from the lake are taken in an upstream, middle and downstream part, each time at 3 different depths (0.3m, 5m and 10m). Water samples from the river are taken at three spots at every cross section: at 25%, 50% and 75% of the width from the water surface. Water samples at all sampling locations are taken by means of 'hand-grab' method and are taken from the top water layer, usually the top 20 cm of the water.

Choices of sample sites are greatly based upon data from PJT-I and upon information provided by Ecoton, BBWS and EPA. To obtain in situ data, the following points were considered:

- I. Sampling in cooperation with PJT-I, EPA and BBWS was done in accordance with their existing fieldwork sampling schedule. Measurements from the handheld WISP-3 are collected in order to correlate in situ spectral with traditional measurements. To be able to correlate data from these sample sites with satellite imagery from the nearest cloudfree overpasses, fieldwork campaigns are planned as much as possible on actual days with a S2 satellite overpass. Per cross section 3 samples are taken: 25%, 50% and 75% of the river width. This is done to be able to determine the variation of water quality parameters over the width, possibly estimating the adjacency effect. Samples with the spectrometer will be taken at the exact same spots as the samples for lab analysis.
- II. Generally, sample sites are chosen in such a way that the chances are biggest to encounter water with the widest range possible in measured values for SWQPs. This is done in order to calibrate the model for a range as wide as possible.
- III. Apart from joining aforementioned organizations on their fieldwork missions, own missions were conducted in order to get an evenly distributed network of sampling locations for the entire basin.

3.2.3.1 Quality assessment of Standard Laboratory Operating Procedure

The EPA uses standardized protocols (i.e. SNI, APHA) to measure each water quality variable in their own laboratory. PJT-1 uses its own laboratories in Malang and Mojokerto. The PJT-1 water quality laboratory management is ISO-certified. BBWS collects water samples and has them analysed at the laboratories of PJT-1.

Water samples taken by myself when conducting fieldwork measurements alone were analysed at the laboratory of the Environmental Engineering Department of ITS (Sepuluh Nopember Institute of Technology). These samples were analyzed using a gravimetric method following an unknown protocol.

3.2.4 WISP-3 reflectance data

After taking WISP-3 measurements, they are uploaded onto a platform provided by Water Insight BV, called WISPweb. Here, metadata is added for every single measurement. On WISPweb, measurements can

be searched, filtered and compared. It is a very useful tool to investigate individual above water spectra for quality assessment. Also basic, visual analysis of the water colour can be performed and spurious measurements can be easily flagged out.

3.2.4.1 Quality assessment of methods with WISP-3 in-situ measurements

From the WISP-3 User Guide (Peters and Laanen, n.d.):

“The WISP3 uses a unique configuration of fiber optics. To validate this approach, WISP3 measurements were compared against other non handheld or mounted spectroradiometers and laboratory concentrations.” The WISP-3 is also calibrated against a NIST (National Institute of Standards Technology) traceable light source.

The handheld WISP-3 radiometer averages 15 automated samples each time the button is pushed. For this study 3 to 5 manually induced measurements (of 15 samples each) per sampling station were performed, in order to do a quality control check on those sets of measurements. Average values of those sets of measurements are used, except when 1 out of all manually induced measurements was more than 20% off (that measurement then was neglected).

The water leaving reflectance $R(0^-)$ is a ratio and should therefore never be lower than 0 or higher than 1. Values higher than 1 should be flagged and not used. High reflectance values can be caused by sun glint or mirror-like reflection of the water surface. Most of the impact from sun glint is seen in the blue-green bands, although sometimes it affects the whole spectrum (higher reflectance / more noise overall).

To validate the estimated TSM concentrations from spectral images derived from the WISP-3 measurements, in situ data from the laboratory is used.

3.2.5 Hyperspectral satellite images

3.2.5.1 Image acquisition

The Sentinel-2 mission consists of two satellites 2A and 2B in a sun-synchronous orbit and is originally taken into operation and is optimized for (monitoring of) land surface conditions. Over the years, it has proven its value for water quality monitoring though. It is used in this research because its products are freely available and because of the high-resolution of the images in the visible and near infrared domain, as shown in table 2.

Table 2: Overview of Sentinel-2 bands in the visible and NIR domain

Sentinel-2 band	Band name	Central wavelength [nm]	Resolution [m]
Band 2	Blue	492	10
Band 3	Green	559	10
Band 4	Red	665	10
Band 5	Red edge 1	704	20
Band 6	Red edge 2	741	20
Band 7	Red edge 3	783	20
Band 8	NIR	833	10

For comparison, results of water sample analysis are taken as often as possible within 2 hours before and after satellite overpass. Individual S2 images are downloaded from the Copernicus Open Access Hub. For each match up with laboratory samples, the atmospherically corrected bottom of atmosphere (level 2A) product as well as the atmospherically uncorrected top of atmosphere product (level 1C) is downloaded for further analysis. Bulk data acquisition of S2 data is done through the GEE platform.

3.2.5.2 Quality assessment of Sentinel-2 optical satellite imagery

A first, visual inspection is undertaken by analyzing the RGB color composite image of the remotely sensed data. Thereby, images with sun glint and cloud cover can be easily identified and manually taken out of the dataset. Also, to check if derived reflectance values actually stem from water pixels and not spurious or land pixels, spectra are plotted containing all bands. In this way a check is possible to see if the typical water signal can be deduced.

3.2.5.3 Sentinel-2 bands simulated from WISP-3 data

The high-resolution WISP-3 data is used to calculate Sentinel-2 output on bands 1 to 7 (averages are taken over from WISP-3 data over the bandwidth of Sentinel-2 bands). In this way, accurate Sentinel-2 like data is produced, without errors introduced by atmospheric correction procedures.

3.3 Data processing WISP-3

This section describes the calibration and fingerprinting procedures to achieve high quality hyperspectral WISP-3 data.

3.3.1 Calibration

During transportation of the WISP-3 to Indonesia, one out of two shock indicators went off. It was decided to use the equipment nonetheless, with possible need of calibration afterwards. First analysis of the results showed indeed unrealistically high water leaving reflectances. After receipt of the WISP-3 by Water Insight, it was at once re-calibrated. The WISP-3 was checked against 4 other WISP-3's (including the Gold Standard WISP-3) and it turned out that the water leaving and sky radiance L_d and L_u channels were way off. The orientation of the lenses were affected severely. E_d measurement values were not affected. After re-calibrations, resulting $R(0-)$ were now between 0 and 1, as expected. The shapes of the spectra are maintained throughout the recalibration process, the numbers are normalized.

The WISP-3 provides values for L_w , L_d and E_d at 401 bands. Also, subsurface irradiance reflectance values $R(0-)$ are directly calculated and provided, using a constant value for ρ (sky correction).

3.3.2 Stefan Sims' fingerprinting algorithm

Because of the extremely high turbidity levels encountered, sun glint seemed to be a problem in a substantial part of the measurements. It was decided to correct for this sun glint by using the fingerprinting algorithm developed by Simis and Olsson (2013). This algorithm optimizes the sky correction factor ρ depending on features specific to each measurement. Optimization of ρ is done based on identification of atmospheric absorption features that are present in the upwelling and downwelling radiance received by the sensors. The algorithm provides a unique value of ρ for each measurement. With optimized ρ values - unique for every measurement - the $R(0-)$ and R_{rs} values showed overall slightly lower values. See [Appendix A](#) for an overview of the effect of fingerprinting on the spectra of 27 selected matched-up measurements.

3.4 Data processing hyperspectral satellite images

This section shows a short overview of the atmospheric correction models used, of how atmospheric correction of a L1C S2 image is forced by a ground control point and how clouds are masked before using S2 images for analysis.

3.4.1 Atmospheric correction models

For this study, L1C uncorrected data and atmospherically corrected data by Sen2Cor, C2RCC and ACOLITE algorithms are used. All these processors are, all in their own way and with different levels of accuracy,

able to correct for the effect of the aerosol contributions. For each AC model the followed procedures are outlined in the subparagraphs below, along with parameter values used (if applicable).

3.4.1.1 Sen2Cor

Since March 23, 2016 Sentinel-2 L1C data has been available in Google Earth Engine. On March 27, 2019 also S2 L2A was added to the GEE catalog. This creates possibilities to process images in bulk for whole time series. Sen2Cor data was computed and released from late 2018 onwards by ESA. All Sen2Cor processing has been done on Google's servers, in the cloud on.

3.4.1.2 C2RCC

To be able to process L1C images into C2RCC and ACOLITE corrected images, downloaded copies of L1C images are necessary. Therefore, L1C is collected from The Copernicus Open Access Hub and processed using a built-in feature of SNAP to achieve C2RCC corrected images. SNAP can also be used for reading the output files and for extracting specific pixel values corresponding to in situ sampling stations. To use the C2RCC algorithm, first the whole scene has to be resampled to the same resolution (10m is chosen, corresponding to the resolution of band 2, 3, 4 and 8). For the C2RCC processor, the valid pixel expression is changed from $B8 > 0 \ \&\& \ B8 < 0.1$ to $B8 > 0 \ \&\& \ B8 < 0.3$, to avoid masking out of large parts of the Brantas river. The temperature is adjusted to reflect the yearly mean river water temperature of 28 °C (standard is 15 °C). Also, the option is checked to 'Output AC reflectances as Rrs instead of Rhow', as to achieve values which can be compared directly without any conversions to outcomes of other AC models.

3.4.1.3 ACOLITE

ACOLITE can be run using a graphical user interface (GUI) or a command-line interface (CLI). The GUI offers only limited configuration (limited file input/output, settings, output parameters and loading/saving of settings files). Therefore this study uses the CLI mode to make full use of the models capabilities. The specific aquatic related parameters are set to `l2w_parameters = Rrs_*,spm_nechad2016,chl_re_moses3b74`, the standard `l2w_mask_threshold = 0.0215` is set to `l2w_mask = False` to avoid any unwanted masking out of narrow river segments. Due to the high sediment loads, NIR bands give high reflectance values making water pixels susceptible for being masked out. The output is stored as a .nc (netCDF) file and can be opened, read and manipulated in SNAP.

3.4.1.4 Forcing atmospheric correction

To use forced atmospheric correction on a S2 image, a calibrated WISP measurement from WISPweb is used as a ground control point. First, from the WISP data, the remote sensing reflectance (R_{rs}) is calculated. Next, the top-of-atmosphere reflectance data from the satellite are retrieved. Now using the pin manager within the SNAP environment, precise pixel values can be obtained for the exact location where the WISP measurement was taken. From here, the reflected light which is assumed to be due to the atmosphere can be calculated, as the difference between the WISP measurement and the TOA value of the pixel. The satellite TOA data for S2 is already converted to irradiance reflectance. What is derived from the WISP data is radiance reflectance, so there is just a factor PI difference between WISP and satellite units. Now, as a last step, the by WISP-data forced atmospherically corrected data for the whole image can be calculated using the band-math tool of SNAP. A more detailed approach can be found in the manual on forced AC by Peters and Laanen (n.d.).

3.4.2 Cloud masking of L1C and L2A products

To detect clouds, cirrus, cloud shadows and water pixels in the Sentinel-2 MSI images, decision trees as well as the classical Bayesian approach are used, as provided by Hollstein et al. (2016). The method was adapted to be used in GEE by Rodrigo E. Principe and made open source in geetools.

3.5 Development of multi-conditional TSM algorithm

This section describes the method followed to develop the multi-conditional TSM algorithm.

3.5.1 Basic TSM models tested

First, the built-in WISP-3 models are mimicked, according to algorithms developed by Rijkeboer (2000). This is done to see how well the different models perform and to see if they can be used and tuned to local circumstances. Results are shown in [Appendix B](#). The built-in algorithms are considered suitable for a range of moderately to highly turbid waters. In this case however, investigated water bodies turned out to be extremely turbid, which resulted in the WISP-3 algorithm reaching its maximum detection limit. This led to significant underestimation of TSM concentrations. Secondly, basic, well known and well defined TSM models were tested. The 7 bands in the visible spectrum of the Sentinel-2 (based on WISP-3 averages) are related to results of laboratory measurements. Simple and multiple linear regression is performed to test 1 band and 2 band combination algorithms. The end result is a 1 and a 2 parameter empirical algorithm based on single bands or band combinations of bands 1 to 7 tuned to local circumstances, calibrated on high-resolution WISP-3 data. The same approach has been followed using the original WISP-3 high-resolution data, resulting in empirical algorithms based on single bands or band combinations of the 401 bands (400 – 800 nm). All results are shown in [Appendix C](#) based on individual WISP-3 bands and in [Appendix D](#) for the S2 simulated bands. [Appendix E](#) shows an inter-comparison of TSM algorithms based on single and multiple WISP-3 and S2 bands. Derived algorithms either perform moderately over the whole range of TSM concentrations, or only well on small, specific ranges. Therefore, these results are not considered satisfactory. The development of a multi-conditional TSM algorithm will combine the models, each performing best within their own range.

Development of the multi-conditional TSM algorithm is based on linear relations for low to medium TSM concentrations, based on reflectances in the green and red band. For high to extremely high TSM concentrations, a polynomial relationship in the red edge NIR band is used. For each of the three to be used, separate TSM models, the dataset is split in 60% for calibration and 40% for validation part. By taking these steps, the method developed by Novoa et al (2017) is roughly followed.

3.5.2 Algorithm bounds selection

The switching reflectance $R(0^-)$ values can be best selected based on the saturation behaviour of the most sensitive band(s). The selection is done by comparing the in situ $R(0^-)$ reflectance values of the green vs red band and the red vs NIR band. The data points are modelled using a logarithmic regression curve. This curve starts linearly and bends at the point where the saturation of the most sensitive bands starts occurring (although it plots as a straight line on a logarithmic scale). The actual value of this saturation point is computed where the first derivative of the regression curve equals 1 (slope = 1). This is the point between a horizontal (complete saturation) and vertical line.

3.5.3 Multi-conditional TSM algorithm validation

Validation of the performance of the multi-conditional algorithm based on WISP-3 data is done by the 40% data saved for validation. Validation of the performance of the multi-conditional algorithm based on S2 data is done by comparing historical data provided by PJT-1 and EPA with modelled values.

3.5.4 Model and algorithm performance

The statistical parameters used to describe the models performances r^2 , RMSE, and NRMSE are calculated using the Python (Notebook) code as shown in figure 4.

```

import numpy as np
import pandas as pd
import re
import math
from sklearn.metrics import r2_score, mean_squared_error

#Define Epsilon
EPSILON = 1e-10

#Define functions to calculate specified parameters
def _error(actual: np.ndarray, predicted: np.ndarray):
    """ Simple error """
    return actual - predicted

def _percentage_error(actual: np.ndarray, predicted: np.ndarray):
    """
    Percentage error
    Note: result is NOT multiplied by 100
    """
    return _error(actual, predicted) / (actual + EPSILON)

def mse(actual: np.ndarray, predicted: np.ndarray):
    """ Mean Squared Error """
    return np.mean(np.square(_error(actual, predicted)))

def rmse(actual: np.ndarray, predicted: np.ndarray):
    """ Root Mean Squared Error """
    return np.sqrt(mse(actual, predicted))

def rmspe(actual: np.ndarray, predicted: np.ndarray):
    """
    Root Mean Squared Percentage Error
    Note: result is NOT multiplied by 100
    """
    return np.sqrt(np.mean(np.square(_percentage_error(actual, predicted))))

def nrmse(actual: np.ndarray, predicted: np.ndarray):
    """ Normalized Root Mean Squared Error """
    return rmse(actual, predicted) / (actual.max() - actual.min())

#Calculate specified parameters
r2_score(actual, predicted)
rmse(actual, predicted)
rmspe(actual, predicted)*100
nrmse(actual, predicted)*100

```

Figure 4: *The statistical parameters used to describe the models performances R2, RMSE, and NRMSE and how they are calculated using the following Python (Notebook)*

3.6 Development of model based on linear regression of S2 match-ups with historical in situ measurements

The by this study developed MCA can be used on S2 derived remote sensing reflectances, given an accurate estimation of reflectance values by a valid atmospheric model. For time series analysis this means processing over 290 S2 L1C products (2015 - 2020) into AC corrected images. By doing so, pixel values can be extracted for match-up with the in situ historical TSM dataset. Each run takes approximately 50 min (ACOLITE) until 8 hours (C2RCC). Executing this proposed method exceeds available computational power and time given this study, if doing this for all available images. Therefore, only L1C (2015-2020) and L2A (2018-2020) are available for bulk processing. Since reflectance values in L1C (RMSPE 320%) and L2A (RMSPE 211%) are so far off from actual values (compared to WISP-3 measurements), predicted values from S2 cannot be used as input for the MCA developed by this study. What can be, and is done, however is matching the historical dataset with TSM values from the Brantas project stakeholders with the S2 L1C dataset 2015-2020. Based on this new dataset with 42 matched values, logarithmic regression can be performed to derive an algorithm for calculating TSM concentrations

based on Rrs from S2. Since only band 7 can be used, the method followed is a simplified version of the one used to develop the MCA.

3.7 Summary of workflow from first idea to end product

Figure 5 shows a flowchart with an overview of all general process steps to take by this study, as a summary of this chapter. To estimate TSM concentrations a multi-conditional algorithm is developed using linear regression for low to medium TSM concentrations based on green en red band reflectance values and polynomial regression for high to extremely high TSM concentrations based on the red edge NIR band.

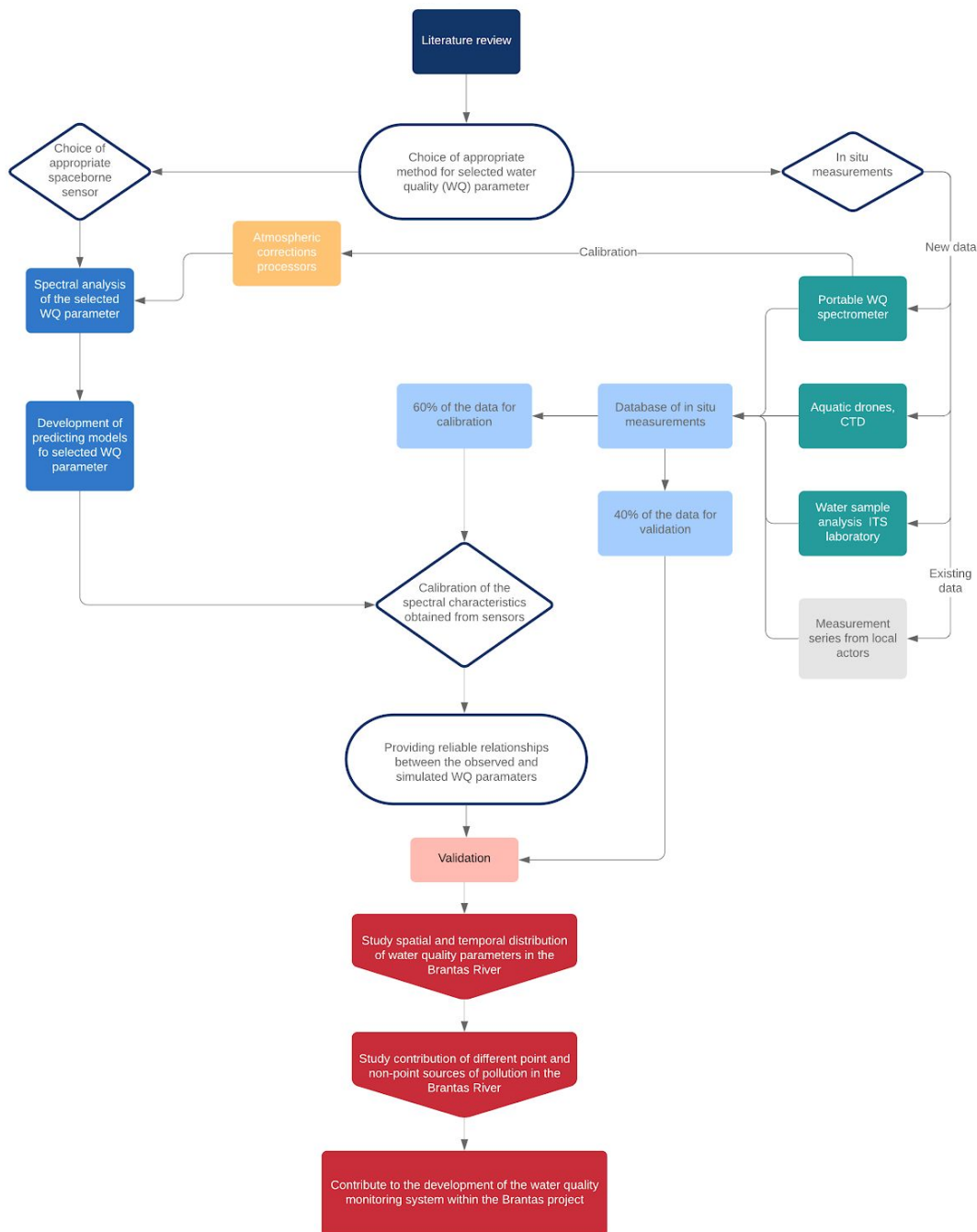


Figure 5: The flow chart shows an overview of all general process steps to take in this study. It is adopted and modified from Gholizadeh et al. (2016).

4

Results

In this section, results are shown - and briefly discussed - starting from scratch. Starting with analyzing in situ hyperspectral radiometer measurements until lastly applying the multi-conditional algorithm on satellite data, in various ways. First, some typical water reflectance spectra are shown, as well as a description of bio-optical properties of the Brantas River system as measured during the fieldwork campaigns. Relationships between spectra and TSM concentrations are shown, modelled and used to build the multi-conditional algorithm. After, the algorithm is tested on Sentinel-2 data to check how well the model(s) perform(s).

4.1 Typical water reflectance spectra

Development of the multi-conditional algorithm is based on the database of WISP-3 subsurface irradiance reflectance values $R(0-)$ from 27 measurements corresponding to laboratory analysis, from samples collected between December 2019 and March 2020. Figure 6 shows some typical spectra, after re-calibration and fingerprinting following the method described by Simis and Olsson (2013). Rapidly increasing values for $R(0-)$ for low concentrations of TSM (7 - 65 mg/L) are observed in the range of 400-600 nm. From figure 6 it becomes apparent that the reflectance in the red band is more sensitive than the reflectance in the green band to TSM concentration changes between 35 - 132 mg/L. Sensitivity for low TSM concentrations in the NIR band are low, but rapidly increase for concentrations higher than 65 mg/L, and for extreme high concentrations it is the most sensitive band.

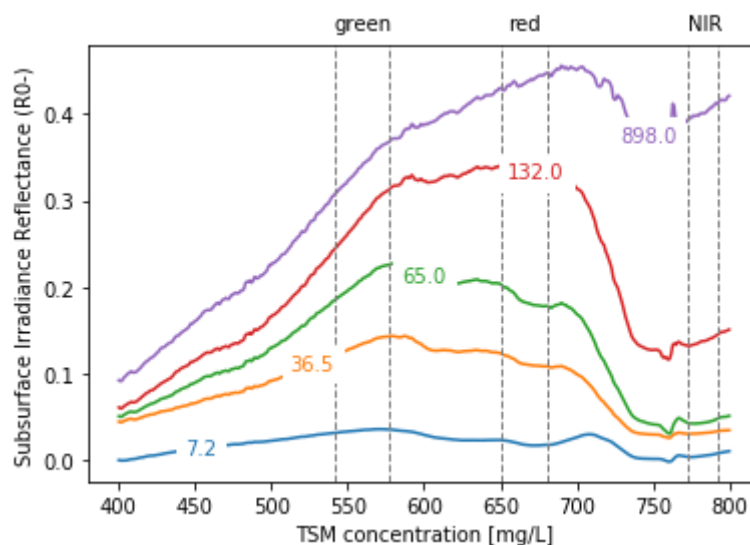


Figure 6: Selected subsurface irradiance reflectance values $R(0-)$ for different TSM concentrations (mg/L) measured in the Brantas River. Vertical lines depict the green (541-577 nm), red (650-681 nm) and NIR red-edge (773-793 nm) bands of the Sentinel-2 satellite mission sensors.

The overview of selected reflectance spectra in figure 6 also shows the extremely turbid nature of the Brantas River surface water. High turbidity levels are easily recognized by the typical tail signature (high reflectance values > 750 nm). Most measurements show spectra with a tail similar to the 898 mg/L example from figure 6.

Figure 7 shows generally increasing TSM concentrations when following the river downstream. The high peak at Mojokerto 11 BUP is caused by inflow of a tributary. So, the river behaves in this respect as expected, showing increasing TSM concentrations from increasing run off, tributaries and increasing urbanization along the river stretch. Figure 7 shows combined data from December 2019 and March 2020 and therefore does not show any detailed information on the river system, other than showing a clear, general pattern.

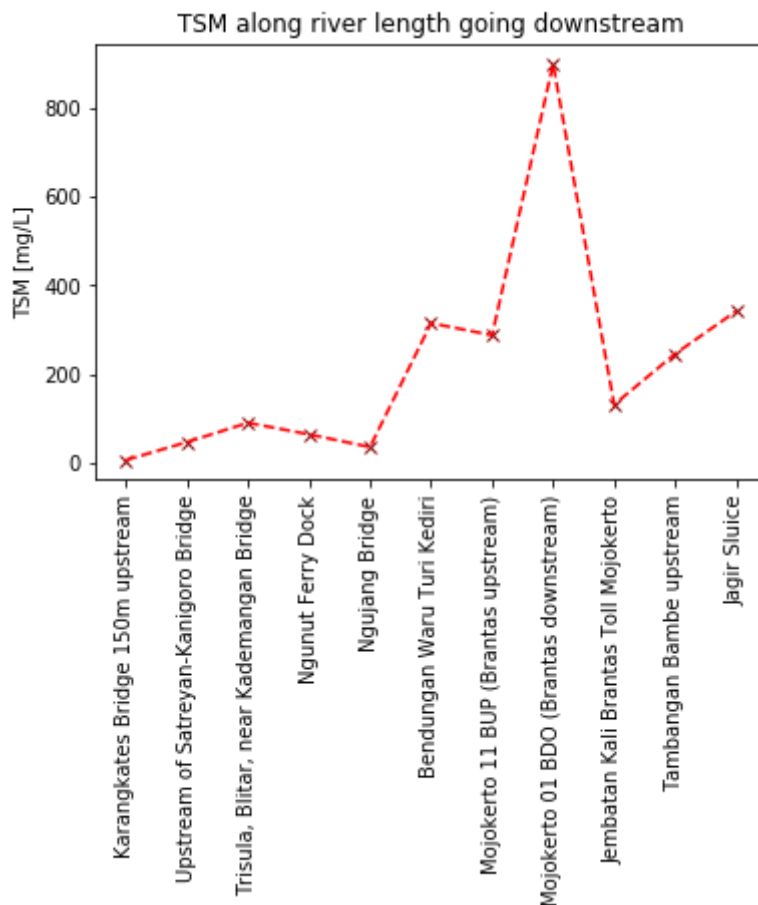


Figure 7: TSM concentrations as measured by laboratory going downstream from left to right, in the period between December 2019 and March 2020. As expected, in general, TSM concentration increases when going downstream. The high peak at Mojokerto 11 BUP is caused by inflow of a tributary.

4.2 Bio-optical properties of the Brantas River surface water

All measurements considered in this research are taken downstream of the reservoir Waduk Sutami. All measurements downstream of Kediri (lets say, halfway) show high reflectance values for all bands >750 nm: the distinctive signal for extremely turbid water. Most measurements also seem to have surface reflectance added to the signal. This fits the turbid profile, since high turbidity levels results in less absorption, which was already recognized by Oxford (1976). An increased backscatter effect in the

direction of the incident light source is observed, which is characteristic for extremely high turbidity samples. In most measurements, no clear signature of Chl-a or CDOM was detected. Turbidity dominates most of the spectra, all the time.

Some measurements of the more upstream area of the river system show a peak around ~700 nm, which is interesting. Literature indicates this peak to be related with an increase of Chl-a concentration that displaces the peak position in the NIR part. This is typically observed in highly turbid or productive water bodies (Z. Wang et al. 2017). Some spectra show a slight dip for phycocyanin absorption at 620 nm. It must be noted these observations only hold for the measurement period of this research: December 2019 - March 2020. Details of spectra of three measurements are shown below, to demonstrate the highly variable nature of the river system and to show some interesting features.

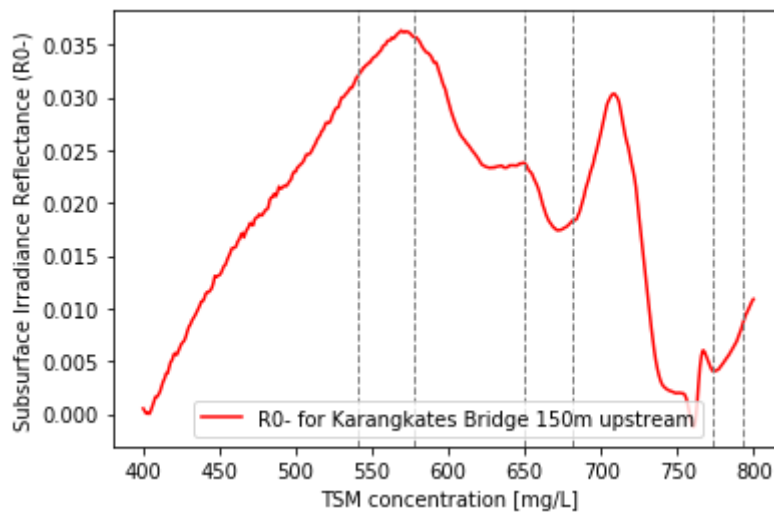


Figure 8: WISP-3 subsurface irradiance reflectance for sample location 150m upstream of Kranagkates Bridge, in the upstream region, just 1.5 km downstream of the Waduk Sutami dam. Corresponding laboratory measurement shows a TSM concentration of 7.2 mg/L.

Figure 8 shows $R(0-)$ for a location near Karangates Bridge in the upstream part of the middle section of the Brantas River, about 11 km upstream of Blitar, just 1.5 km downstream of the Waduk Sutami dam. The right bank is sparsely populated, the left bank mostly agriculture lands. Fairly clear water is observed (the clearest of the whole dataset). As is often the case for inland lakes and waters, the middle part of the reflectance is pronounced. Since this is the region for green light, it indicates the presence of algae. Chl-a typically has a high absorption at 665 nm and fluorescence emission at 710 nm, which both can clearly be seen here. The spectrum in figure 8 shows a slight dip for phycocyanin absorption at 620 nm. Also, the mean specific phytoplankton absorption coefficient at 676 nm is visible. Bottom visibility at this particular location is confirmed by the elevated signal >750 nm where no high sediment load is observed, also a peak could be expected at 810 nm (from benthic plant for example). The associated light attenuation $K_d = 2.4$ corresponds with a Secchi disk depth of 0.47m, which would have been the water depth approximately.

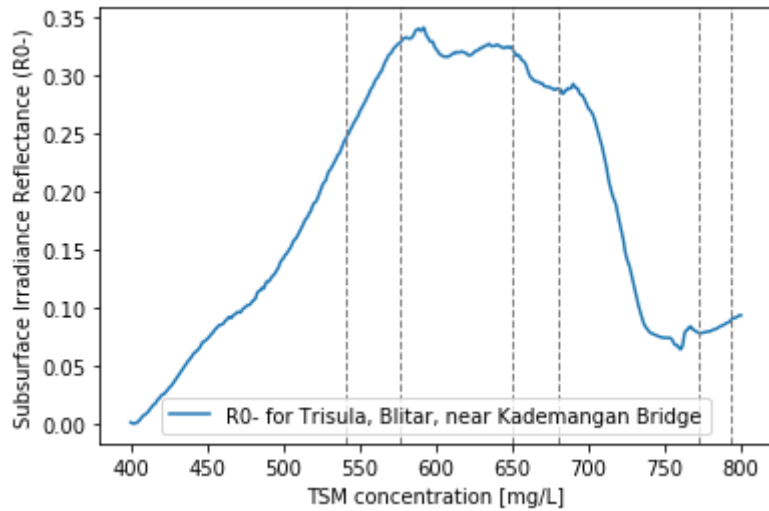


Figure 9: WISP-3 subsurface irradiance reflectance for sample location in Trisula, Blitar, in the upstream region. Corresponding laboratory measurement shows 91 mg/L TSM.

Figure 9 shows $R(0-)$ for a location near a populated area in the upstream part of the middle section of the Brantas River. It is located roughly 13 km downstream of the Waduk Sutami dam (reservoir). The signature shows a peak for sediment load around 650 nm. The prominent dip near 765 nm results from atmospheric conditions: this dip is caused by oxygen in the atmosphere. This sample is pronounced especially in the green and red part of the spectrum. This water appears brown-reddish, due to the high sediment load.

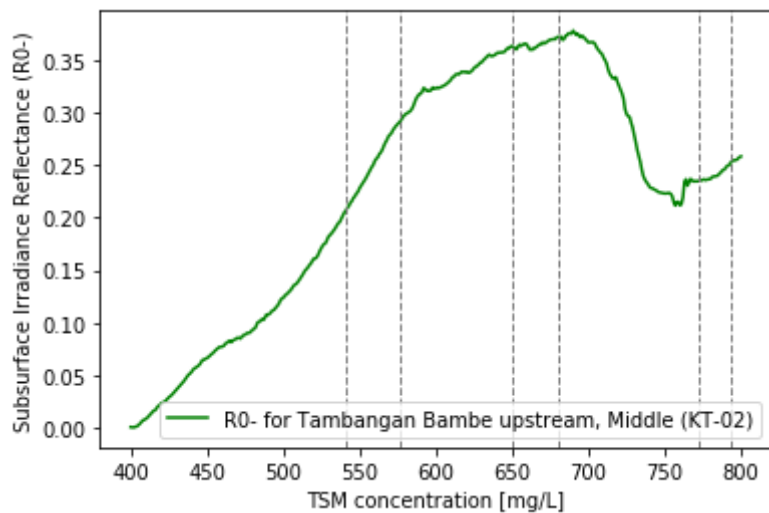


Figure 10: WISP-3 subsurface irradiance reflectance for sample location in Wringinanom, in the downstream, industrialized region of the Brantas River. Corresponding laboratory measurement shows a TSM concentration of 238 mg/L.

Figure 10 shows $R(0-)$ values for a location at Tambangan Wringinanom (a ferry service near ECOTON office, taken on 08-02-2020). Here in the lower part of the Brantas river, the river is named Surabaya river. The location is still 28 km upstream of Surabaya city, but already in a heavily populated area and in the important industrial district of Gresik. This spectrum shows high overall reflectance >750 nm: indicating very turbid water. The effect of surface reflectance added to the signal is probably also present.

The peak around 700 nm could be due to highly turbid water or productive waters with an increase in Chl-a displacing the peak position from 710 to 700 nm (Z. Wang et al. 2017).

4.3 Relationship between WISP-3 and TSM concentration

So, now a general understanding of the bio-optical properties of the river system have been established, we can focus on WISP-3 spectra versus TSM concentration solely, to derive relationships for developing an algorithm to estimate these TSM concentrations. The figures below show relationships of TSM concentrations and the R(0-) reflectances in bands green, red and NIR (respectively S2 band 2, 3 and the red edge band 7). The values used are derived from the high-resolution WISP-3 measurements and averaged for the respective total band widths of the corresponding Sentinel-2 bands. This is done because in the end the goal is to use Sentinel-2 remote sensed data to estimate TSM concentrations. By doing so, a realistic estimate is made for values in the S2 bands. The next paragraphs and accompanying figures show the relationship between reflectances and TSM concentrations of the bands 2, 3 and 7.

Figure 11 emphasises a linear relationship between the green band and TSM concentration < 30 mg/L. The linear correlation is good ($r^2 = 0.91$, RMSE = 5.3 mg/L and NRMSE = 13.2%). It can be clearly seen that the signal gets saturated quickly, for TSM concentration of above 30 mg/L the signal already gets scattered. Figure 12 shows a similar pattern for the red band, which saturates at higher TSM concentrations. Above 150 mg/L the signal is 100% saturated, but scattering already starts at around 80 mg/L. Also here a good linear fit can be achieved for lower concentrations ($r^2 = 0.92$, RMSE = 12.6 mg/L and NRMSE = 10.1%). Early research (Jerry C. Ritchie, Cooper, and Schiebe 1990; J. C. Ritchie and Cooper 1991) already shows that if the range of suspended sediment is roughly between 0 and 50 mg/L reflectance from almost every wavelength will be linearly related to suspended sediment concentrations. This research however shows the linear relationship holds for even slightly higher concentrations of TSM.

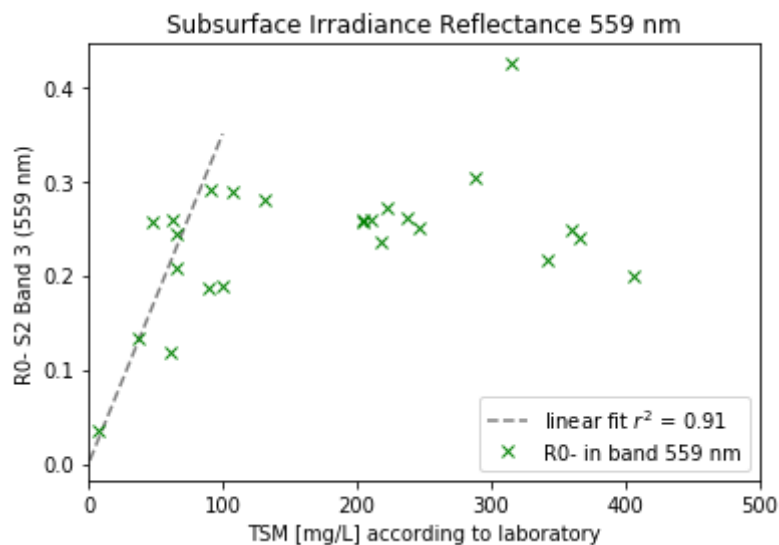


Figure 11: Scatter plot showing comparison between TSM concentration and reflectance values in S2 green band (B3, central wavelength 559 nm). It can be clearly seen that the signal gets scattered for concentrations > 30 mg/L and is fully saturated for TSM concentrations > 100 mg/L.

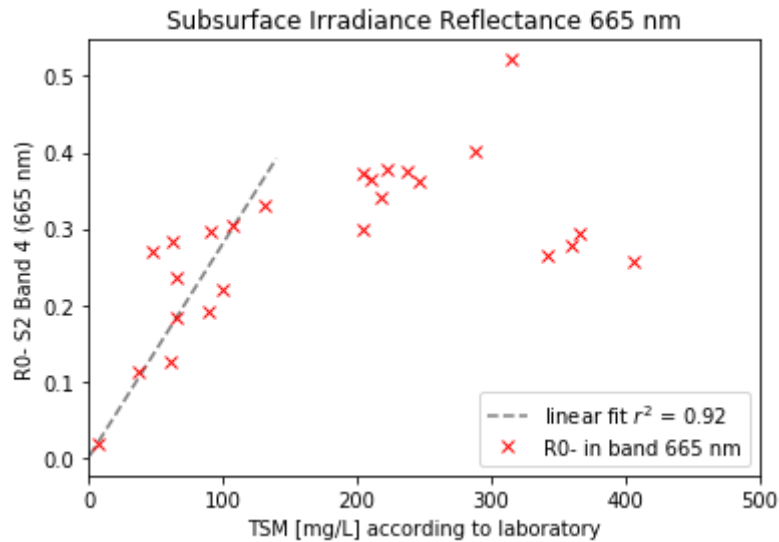


Figure 12: Scatter plot showing comparison between TSM concentration and reflectance values in the S2 red band (B4, central wavelength 559 nm). The relationship follows a similar pattern as the green band, at different concentrations: the signal gets scattered for concentrations > 80 mg/L and is fully saturated for TSM concentrations > 150 mg/L.

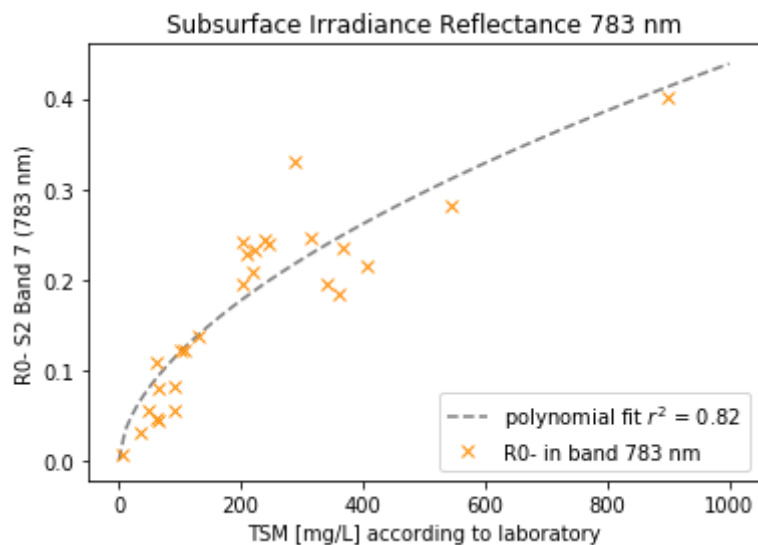


Figure 13: Scatter plot showing comparison between TSM concentration and reflectance values in the S2 red-edge band (B7, central wavelength 783 nm). The relationship follows a different pattern than the green and red band, without saturation for higher TSM concentration.

As TSM concentrations increase, a curvilinear relationship is observed. This is demonstrated by figure 13 with a very good polynomial fit for higher TSM concentrations, without any signs of saturation. The polynomial fit is reasonably well with $r^2 = 0.82$, RMSE = 58.3 mg/L and NRMSE = 7.9%. This behaviour was also already recognized by Ritchie et al. (1990) and Ritchie and Cooper (1991) and recently confirmed by Nova et al. (2017). Figure 14 shows similar increase in reflectance values for the green and red band, and a clearly sharper increase of both the green and red band compared to the red edge NIR band. This proves the higher sensitivity in the green and red band for lower TSM concentrations, compared to the NIR band.

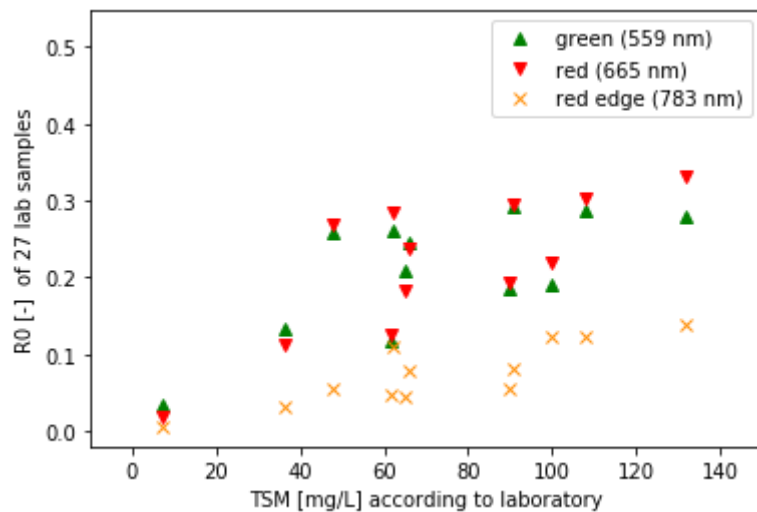


Figure 14: *in situ* reflectances $R(0)$ for TSM concentrations until 140 mg/L, showing similar sensitivity in the green and red band, and a clearly lower sensitivity for the red edge NIR band.

All the above is summarized in figure 15 below. The green band really shows full saturation, the red band nearly full and the NIR band shows a continuing relationship for high TSM values. The flattening of the curves combined with different sensitivity of the available bands to changing TSM concentrations, is best utilized in a multi-conditional approach for developing an algorithm to estimate TSM concentrations.

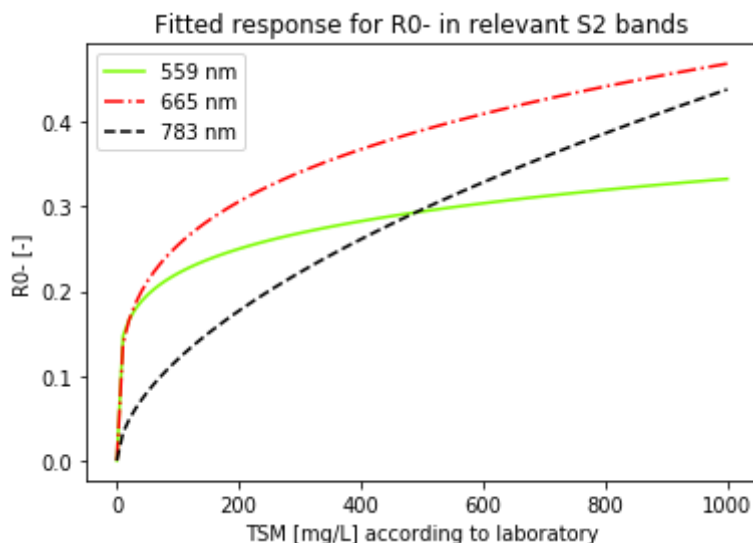


Figure 15: *the good linear relationship for low TSM concentrations but flattening of the curves in the green and red band for higher TSM concentrations suggest to use a multi-conditional algorithm development approach, where the green and red band are best used for lower TSM concentrations and the NIR band can be used for high TSM values, following the still clearly visible relationship at high TSM concentrations.*

4.4 Multi-conditional TSM algorithm based on WISP-3 data

The goal is to develop an algorithm to estimate TSM concentration from water leaving reflectance values. The first two paragraphs have pointed out that low TSM concentrations are best estimated using the green band linear relation, moderate TSM concentrations by the red band linear relation and high and extremely high values by the polynomial relationship in the NIR band. These characteristics are best modelled using a multi-conditional algorithm. For this, separate models will be used as described above. When to switch from one model to the next is based on the saturation of the most sensitive band. So, now the values for the switching bounds for switching from one model to the next have to be determined. The next paragraph shows how these bounds are calculated.

4.4.1 Switching bounds selection

The switching reflectance $R(0-)$ values are selected based on the saturation behaviour of the most sensitive bands. The selection is done by comparing the in situ $R(0-)$ reflectance values of the green vs red band and the red vs NIR band. The data points are modelled using a logarithmic regression curve. Figure 16 shows the scatterplot for the green band vs red band. We earlier already saw (figure 14) that sensitivity for the green and red band are almost similar (green band slightly more sensitive than the red band), which is proven by what we see in figure 16 (the points almost plot a straight line). This is not in line with results found by Novoa et al. (2017), which showed decreasing sensitivity in the green band for higher reflectance values in the red band. Because in this case the sensitivity does not differ greatly, no point will be found where the slope of the tangent of the regression curve will be 1. If the tangent anywhere would have had a slope of 1, the corresponding y-intercept value would be the value for the switching bound. Therefore, a switching bound for changing between algorithms based on the green and the red band will be done iteratively, in such a way that it yields the highest r^2 value for the model as a whole. This will be done simultaneously with optimizing the performance of the multi-conditional algorithm, described in the next paragraph.

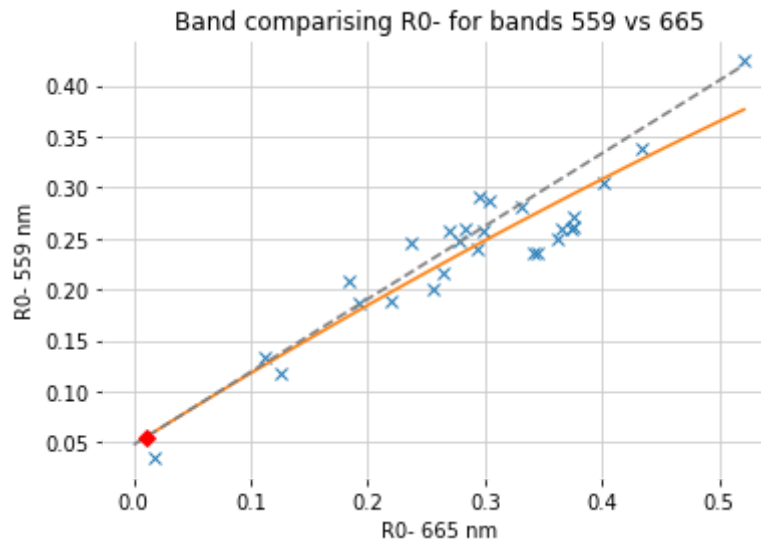


Figure 16: Scatterplots of reflectance $R(0-)$ at 559 vs 665 nm for the in situ measurements. This comparative plot shows a slightly higher sensitivity in the green band than the red band TSM concentrations, being almost similar. The orange solid line corresponds to the logarithmic regression line between the green and red band. The dashed grey line is the tangent in point (0.01, 0.05), shown as a red diamond in the figure. As the tangent is drawn in the figure, it is the steepest it gets, with a slope of 0.71.

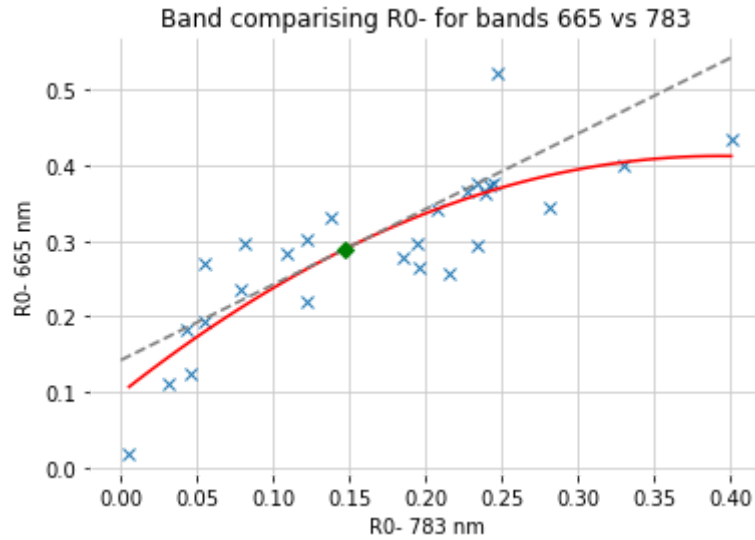


Figure 17: Scatterplots of reflectance $R(0-)$ at 665 vs 783 nm for the in situ measurements. The red solid line corresponds to the logarithmic regression line between the red and red edge NIR band. The dashed grey line is the tangent in point (0.15, 0.29), the point is highlighted as a green diamond in the figure. Here the tangent has slope of 1, the corresponding y-intercept value for the switching bound is 0.14.

Figure 17 shows the comparative plot between the red band and the NIR band. For lower values of TSM concentration the red band is more sensitive, shown by the steeper increase in $R(0-)$ values for the red band, compared to the NIR band. Also, the saturation of the red band is clearly visible for higher reflectance values. The figure shows how the switching value $s_{665-783}$ is derived for switching from the red to the red edge NIR band algorithm. It corresponds to the y-intercept of the tangent of the regression curve where the slope of the tangent equals 1. This is at the point (0.15, 0.29). The corresponding y-intercept value for the switching bound is 0.14. All interval bounds are based on the $R(0-)$ value in the red band, as this is the intermediate band between the green and the red edge NIR band. The overall observed behaviour is very similar as found by Novoa et al. (2017), the value for the switching bound for switching from the red to the NIR band slightly higher (0.14 versus 0.12).

4.4.2 Performance of multi-conditional algorithm

Now, after the bounds have been determined, the performance of the algorithm can be tested. For each relationship in the appropriate band, linear or logarithmic regression functions are modelled. From these, parameter values are found for the TSM models. The models are shown in table 3, together with their respective parameter values. The table also shows which switching bound values are used, and which TSM concentration range is associated with it.

Table 3: TSM models and associated switching bound values and TSM concentrations for three models used in the multi-conditional algorithm. The model using reflectance information from the green and red band are linear, the model based on the NIR red edge band is a polynomial function.

Interval range of R(0-) values in the red band	TSM model	Application range of TSM concentration (mg/L)
$R(0-)_{\text{red band}} \leq 0.057$	$\alpha * R(0-)_{\text{green band}}$	0 - 30
$0.057 < R(0-)_{\text{red band}} \leq 0.142$	$\beta * R(0-)_{\text{red band}}$	30 - 80
$0.142 < R(0-)_{\text{red band}}$	$\gamma * R(0-)_{\text{NIR}}^2 + \delta * R(0-)_{\text{NIR}} + \varepsilon$	> 80

With: $\alpha = 203.66$, $\beta = 329.28$, $\gamma = 4431.62$, $\delta = 36.36$ and $\varepsilon = 44.45$.

Now, using the multi-conditional algorithm on the S2 band reflectance values, averaged from the WISP-3 measurements, the performance of the model can be tested. It is compared to the original 27 laboratory measurements gathered during the fieldwork campaigns, as shown in figure 18. The performance of the model is quite well with values for statistician parameters as shown in table 4 below. Scatterplot with residual values is shown in figure 19.

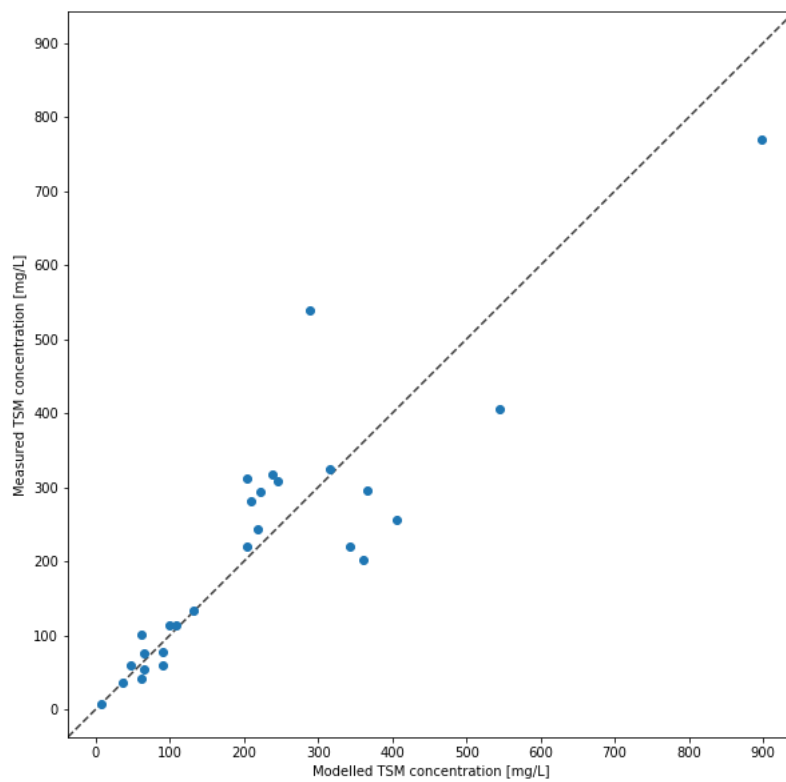


Figure 18: Modelled TSM concentrations for the 27 matched up measurements by the multi-conditional algorithm vs the laboratory results. The model performs quite well with $r^2 = 0.79$.

Table 4: showing statistical parameters for the multi-conditional TSM algorithm

r^2 [-]	0.79
RMSE [mg/L]	66.5
NRMSE [%]	9.71

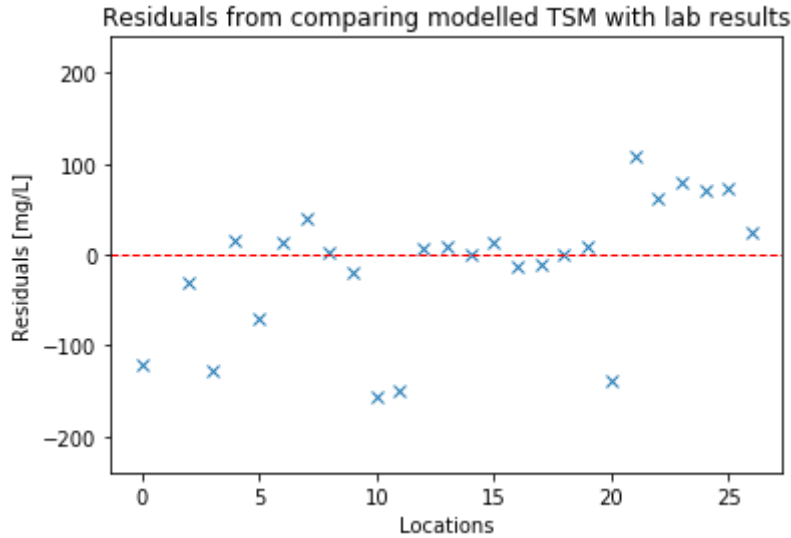


Figure 19: Residuals from comparing the modelled TSM vs laboratory values. Overall the model functions well, though still a considerable number of estimates is more than 50 mg/L off.

From figure 18 and figure 19 it becomes clear that the model performs well for TSM concentrations up to 250 mg/L but is less accurate in estimating the peaks depicting TSM concentrations of 300 mg/L and higher. More match-ups between in situ spectral and in situ laboratory measurements are necessary to achieve more accurate results, since the used database only consists of 27 matched measurements.

4.5 Exploring Sentinel-2 data

Now, having derived a multi-conditional algorithm for TSM concentrations in the Brantas River based on in situ spectral measurements, the next step is to involve satellite remote sensed data. It is generally acknowledged that accuracy of satellite images is greatly affected by - amongst others - atmospheric correction procedures and uncertainties (Gernez et al. 2015). Therefore, ACOLITE and C2RCC processors will be used, being two of the most promising models for aquatic purposes according to Warren et al. (2019). Results will be compared to the Sentinel-2 standard applied Sen2Cor results atmospherically uncorrected images to indicate difference in performances of the models.

4.5.1 Atmospheric correction of S2 data

To be able to assess the performance of the selected AC models, it is necessary to compare their results to the above water in situ spectral measurements from the WISP-3, assuming it is the closest to the truth as can be achieved. To be able to do so, match-ups are needed between satellite images and in situ measurements. The WISP-3 dataset is matched with S2 L1C images to find these match-ups.

4.5.1.1 Match-ups from recent fieldwork missions for atmospheric correction

[Appendix I](#) shows an overview of in situ sampling days, region and sampling stations, dates from which Sentinel-2 images are available and corresponding cloud cover. Only match-ups exist for 1 sample on 28-02-2020 and 9 samples on 24-03-2020 due to high cloud cover percentage during the fieldwork campaign period. So unfortunately extensive (statistical) analysis cannot be performed. Nonetheless the found match-ups provide valuable information, which is shown below.

4.5.1.2 Comparing uncorrected and AC model results and performances

Figure 20 shows 1 match-up from 28-02-2020 at Jagir Sluice. From the figure it can be seen that the effect of the atmosphere on measured Rrs is biggest in the lower wavelengths. For wavelengths > 605 nm L1C and L2A show very comparable Rrs values. Overall, taking the above water WISP-3 measurement as ‘the truth’, the S2 AC L2A clearly overestimates Rrs greatly, where the C2RCC processor seems to underestimate Rrs. From this one measurements, ACOLITE seems to perform best. To check if these assumptions hold, 23 other locations are checked for the same image (28-02-2020). Since only a single WISP-3 measurement matches for that date, the whole image is atmospherically corrected (forced by WISP-3). This only holds by assuming that the difference between WISP-3 measurement Rrs and L1C Rrs at Jagir Sluice, holds for every pixel in the image (constant atmospheric influence for the whole image). Results are shown in [Appendix J](#), which show that the aforementioned assumption does not hold. Forced by WISP-3 spectra differ greatly compared to other spectra, and even result in negative values.

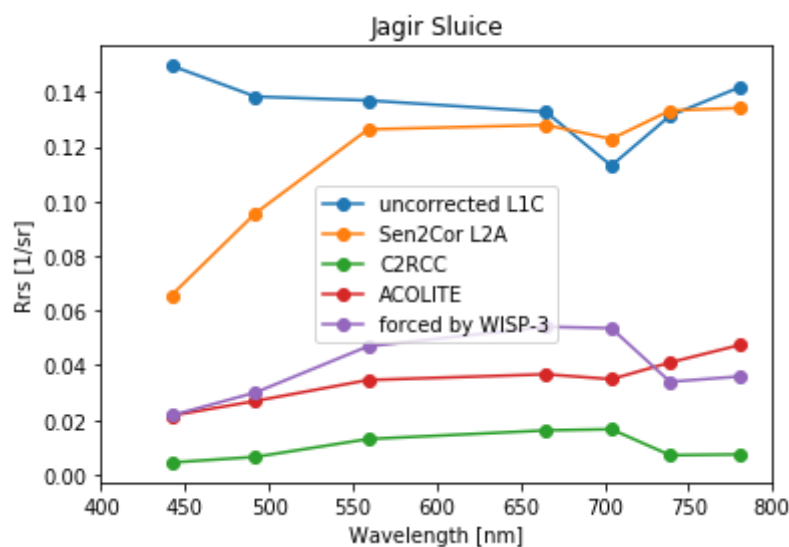


Figure 20: Comparison of spectra derived by using a set of AC models for Jagir Sluice on 28-02-2020, showing the effect of the atmosphere on measured Rrs and performances of the AC models compared to a ground truth measurement. The S2 L2A seems to greatly overestimate the Rrs values, whereas the C2RCC underestimates them. ACOLITE gives the best result.

The search for match-ups between above water spectral measurements and satellite imagery also gives 9 hits for 24-03-2020. That day, in situ measurements were taken on Waduk Sutami (WS). Figure 21 shows spectra derived for one of the locations. Also here, S2 L2A greatly overestimates Rrs. C2RCC performs best at low and high wavelengths, ACOLITE performs best for the green, red and red edge band 1. Comparisons for all locations matched on 24-03-2020 are shown in [Appendix K](#).

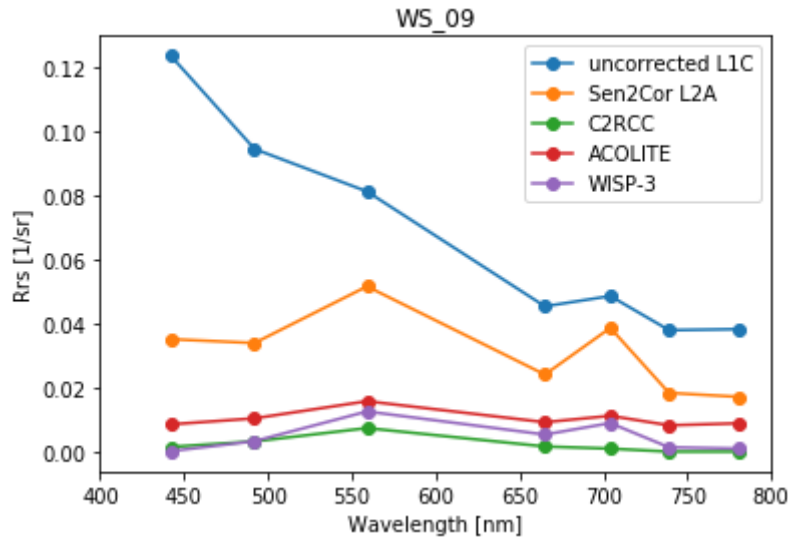


Figure 21: Comparison of spectra derived by using a set of AC models for a sample location on Waduk Sutami on 24-03-2020, the S2 L2A seems to greatly overestimate the Rrs values. C2RCC performs best at low and high wavelengths, ACOLITE performs best for the green, red and red edge band 1.

4.5.1.3 TSM concentration estimates based on AC corrected Rrs values

Based on the above derived atmospherically corrected Rrs, TSM concentrations can be estimated using the MCA derived by this study for the above mentioned match-ups. For comparison, the MCA is also applied to the L1C Rrs values, using only the information from the NIR band (least atmospheric influence). Figure 22 shows the resulting TSM estimates graphically, plotted against the TSM concentrations estimated by WISP-3 spectra. Outcomes of one extra model are visualized in this figure as well, labelled L1C (LR S2). These values are derived from a newly developed single band polynomial model calibrated on match-ups between S2 data and historical in situ laboratory TSM measurements (see [4.5.2.3 Algorithm based on S2 atmospherically uncorrected L1C data and historical in situ dataset](#)).

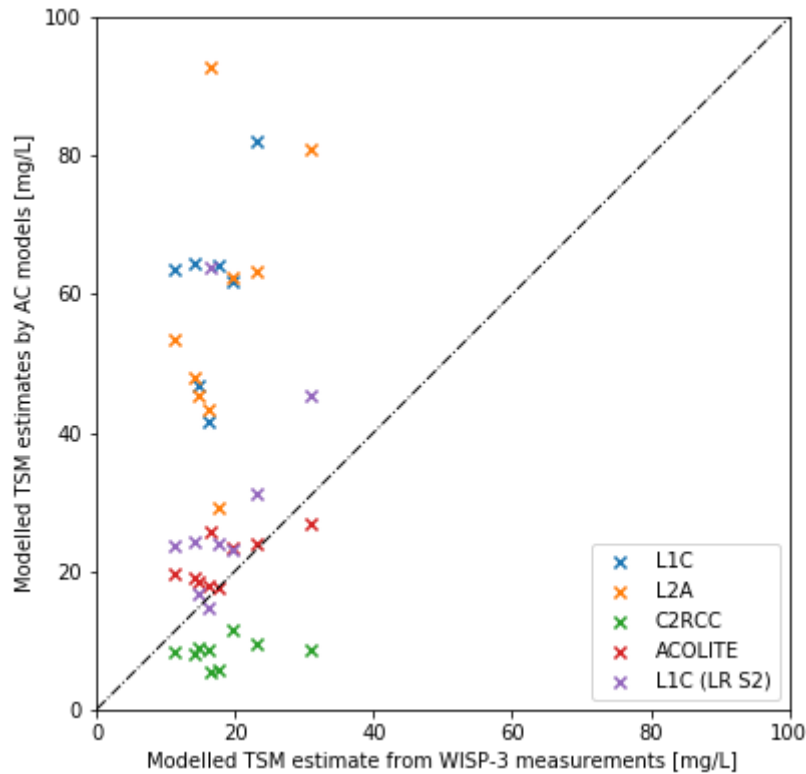


Figure 22: Resulting TSM estimates derived by using Rrs values computed using the ACOLITE, C2RCC and Sen2Cor processors for the match-ups found on 28-02-2020 and 24-03-2020. Estimates are plotted against the TSM concentrations estimated by WISP-3 spectra.

Although this dataset is too small to derive statistically trustworthy outcomes, table 5 shows an indication of RMSE (mg/L) and NRMSE (%). From both the figure and the table it becomes clear that for this dataset ACOLITE performs best (RMSE = 5 mg/L), followed by C2RCC (RMSE = 11,3 mg/L) and Sen2Cor (RMSE = 42,8 mg/L). Using uncorrected L1C Rrs as input performs worst (RMSE = 69,7 mg/L).

Table 5: An indication of RMSE, and NRMSE values for derived TSM concentrations by using ACOLITE, C2RCC and Sen2Cor processors.

	Bands used	Algorithm used	rmse [mg/L]	nrmse [%]
ACOLITE	Green, Red, NIR	MCA	5.0	25.3
C2RCC	Green, Red, NIR	MCA	11.3	57.5
Sen2Cor	Green, Red, NIR	MCA	42.8	217.2
L1C WISP	NIR	MCA	69.7	353.6

To make better predictions, derive stronger relationships and get better calibrated model parameters, more match-ups between in situ spectra and satellite imagery are needed. Because of persistent cloud cover during the fieldwork missions, these could not be obtained. A big(ger) dataset of match-ups does exist though, being match-ups between historical in situ water sampling by laboratory and satellite imagery, dating back to 2015. What if this data is used to derive a new algorithm? It will be based solely on L1C (since validating performance of AC models is not possible without ground truth measurements) matched with in situ derived TSM concentrations. The results of this method are shown in the next paragraph.

4.5.2 Using uncorrected S2 data for TSM estimations

Due to its very nature, the effect on recorded reflectances by the atmosphere is biggest in the lower wavelengths of the visible spectrum, and smaller in the NIR. If differences in TOA and BOA reflectances are negligibly small - considering it as input for a model - no AC is needed at all. To explore this possibility, first all reflectance values measured in B7 (red edge NIR, central wavelength of 783 nm) of S2 are examined more closely. This band is chosen since it is the band with the highest wavelengths which can still be compared by WISP-3 measurements (WISP-3 range goes up to 800 nm). The next paragraph shows an exploration of the vast amount of (atmospherically uncorrected) data offered by the S2 platform.

4.5.2.1 Time series spectral information Sentinel-2 bands

Since its launch, the readily available data from the S2 platform comes in an atmospherically uncorrected format called level 1C, or L1C. Since December 2018, also atmospherically corrected images can be downloaded as level 2A, or L2A. This correction is done using the Sen2Cor algorithm, optimized for use over land surfaces. Since the influence of the atmosphere is small in the NIR region, it is expected that the L1C and L2A show small or even negligible differences.

For this research a combined historical database was built holding measurements from EPA, BBWS and PJT-1 with a total of 58 measuring stations for the river basin under consideration. For all of these, time series have been computed for S2 B7 L1C and L2A reflectance values. Computed time series are visualized in [Appendix F](#). A selection of these series is shown below in figure 23, figure 24, figure 25 and figure 26. These figures clearly show small differences between reflectance values in the L1C and L2A products for most locations. Still, differences are observed which could be large enough to have a significant effect on the calculated TSM concentration based upon these reflectance values. Moreover, all locations show, some more pronounced than others, a strong seasonal effect.

When trying to understand the seasonal effect, one has to understand the local, general weather system. On Java island, most of the weather stations show a very distinctive wet and dry seasonal variation due to the Malaysian-Australian monsoon (Lee 2015; Aldrian and Djamil 2008). The dry season is generally from April - October, making the monsoon last from November until the end of March. Rainfall occurs mostly in short, heavy bursts. From the figures below it can be seen that in January, during the peak of the rainy season, reflectance values are highest, around the start of July, during the dry season, lowest. This makes perfect sense considering the increasing amount of soil particles washed away by runoff. Also, density of images is highest in the dry season (no clouds), and lower in the rainy season (especially during the peak in January). The S2A satellite was launched June 23, 2015, so that is where the time series starts. The second satellite S2B was launched March 7, 2017, which is clearly visible by the sudden increase of density of measurements. Also, after every launch, one can expect that in the months following small changes to procedures, calibrations and other adjustments are made, possibly affecting the measured reflectance values. That might explain the more scattered data points observed in the figures below, just after every launch date.

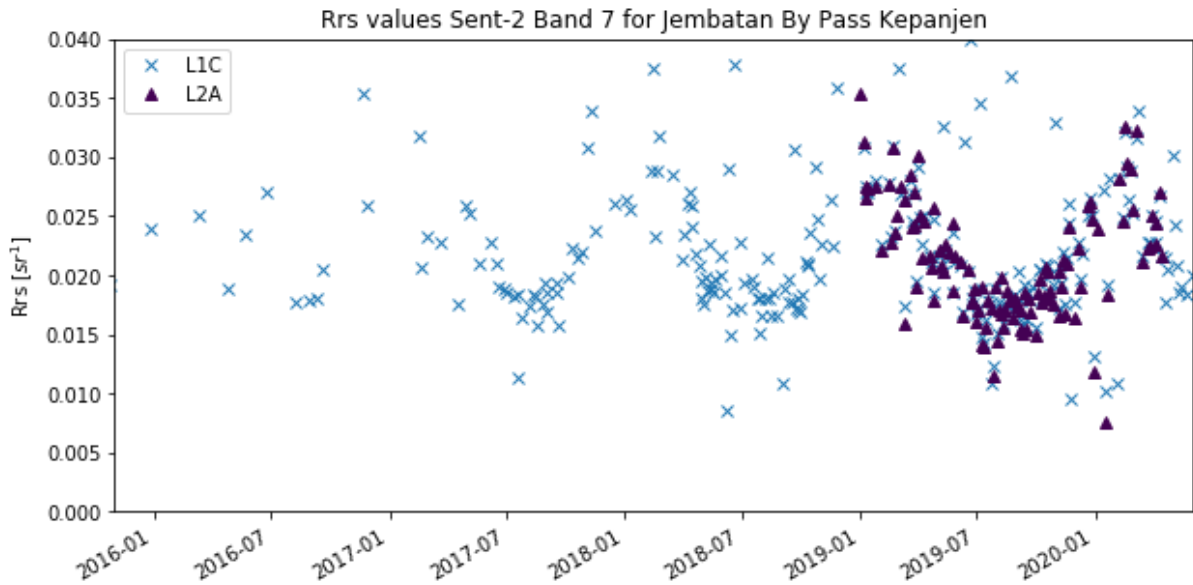


Figure 23: Remote sensing reflectances R_{rs} (sr^{-1}) for S2 B7 L1C and L2A compared for location Jembatan By Pass Kepanjen. A strong seasonal effect can be observed. In January, reflectance values are highest, in summer around the start of July, lowest.

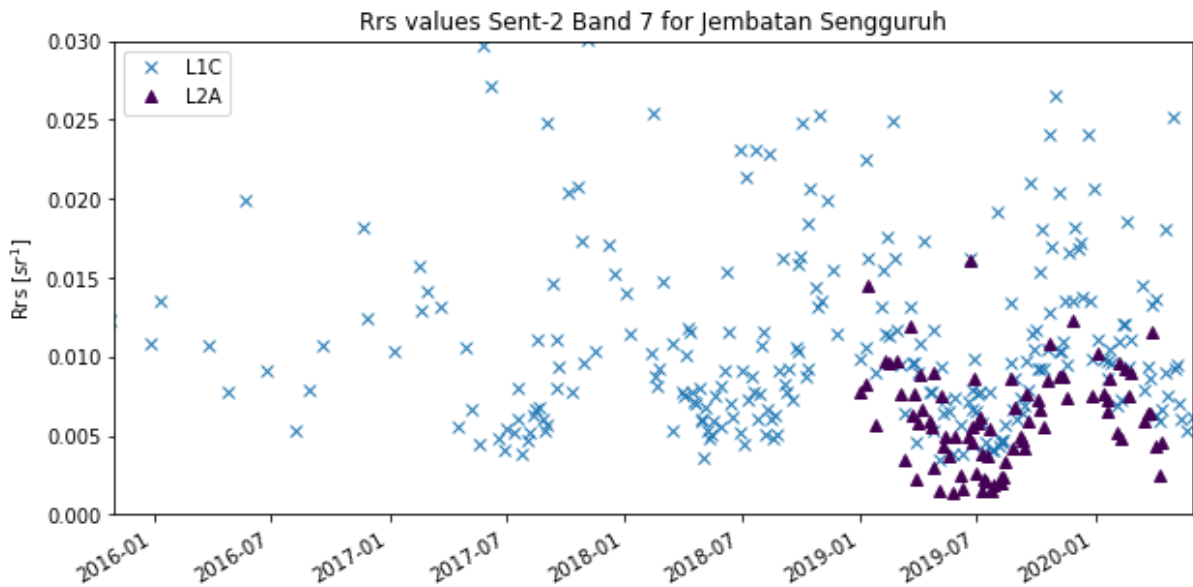


Figure 24: Remote sensing reflectances R_{rs} (sr^{-1}) for S2 B7 L1C and L2A compared at location Jembatan Sengguruh. L2A values are considerably lower for this location.

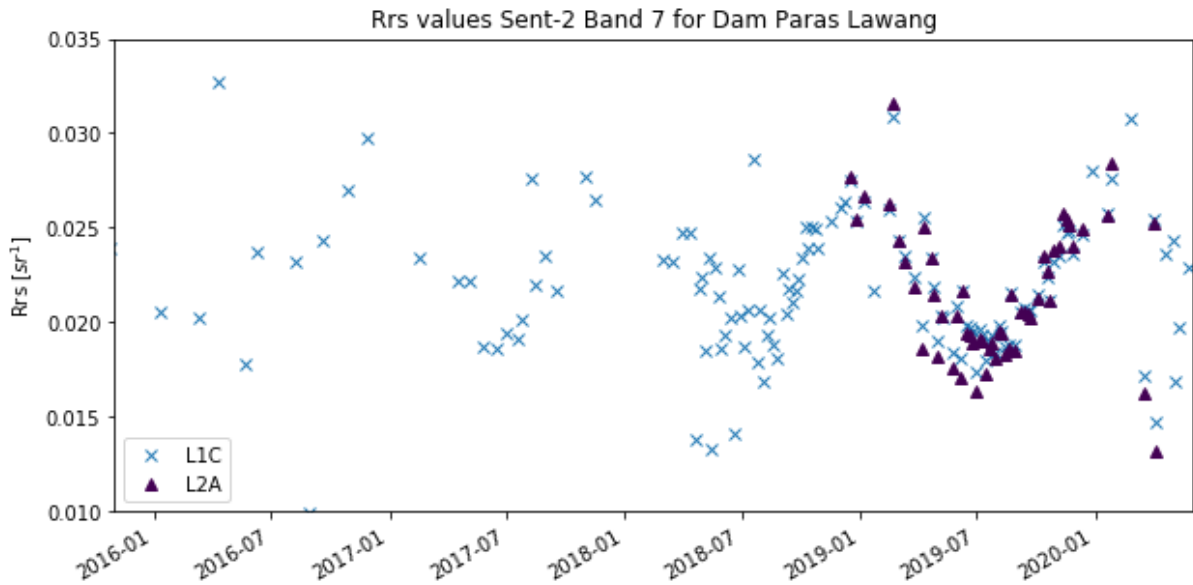


Figure 25: Remote sensing reflectances R_{rs} (sr^{-1}) for S2 B7 L1C and L2A compared at location Dam Paras Lawang.

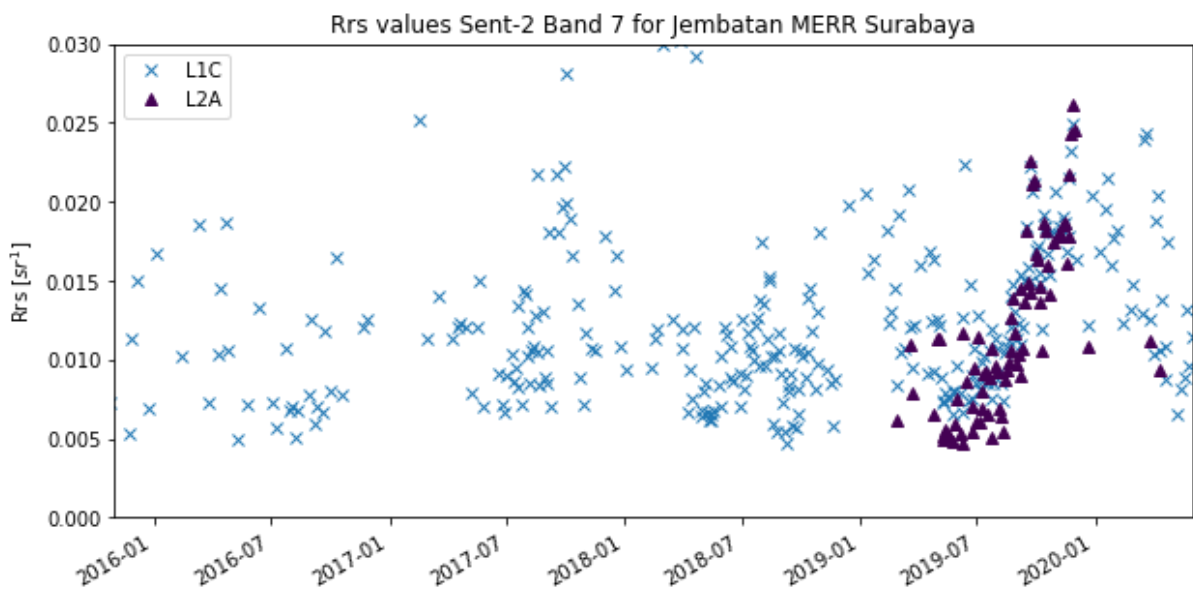


Figure 26: Remote sensing reflectances R_{rs} (sr^{-1}) for S2 B7 L1C and L2A compared at location Jembatan MERR Surabaya.

4.5.2.2 Match-ups between uncorrected S2 data and TSM measurements from historical data in situ measurements

After having established a general understanding of how reflectance values in the red edge NIR (band 7) domain vary in space and time, the next step is to determine if a clear relationship between reflectance values from S2 band 7 and TSM concentrations exists (as is found for TSM concentrations and above water radiometric measurements). To achieve this goal, the historical database of BBWS, EPA and PJT-1 is explored and matched with results as shown above. Match-ups between those in situ measurements and satellite imagery - given a positive correlation can be found - can serve as a database to derive parameters for a new model. This model then is solely based on satellite data and in situ laboratory measurements (called L1C LR). In paragraph [4.5.1.2 Comparing uncorrected and AC model results and performances it](#)

was already shown that L1C differs too greatly from WISP-3 Rrs values to serve as validation for the earlier derived multi-conditional algorithm.

An in situ measurements database from 15-02-2019 to 15-11-2019 was provided by PJT-1. From this, 45 match-ups are found matching satellite imagery taken the same day. The same search and matching strategy was performed on the EPA database dating 14-09-2015 to 24-01-2020. This search resulted in 43 match-ups, with satellite imagery taken the same day. No match-ups are found for measurements from the BBWS. This is no surprise since the database only consists of a few measurements. Until the day of writing this report, no more data was received from BBWS, unfortunately (which is a pity, since theirs is a huge database). In total 86 match-ups were found in the period 15-02-2019 until 24-01-2020. Results are graphically shown in figure 27.

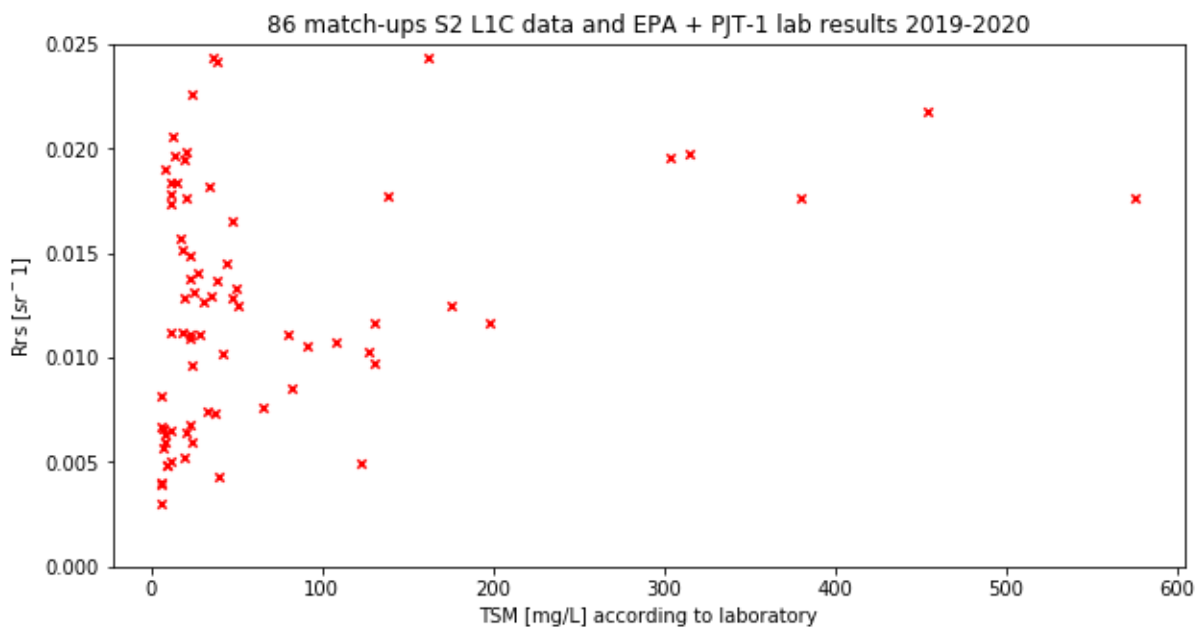


Figure 27: Match-ups between in situ historical TSM data from PJT-1 and EPA and S2 band 7 L1C reflectance values. A lot of noise can be observed in the data, especially for low TSM concentrations.

Figure 27 shows that when simply plotting Rrs values against laboratory TSM values, as was done as the first step when analyzing WISP-3 measurements, a relationship seems to be visible, but not so strong at all. A first attempt at answering what happens here, and why, is done by plotting a 3rd characteristic as colour in figure 28 and figure 29. In the first case, the season in which the measurements are taken is shown in a different colour and with a different marker. The same flattening curve can be seen as for the relationship between spectral data and laboratory measurements, as was seen earlier (figure 13) for the WISP-3 data. Still, also obviously a lot of noise in this data can be seen, which cannot be explained by seasonality. The differentiation made on dry and wet seasons does not explain the noise. What is remarkable to see however, is that the combination of highest reflectance values and highest TSM concentrations measured are found in the dry season.

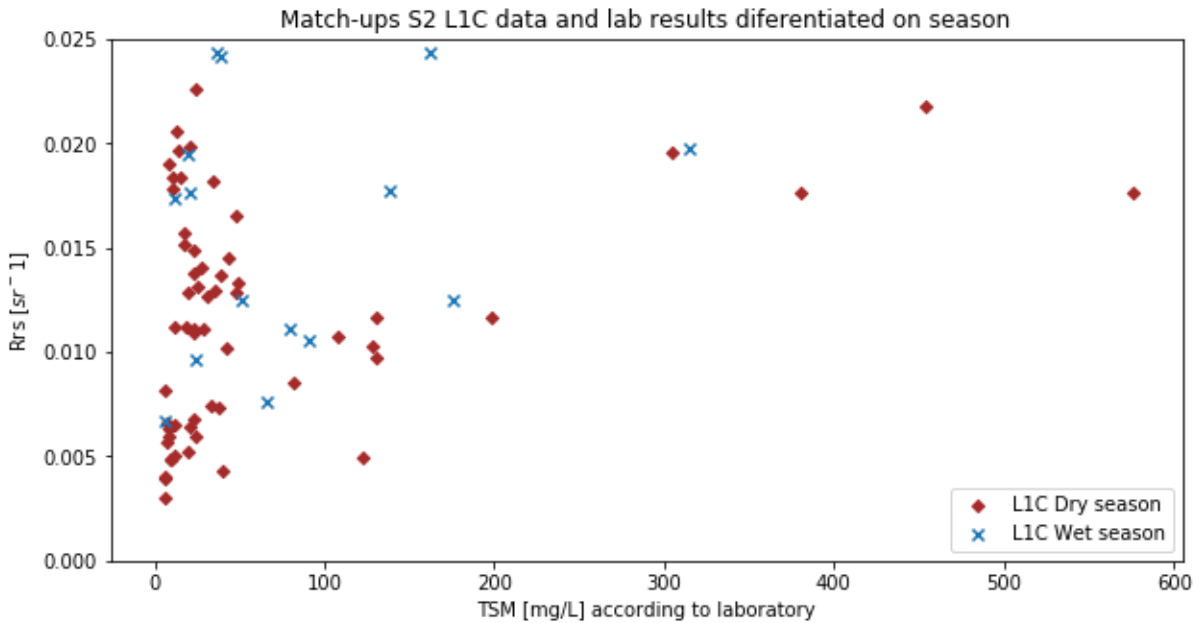


Figure 28: Match-ups between in situ historical TSM data from PJT-1 and EPA and S2 band 7 L1C reflectance values. The noise cannot be explained by the influence of seasonal circumstances.

The same exploration as differentiating on season, has been done for the effect of river width on the noise (see [Appendix G](#), where also Waduk Sutami widths are taken into account, ranging upto over 800m), also showing not be the answer. Since figure 27 shows results combined from all 58 locations, a differentiation on location can be made to know why this effect is observed.

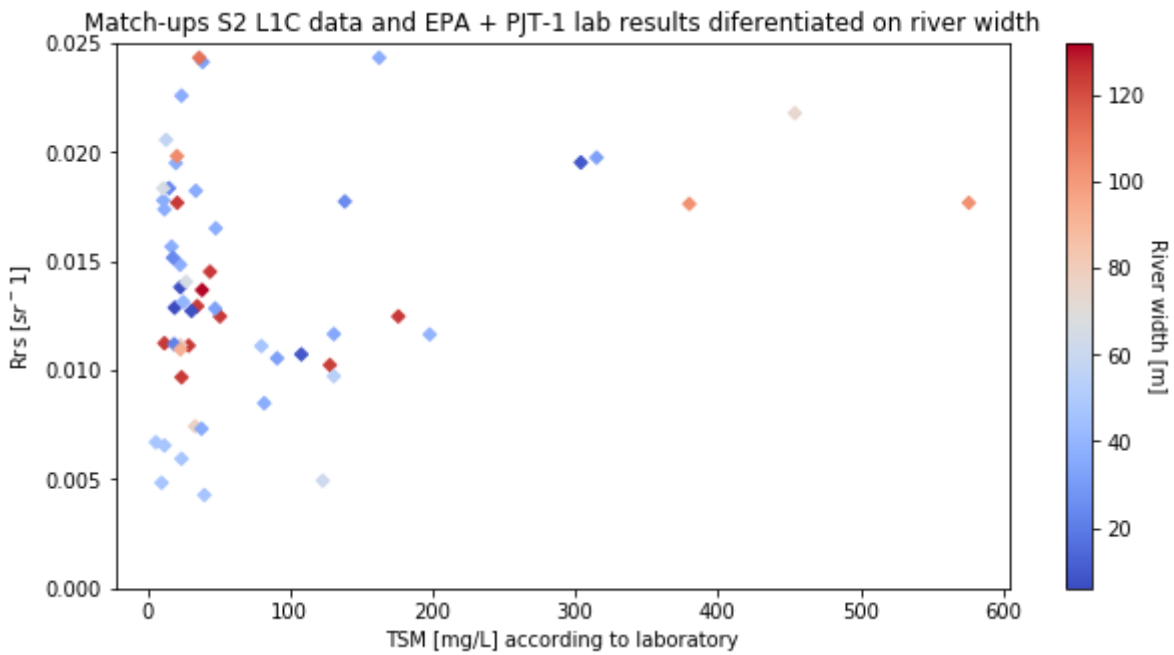


Figure 29: Match-ups between in situ historical TSM data from PJT-1 and EPA and S2 band 7 L1C reflectance values. The noise cannot be explained by the influence of river widths.

Results shown above assume that found values for Rrs stem from actual water pixels. Due to errors in location details or mismatches in georeferencing the satellite imagery, it could be that Rrs values are from actual land pixels. To find out if these accidental land pixels can be pointed out and excluded as non-valid

measurements, whole spectra (all bands) from satellite imagery are plotted and examined. Results for selected measurements (one per location and only for a subset of sampling locations, for illustration purposes) are shown in figure 30 below. All results from all measurements for all locations are shown in [Appendix H](#). From this inspection it can be concluded that location 0, 1, 2, 7 and 20 depict Rrs values which actually can represent the spectrum of a water pixel, whereas locations 5, 6 and 15 represent a spectrum typically derived from a land pixel.

Match-ups L2A combined into plotted spectra for 8 locations

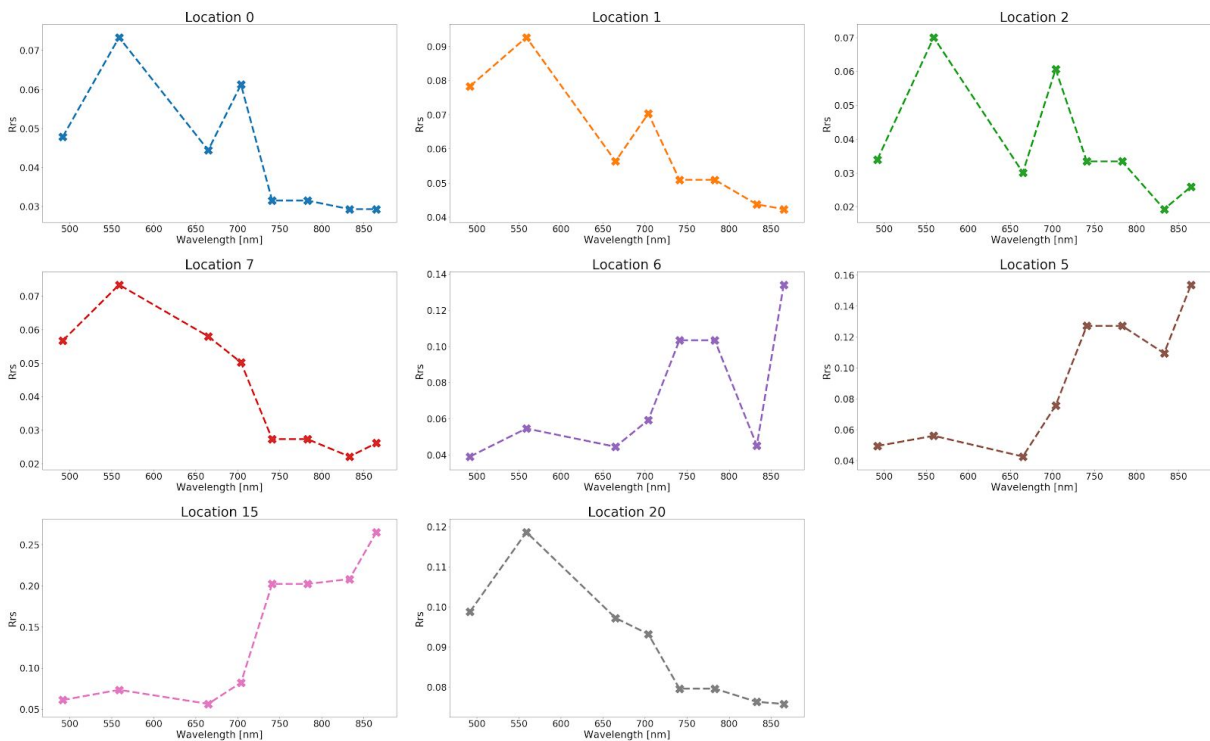


Figure 30: Match-ups of S2 and in situ data, from which spectra are plotted for bands 1- 8, to be able to label pixels as water, land or spurious.

The investigation described above has been done for all sampling locations which have matched in situ measurements with satellite data (the dataset of 86 match-ups). Now, spurious or data coming from land pixels, can be flagged out and neglected. A full list of results of classification of these pixels is shown in [Appendix L](#). After doing so, 44 match-ups remain, which are shown in figure 31.

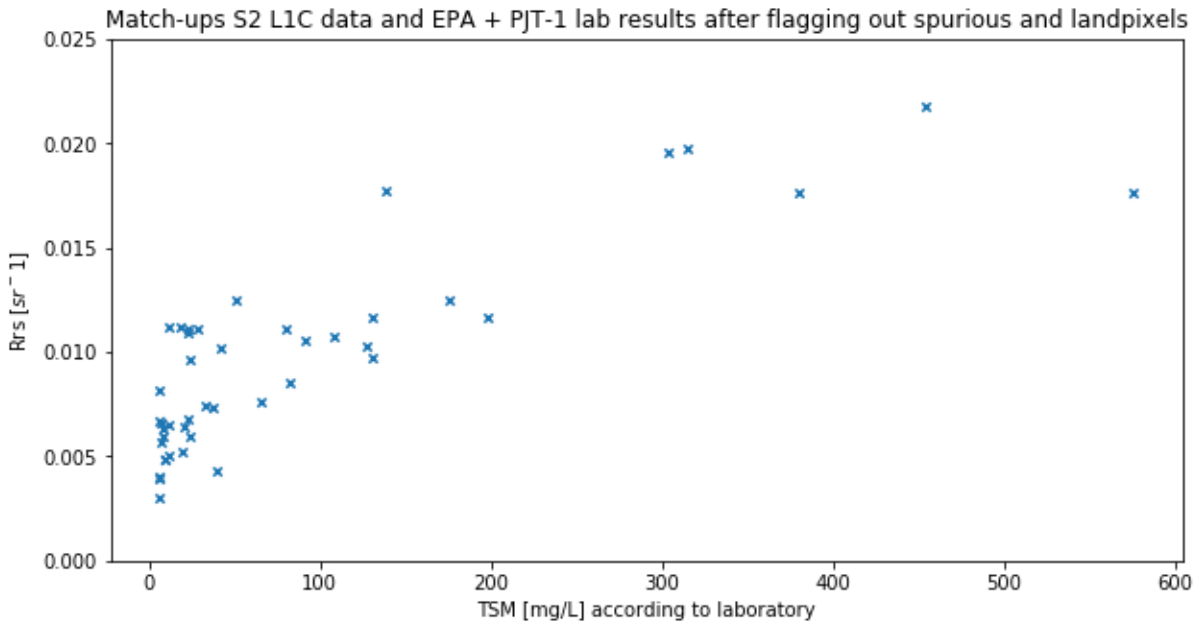


Figure 31: Match-ups S2 L1C data and EPA + PJT-1 lab results after flagging out spurious and landpixels

4.5.2.3 Algorithm based on S2 atmospherically uncorrected L1C data and historical in situ dataset

The curvilinear relationship which is observed is modelled using a polynomial fit. A log transformation is used allowing linear regression to perform the curve fitting. The polynomial fit is reasonably well with $r^2 = 0.75$. Results are shown in figure 32.

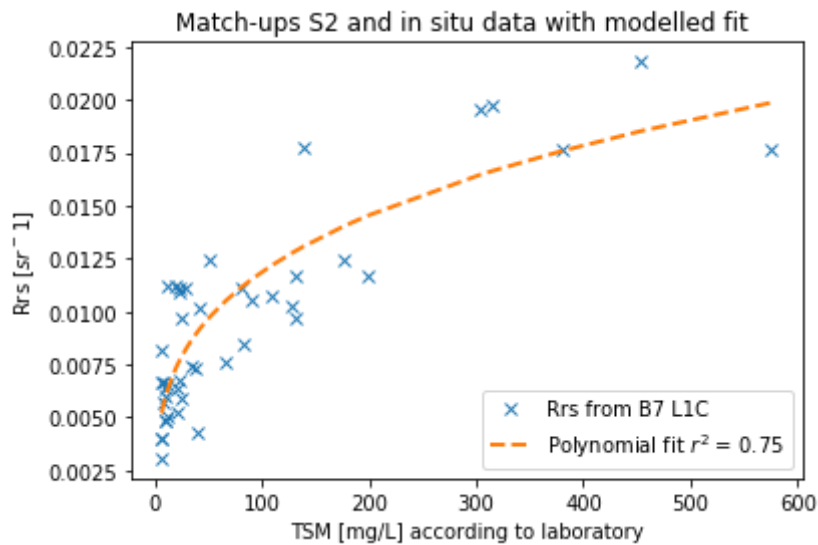


Figure 32: Scatter plot showing comparison between TSM concentration and reflectance values in the S2 (uncorrected) red-edge band (B7, central wavelength 783 nm).

The 2-degree polynomial function reads:

$$\text{TSM [mg/L]} = \zeta * R(0)_{\text{NIR}}^2 + \eta * R(0)_{\text{NIR}} + \theta$$

with: $\zeta = 9431.62$, $\eta = 36.36$ and $\theta = 15.2$.

Now, using the newly developed model on the uncorrected S2 band reflectance values, the performance of the model can be tested. Performance of the model is depicted below in table 6.

Table 6: summarizing performance of the model based on S2 L1C data matched with historical in situ TSM concentrations

r^2 [-]	0.75
RMSE [mg/L]	64.2
NRMSE [%]	11.3

The model outcome is compared to the original TSM laboratory measurements from the match-ups, and plotted against each other as shown in figure 33. Scatterplot with residual values (predicted - actual) is shown in figure 34.

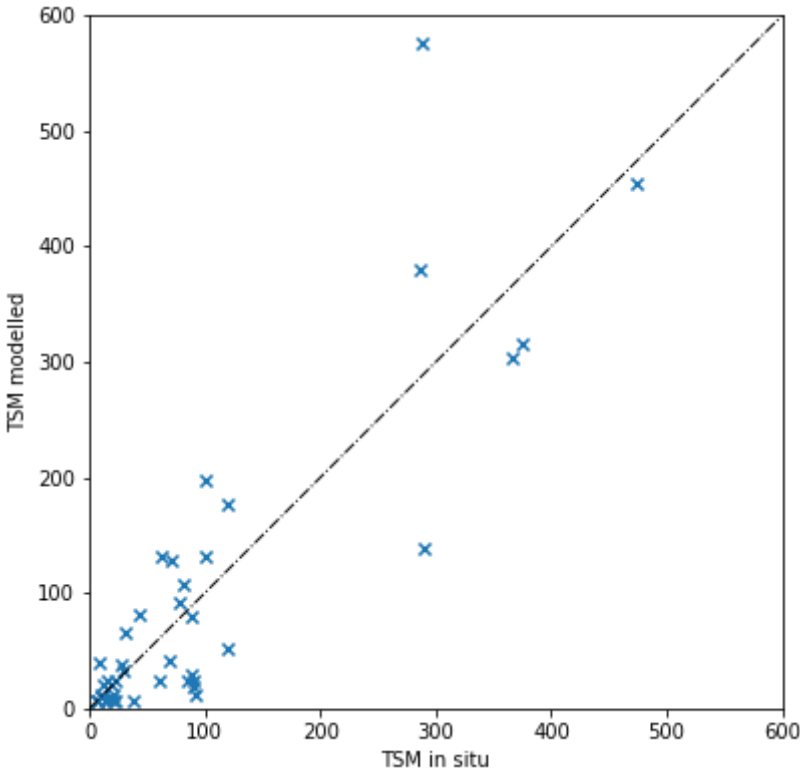


Figure 33: TSM laboratory measurements plotted against the model outcome.

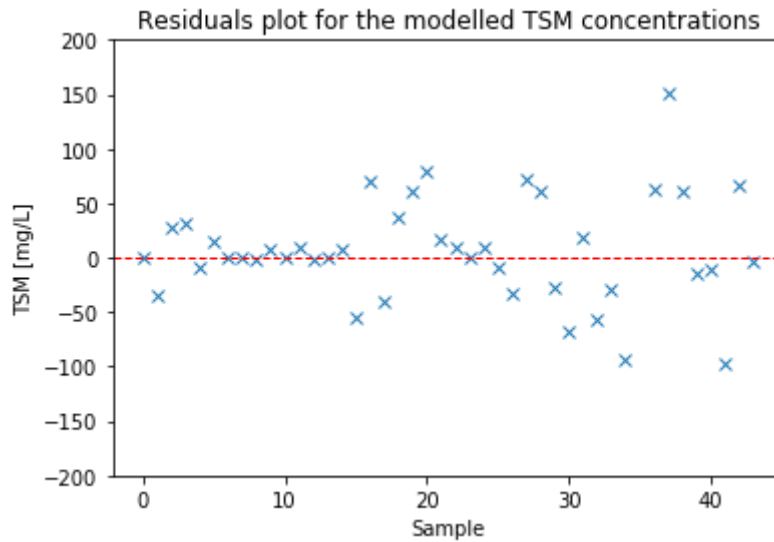


Figure 34: Residuals plot for the modelled TSM concentrations.

4.5.2.4 Time series of modelled TSM concentrations using the model based on S2 L1C data

In this section, a comparison is made between modelled TSM values and laboratory measurements using the model based on S2 data L1C band 7, as derived above. The performance of this method is illustrated in figure 35, figure 36, figure 37 and figure 38 below.

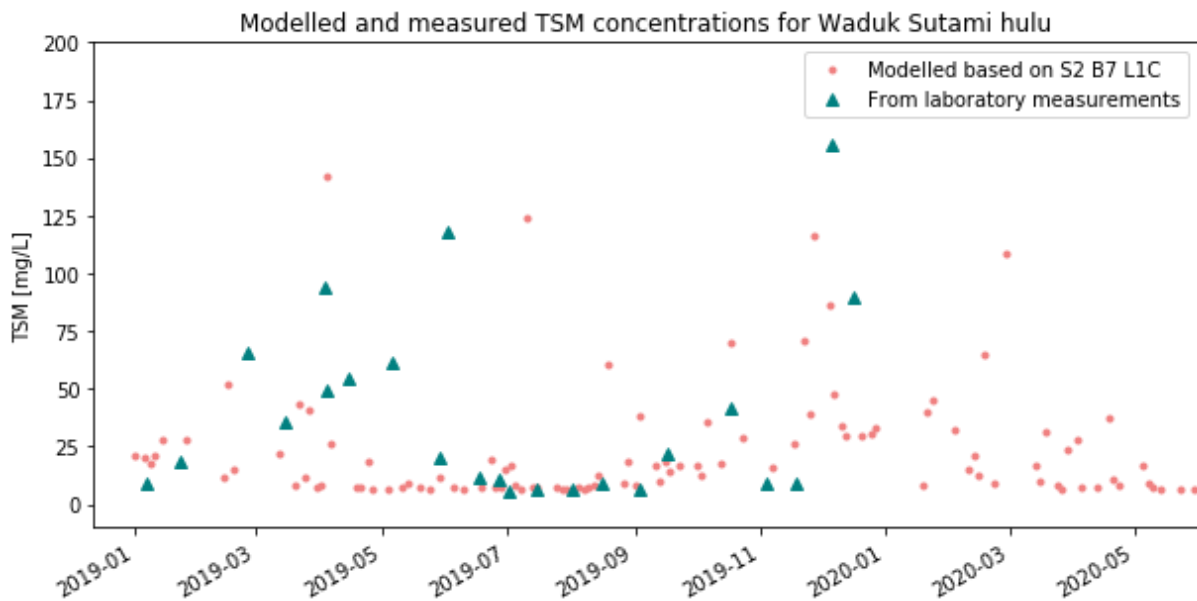


Figure 35: Modelled and laboratory TSM data for Waduk Sutami using the polynomial relationship based on S2 L1C B7 data (atmospherically uncorrected)

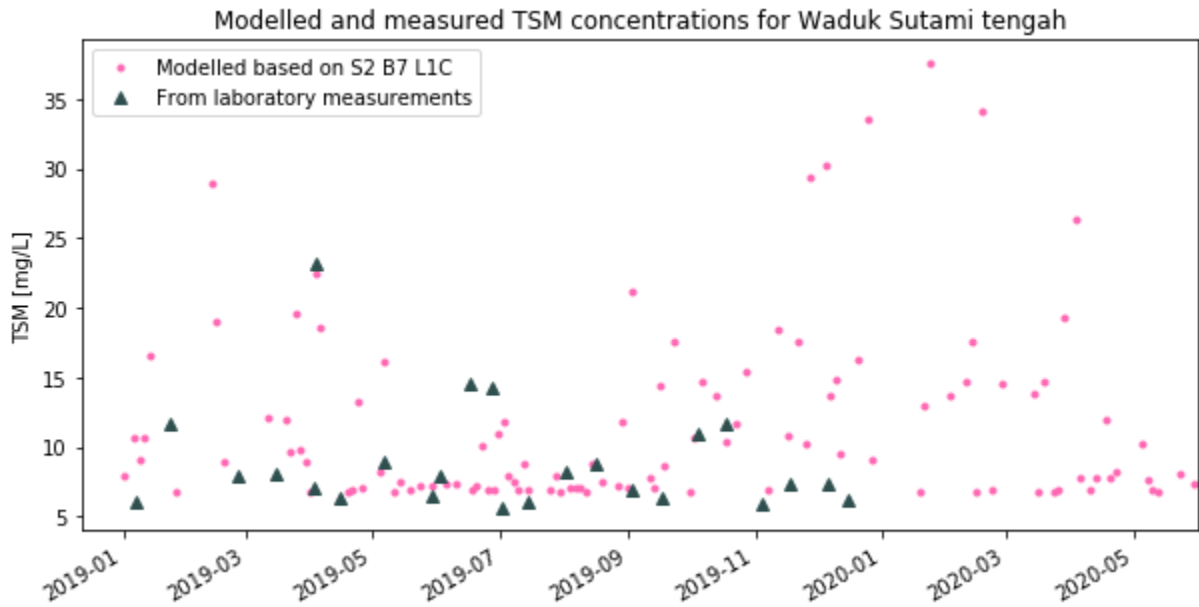


Figure 36: Modelled and laboratory TSM data for Waduk Sutami tengah. Like for Waduk Sutami hulu only the polynomial relationship based on band 7 is used, based on S2 L1C data. Figure 35 and this figure show information from sample sites in the upstream area of the Brantas basin.

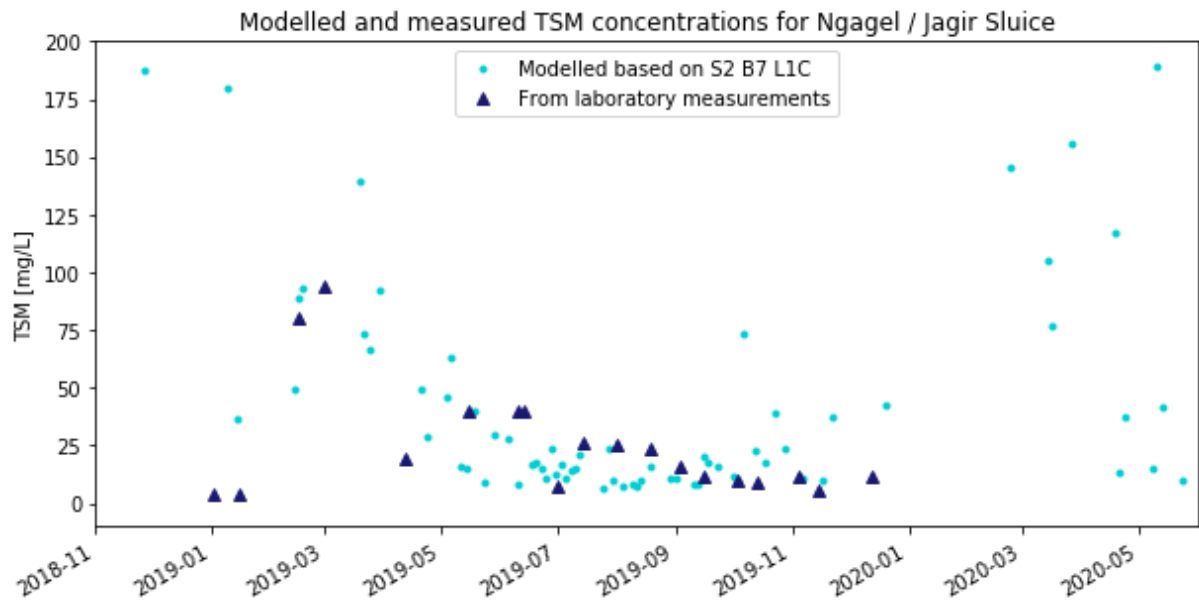


Figure 37: Modelled and laboratory TSM data for Ngagel / Jagir Sluice. This figure shows information from a sample site in the downstream area of the Brantas basin.

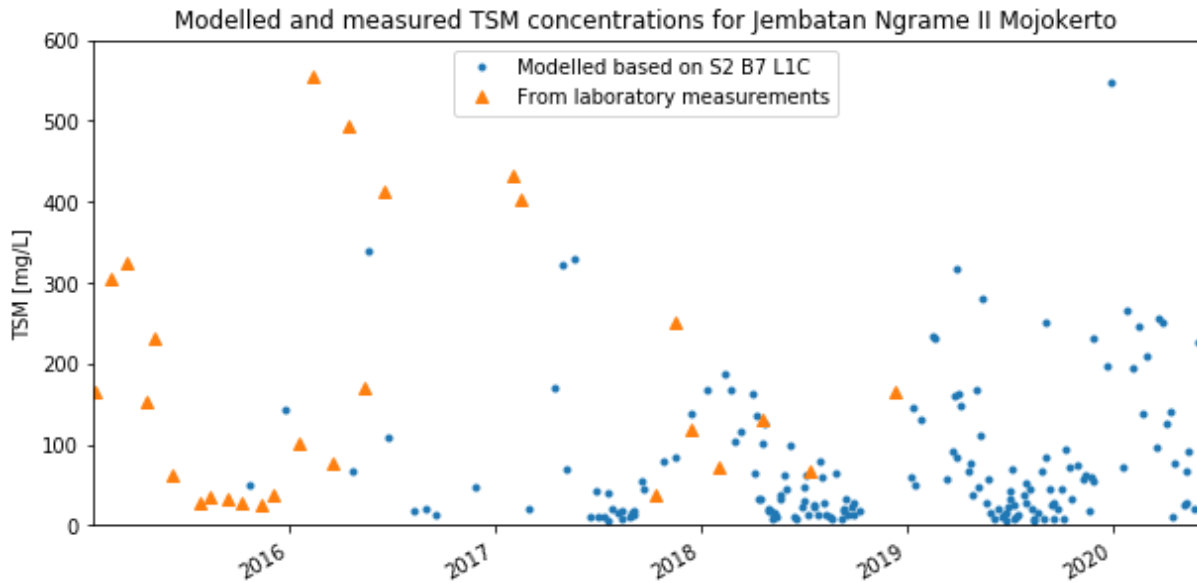


Figure 38: *Modelled and laboratory TSM data for Jembatan Ngrame II Mojokerto location. This figure shows information from a sample site in the downstream area of the Brantas basin.*

For a full overview of the above shown results for all sample sites which are investigated, see [Appendix M](#). Though modelled as well as laboratory measurements are too scarce in numbers to interpolate and construct continuous time series, it can be seen that measured values follow the same trend, it can be concluded that the modelled values reasonably well represent the range expected from laboratory values. Observed high concentrations > 100 mg/L will not be outliers, since they fall within the range of observed values by PJT-1, EPA and results from this research. The range of observed values matches the range of modelled values. What is evident in any case is that the model works reasonably well for low TSM values. For high values no matches with laboratory values can be found, most probably because these high concentrations are related to rainfall events, thus clouds, thus no satellite image.

What also can be observed from the figures above, is an increased scattering of data from late 2019 onwards. It could be an effect of changing rainfall patterns, due to El Nino. After checking it turned out that sea surface temperature conditions in the tropical Pacific remained neutral in terms of the El Niño-Southern Oscillation (ENSO) status, signifying that neither El Niño nor La Niña is currently prevailing (Abram et al. 2020).

From all figures above it is evident that in order to get more accurate results, more match-ups between in situ measurements and satellite imagery are needed, with a smaller time window for matching. However, with the available data, it has been shown that one more way of matching in situ spectral and satellite remote sensed data can be followed. The last section of this results chapter will show snapshots in time of TSM concentrations for the entire basin in two ways.

4.6 Snapshot of TSM concentration in time for entire river basin

This paragraph shows snapshots in time of TSM concentration estimates for the entire Brantas river stretch. Two methods are used: 1) based on the model derived from S2 data and in situ historical data using an atmospherically uncorrected image and 2) based on the MCA using an atmospherically corrected image by the ACOLITE processor, both for the same day (24-03-2020), as shown below.

4.6.1 Using algorithm based on uncorrected S2 L1C data

On average, TSM estimates by the single band algorithm developed for S2 atmospherically uncorrected data results in values 1.5 times higher than the MCA based on ACOLITE corrected data for the reservoir and up to 1.8 times higher for narrow river stretches. Results are shown in figure 39 and figure 40.

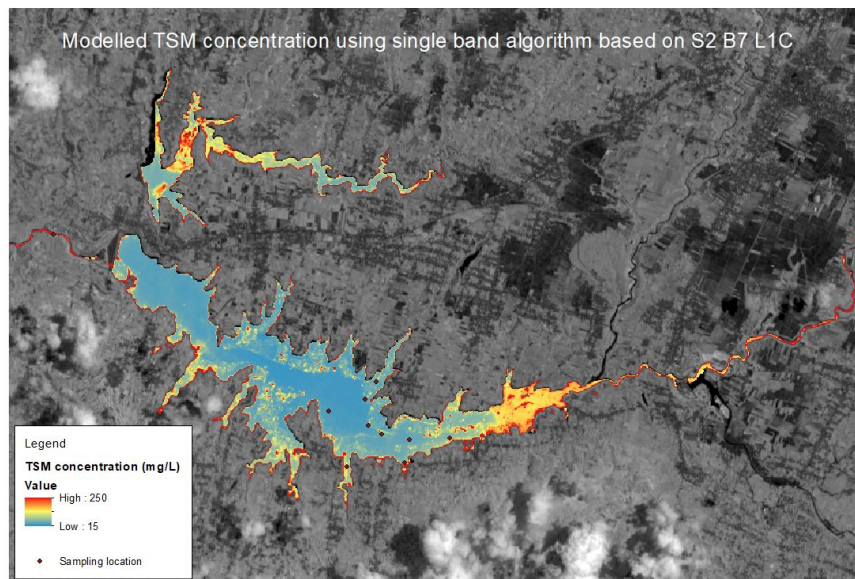


Figure 39: TSM concentrations for Waduk Sutami, modelled by using the single band algorithm developed for S2 atmospherically uncorrected L1C data, image sensed March 24, 2020.

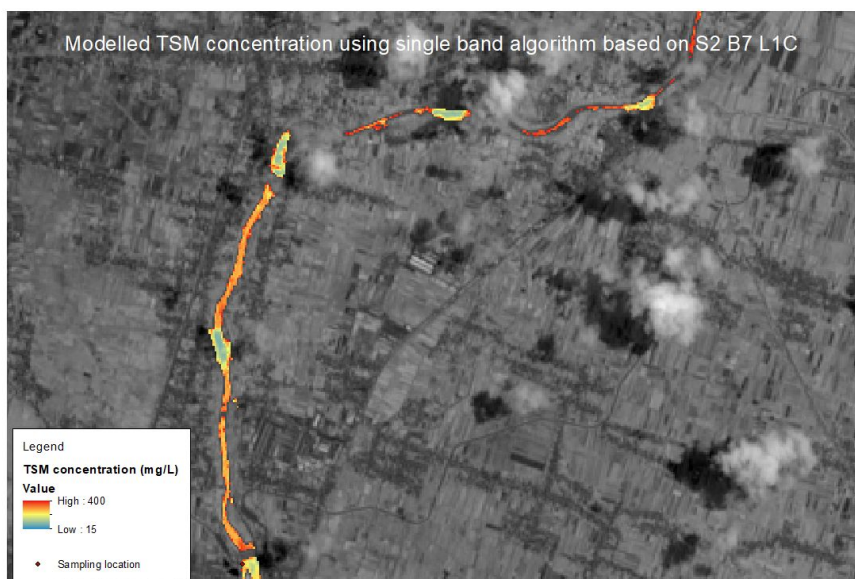


Figure 40: Modelled TSM concentrations for a river stretch near Kediri using the single band algorithm developed for S2 atmospherically uncorrected L1C data, image sensed March 24, 2020. It can be seen that river edges still show unrealistically high TSM values.

4.6.2 Using MCA and atmospherically corrected image by ACOLITE

Estimated values correspond well with the values expected. TSM values are highest at the inflow point, and gradually decrease going downstream through the reservoir. It can be seen that reservoir and river edges still show unrealistically high TSM values. From the figures it can be seen that cloud edge detection

is still a problem, the edges create extremely high reflection values, resulting in very high TSM estimates they are of course not expected to be. Figure 41 figure 42.

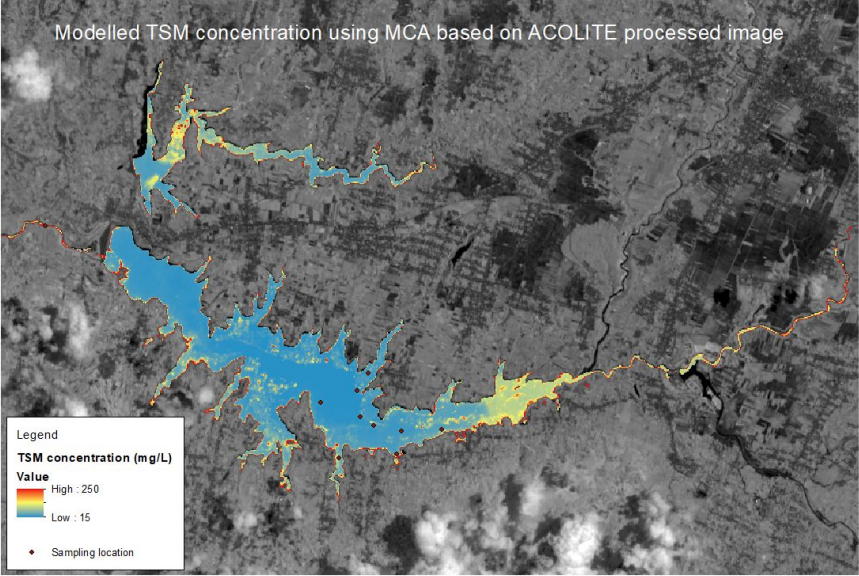


Figure 41: TSM concentrations for Waduk Sutami, modelled by using the multi-conditional algorithm on an atmospherically corrected image using the ACOLITE processor, image sensed March 24, 2020.

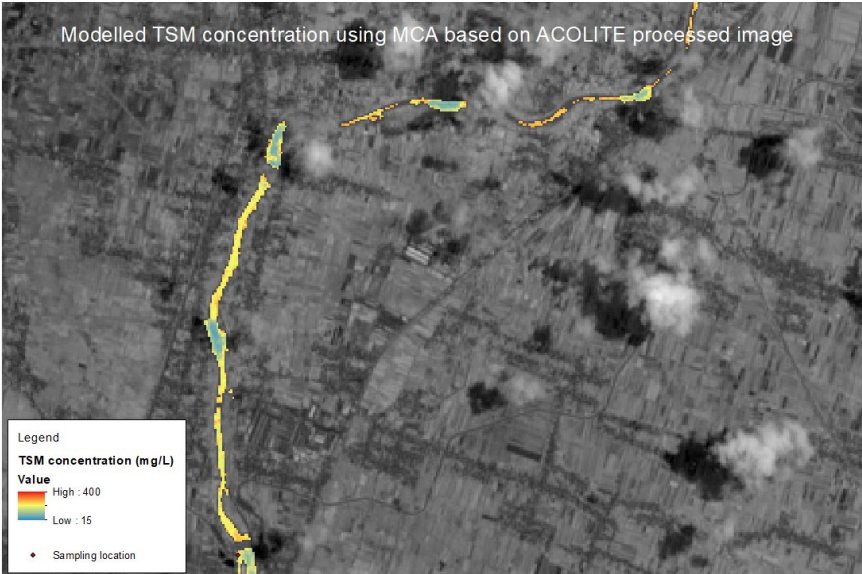


Figure 42: Modelled TSM concentrations for a river stretch near Kediri using the multi-conditional algorithm based on atmospherically corrected S2 products by using the ACOLITE processor. It can be seen that river edges still show unrealistically high TSM values.

Figure 43 below shows three zoomed in details of river stretches with different river widths. From the figure it becomes evident that river widths of less than 40 m become a challenge to estimate TSM concentrations for. Parts with generally higher values than neighbouring cells, which could indicate being a mixed cell or more greatly affected by adjacency effects.

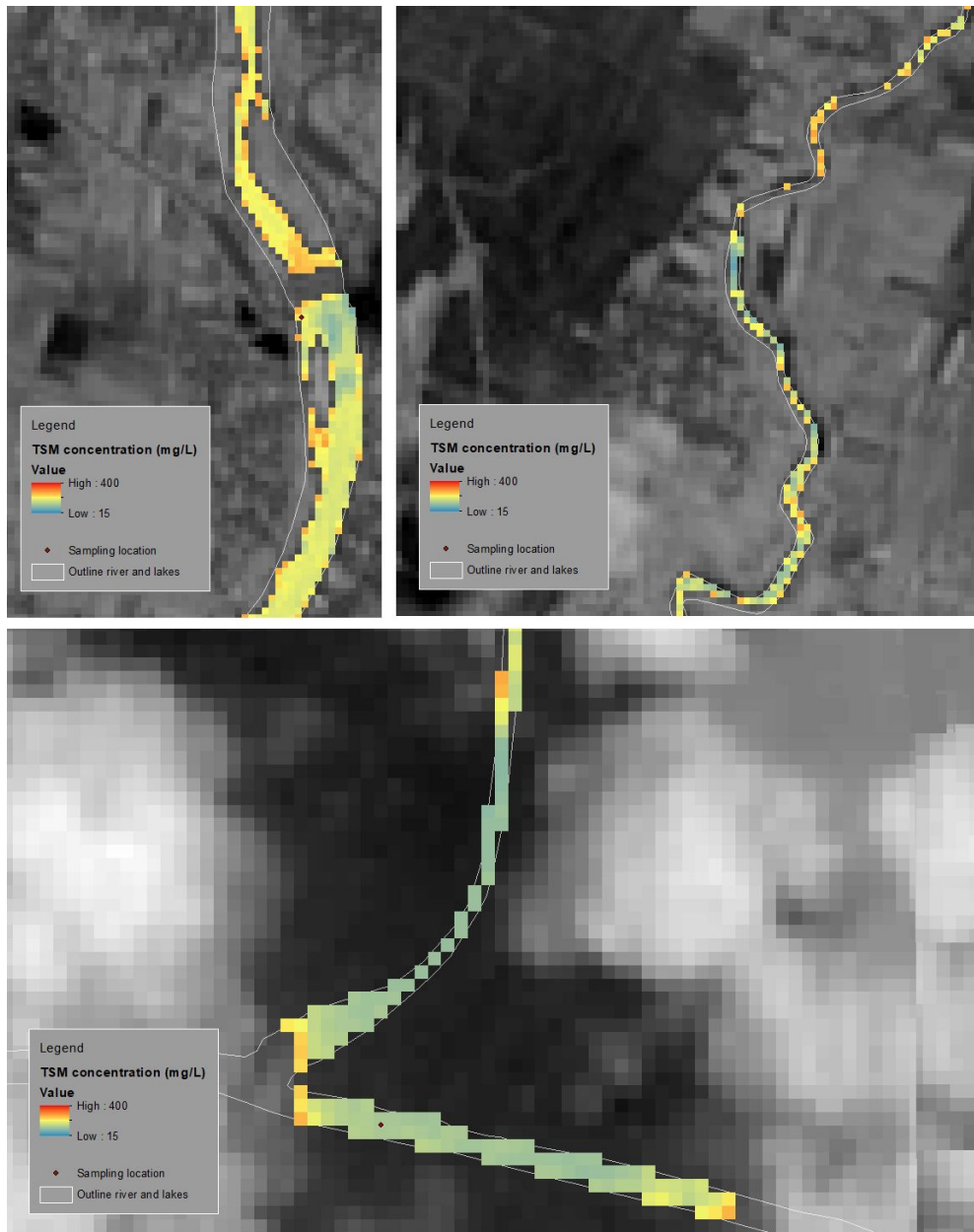


Figure 43: Three zoomed in details of river stretches with different river widths. Top left shows a location near Kediri (with sampling station Bendungan Waru Turi Kediri depicted in the middle of the picture) river widths in this picture ranges from 45 to 180 m. Top right a river stretch just upstream of Waduk Sutami is shown, near Kepanjen. River width varies from 20 to 40 m. The lower image shows the area around sampling station Jagir Sluice, where the Surabaya river splits into Jagir and Mas river. Jagir river continues to the east and is approximately 40 m wide. Mas river going north is not wider than 20 m. At the fork the river measures approximately 65 m.

4.7 Summary of results

Starting with figure 44, it was shown that the good linear relationship for low TSM concentrations saturates (flattening of the curves) in the green and red band for higher TSM concentrations. Therefore, a multi-conditional algorithm is developed, where the high sensitivity of the green and red band for lower TSM concentrations is used in combination with the information from the NIR band for high TSM values, which still clearly shows an increasing relationship at high TSM concentrations. Interval ranges, models used per interval and for which TSM concentration range the models are used are shown in table 7. The performance of the model is summarized in table 8

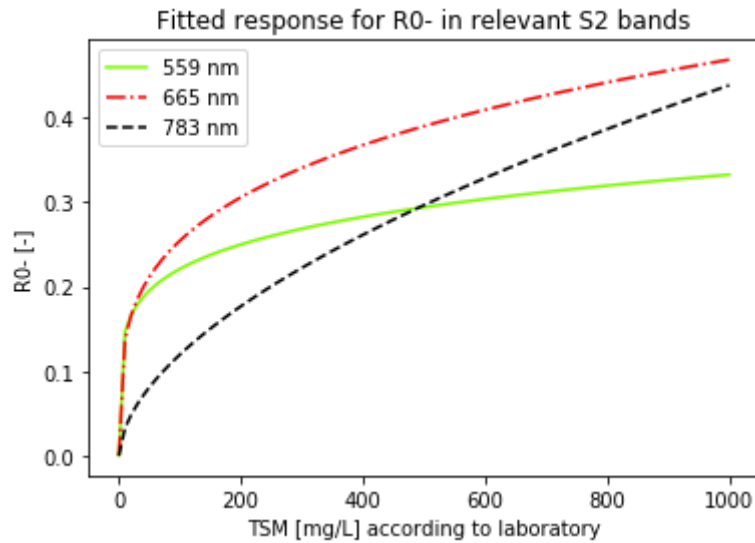


Figure 44: Green en red bands get saturated (flattening of the curves) for higher TSM concentrations, whereas the NIR band keeps holding information even for high TSM concentrations.

Table 7: TSM models and associated switching bound values and TSM concentrations for three models used in the multi-conditional algorithm

Interval range of $R(0-)$ values in the red band	TSM model	Application range of TSM concentration (mg/L)
$R(0-)_{\text{red band}} \leq 0.057$	$\alpha * R(0-)_{\text{green band}}$	0 - 30
$0.057 < R(0-)_{\text{red band}} \leq 0.142$	$\beta * R(0-)_{\text{red band}}$	30 - 80
$0.142 < R(0-)_{\text{red band}}$	$\gamma * R(0-)_{\text{NIR}}^2 + \delta * R(0-)_{\text{NIR}} + \varepsilon$	> 80

With: $\alpha = 203.66$, $\beta = 329.28$, $\gamma = 4431.62$, $\delta = 36.36$ and $\varepsilon = 44.45$.

Table 8: R-squared, RMSE and NRMSE for the MCA

r^2 [-]	0.79
RMSE [mg/L]	66.5
NRMSE [%]	9.7

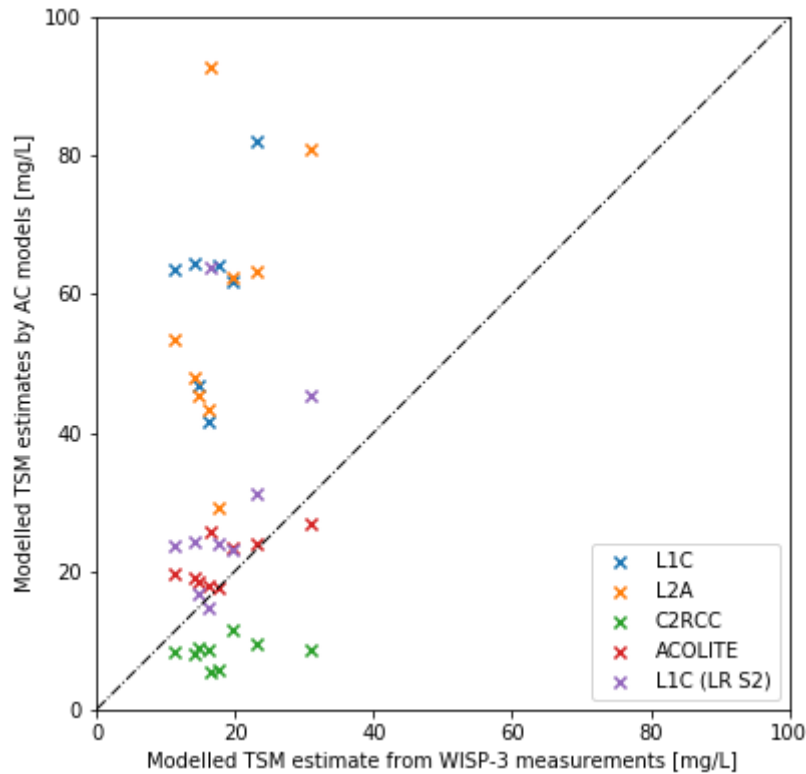


Figure 45: TSM estimates derived by using Rrs values computed by the ACOLITE, C2RCC and Sen2Cor processors for the match-ups found on 28-02-2020 and 24-03-2020. Estimates are plotted against the TSM concentrations estimated by WISP-3 spectra.

After establishing the MCA, different atmospheric correction models were investigated. The resulting modelled TSM estimates are shown in figure 45. Although this dataset is too small to derive statistically trustworthy outcomes, table 9 shows an indication of RMSE and NRMSE. From both the figure above and the table below it becomes clear that for this dataset ACOLITE performs best (RMSE = 5 mg/L), followed by C2RCC (RMSE = 11,3 mg/L) and Sen2Cor (RMSE = 42,8 mg/L). Using uncorrected L1C Rrs as input performs worst (RMSE = 69,7 mg/L).

Table 9: An indication of RMSE, RMSPE and NRMSPE values for derived TSM concentrations by using ACOLITE, C2RCC and Sen2Cor processors. For comparison, also values are given when TSM is estimated from Rrs values given by the L1C S2 product.

	Bands used	Algorithm used	rmse [mg/L]	nrmspe [%]
ACOLITE	Green, Red, NIR	MCA	5.0	25.3
C2RCC	Green, Red, NIR	MCA	11.3	57.5
Sen2Cor	Green, Red, NIR	MCA	42.8	217.2
L1C WISP	NIR	MCA	69.7	353.6

Figure 46 shows the polynomial fit to match-ups between S2 L1C Rrs values and historical in situ TSM measurements. This second model is derived to be able to use the fast amount of data offered by the S2 platform without need of atmospheric correction or above water radiometric measurements and to see how this method compares to the earlier derived MCA.

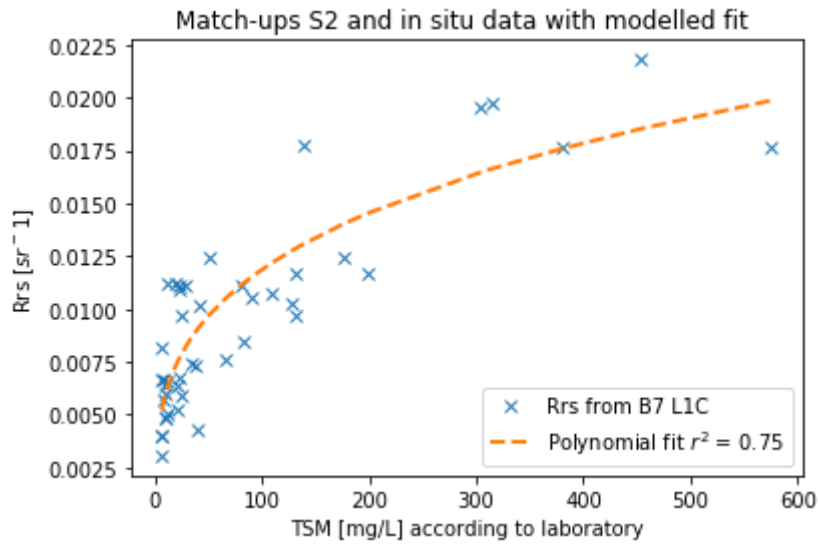


Figure 46: Scatter plot showing comparison between TSM concentration and reflectance values in the S2 (uncorrected) red-edge band (B7, central wavelength 783 nm).

The 2-degree polynomial function reads:

$$\text{TSM [mg/L]} = \zeta * R(0)_{\text{NIR}}^2 + \eta * R(0)_{\text{NIR}} + \theta$$

with: $\zeta = 9431.62$, $\eta = 36.36$ and $\theta = 0.15$.

The newly developed model based on the uncorrected S2 band reflectance values is tested for its performance and shown in table 10.

Table 10: summarizing performance of the model based on S2 L1C data matched with historical in situ TSM concentrations

r^2 [-]	0.75
RMSE [mg/L]	64.2
NRMSE [%]	11.3

5

Discussion

In situ spectral measurements as well as laboratory results show an extremely turbid nature of the Brantas River surface water. A linear relationship between the green band and TSM concentration < 30 mg/L is found ($r^2 = 0.91$, RMSE = 5.3 mg/L and NRMSE = 13.2%). The signal in the green band gets saturated for TSM concentrations > 30 mg/L, which is in contrast with findings of Novoa et al. (2017), who observed saturation occurring already at around 10 mg/L. A similar pattern is observed for the red band, which saturates at higher TSM concentrations of around 80 mg/L (50 mg/L by Novo et al.). Also here a good linear fit can be achieved for lower concentrations ($r^2 = 0.92$, RMSE = 12.6 mg/L and NRMSE = 10.1%). Sensitivity for the green and red band are similar. This contrasts with results found by (Novoa et al. 2017), which show a sharper increase in reflectance for the green band compared to the red for concentrations below 10 mg/L. Observed differences in saturation bounds can be very well caused by the limited number of observations of this study, especially in the low TSM concentration range. However, the sharper increase in red band reflectance compared to NIR bands for concentrations below about 50 mg/L is confirmed by this study. As TSM concentrations increase, a curvilinear relationship is observed. This is demonstrated by a polynomial fit for higher TSM concentrations in the red edge NIR band, without any signs of saturation. Thereby the same behaviour is observed as seen by Ritchie et al. (1990) and Ritchie and Cooper (1991). The polynomial fit is reasonably well with $r^2 = 0.82$ but results in fairly big errors (RMSE = 58.3 mg/L and NRMSE = 7.9%). The overall performance of the model (combining the three separate models) is acceptable with a r^2 value of 0.79, but also high estimated error values with RMSE = 66.5 mg/L and NRMSE = 9.7%. The overall model behaviour though is very similar as found by Novoa et al. (2017). RMSE values get high for the model based on the NIR and and for the overall multi-conditional algorithm. Outliers are observed, especially for high TSM laboratory values, where reflectance values stay relatively low. This might be caused by the fact that particles in the upper water layer in extremely turbid water mask out information from lower layers in the water column. Also, fluctuations observed in laboratory TSM values are expected to be caused by the fact that the database holds data from 4 different laboratories. Some follow different protocols, and one laboratory uses an unknown protocol. When examining errors in between observed and predicted values, the influence of each individual error on the overall RMSE is proportional to the size of the squared error. This results in large errors having a disproportionately large effect on the RMSE (high sensitivity to outliers) (Willmott and Matsuura 2006; Pontius, Thontteh, and Chen 2008).

The high turbidity levels lead to an increased optical complexity, for inland water which is already complex to investigate by remote sensing. Especially atmospheric correction poses a challenge (Vanhellemont and Ruddick 2015; Sterckx et al. 2015). Sen2Cor, ACOLITE and C2RCC processors were used by this study to atmospherically correct TOA reflectance values. These processors are freely available. Only a view match-ups were achieved between field reflectance data measured simultaneously and S2 images. Therefore, no thorough validation of the performance of the different AC models can be undertaken. Nonetheless, when examining the 10 match-ups which are found and compared to the above water reflectance values, it can be concluded that ACOLITE produces the smallest error (RMSE = 5.0 mg/L), followed by C2RCC (RMSE = 11,3 mg/L) and Sen2Cor (RMSE = 42,8 mg/L). If S2 TOA (L1C) data can be used directly, for example the NIR bands where atmospheric interference is smallest, no

atmospheric correction is required altogether. Therefore, performance of the NIR polynomial fit was tested on L1C data from B7. This resulted in a RMSE of 69,7 mg/L for the set of 10 match-ups. The S2 L2A (Sen2Cor) seems to greatly overestimate the Rrs values (up to 3 times as high as WISP-3 control measurements), C2RCC performs best at low and high wavelengths (band 1, 2 (blue) and 8 (NIR)), ACOLITE performs best for band 3 (green), band 4 (red) and band 7 (red edge 1). Generally speaking C2RCC underestimates Rrs values slightly, whereas ACOLITE gives the best result overall.

The poor performance of Sen2Cor could be very well caused by the algorithm approach which uses the dark dense vegetation approach (DDV method). This method is clearly better adapted to the atmospheric correction of land surfaces (Kaufman and Sendra 1988). All results from Sen2Cor, C2RCC and ACOLITE follow the same pattern quite well. However, big differences are observed in absolute Rrs values. Since TSM estimates are calculated directly from these values (and not from a ratio for example), large effects are also observed in final estimated TSM concentration values. That using Sen2Cor results in greatly overestimated Rrs values is no surprise, since the processor was developed for land surfaces and lacks sensitivity to be used on (small) water bodies. In particular, Sen2Cor produces high values in the blue part of the spectrum, up until 3.5 times as high as above water reflectance values. This may be due to sunglint, but most probable because of atmospheric correction errors which are more pronounced in the case of water leaving signal. Toming et al. (2016) states that Sen2Cor will likely be the first choice for many users to test. This may well be, but it is strongly advised not to use it for any final estimation of TSM values. For first explorations however, it is an attractive product since it is readily available either from the Copernicus Open Access Hub or from Google's servers by requesting it via Google's Earth Engine.

Skipping atmospheric correction altogether would greatly reduce workload and needed resources. Atmospheric effects are biggest in the blue part of the spectrum. Effects decrease nearly exponentially with increasing wavelength. The red and NIR bands are relatively least affected by atmospheric effects. Since TSM show good relationship with the NIR band, it is worthwhile investigating if TOA NIR remote sensing reflectances can be used to estimate TSM concentrations. Indeed, Toming et al. (2016) showed that results obtained with TOA reflectance values were better than with BOA reflectance values in case of all studied parameters, when using Sen2Cor as AC processor. This study investigated the influence of the atmosphere by comparing L1C and L2A products in the red edge NIR band (band 7). For most of the nearly 60 locations it showed differences are as small as to be considered negligible. Nearly all investigated S2 red edge NIR band reflectance data showed a strong seasonal effect. It can be seen that in January, during the peak of the rainy season, reflectance values are highest, around the start of July, during the dry season, lowest. This makes perfect sense considering the increasing amount of soil particles washed away by increasing runoff during the rainy season. Also, density of images is highest in the dry season (no clouds), and lower in the rainy season (especially during the peak in January). Confirming these temporal variations in TSM concentrations (and most likely other water quality parameters) seen by conventional point sampling methods is vital for comprehensive assessment and management of the Brantas river system.

Having confirmed the relatively small atmospheric influence in the NIR end of the spectrum, match-ups are searched between S2 TOA data in band 7 and in situ laboratory TSM concentrations from a historical database (2015-2020). Analyzing the historical database gave nearly 90 match-ups. When plotting Rrs values against laboratory TSM values, the expected curvilinear relationship is visible, along with a lot of noisy data. Inspection of all individual measurements was necessary by examining the full spectra (band 1-8) for every sample. By doing so, spurious and land pixels could be identified and deleted. It turned out to be a vital process to understand the data. Mismatches can be due to measurement errors, archiving errors or because of mismatches in georeferencing the raw satellite data. Based on the cleaned up dataset of match-ups a new model was developed, performing comparably to the multi-conditional algorithm based on WISP-3 derived simulated S2 data with $r^2 = 0.75$, RMSE = 64,2 mg/L and NRMSE = 11,3%. A reason for the derived high RMSE can be the fact that match-ups are now considered valid if the measurement is

taken on the same day. Due to the high frequency dynamics of the river and its constituents, a smaller time window is suggested. The best would be to work with a maximum of 30 min before and after satellite overpass. To actually know how dynamics of the river behave, future research could focus on taking multiple in situ laboratory or spectral measurements to map variations within one day. Thereby information is gathered to decide on the maximum allowed time window. By using the model based on S2 and historical data, sensitivity to atmospheric correction in the lower wavelength bands is no issue anymore. This matching process could also be undertaken by the ACOLITE processor corrected images, with use of the multi-conditional TSM algorithm. This will most likely result in the best performance and most accurate TSM estimates. The scope of this study however lacks the time as well as the computational power to have done so. Therefore, TSM estimates are modelled based on the polynomial relationship in the red edge NIR band. The modelled values very well represent the from laboratory values expected range of concentrations. High concentrations fall within the range of observed values by PJT-1, EPA and results from this research. The range of observed values matches the range of modelled values. Density of either the in situ measurements nor the modelled estimates is high enough to compute actual time series. Statistical analysis of the model performance therefore will need more data from shorter time intervals as input.

When computing snapshots in time of TSM estimates for the whole river from source to mouth, ACOLITE in combination with the MCA produces realistic values. For the reservoir Waduk Sutami for example TSM values are high at the inflow point, very similar to in situ measurements, and gradually decrease going downstream through the reservoir. Modelled values represent the sparsely available in situ measurements very well. When examining river stretches, it can be seen that river edges still show unrealistically high TSM values. Also cloud (edge) and cloud shadow detection is still a problem. Cloud edges result in very high TSM value estimations where - of course - they are not expected to be. Also trees and river banks overgrown by bushes pose challenges to accurately estimate TSM values. When using TOA uncorrected reflectance values from band 7 and model based on match-ups from that information, for the reservoir and broad waterways 1.4 times higher TSM estimates are found, for narrower river stretches this factor goes to 1.7.

ACOLITE seems to be the clear winner if it comes down to which AC processor should be used. When choosing an AC model however, correction of inherent effects like sunglint and adjacency of land pixels should be also assessed. However, ACOLITE does not apply an adjacency correction approach. The processor does need a dark pixel from shadowy land, and thereby land pixels can contribute to the contamination of the measured reflectance value of adjacent water pixels. In situations where large reflectance contrasts occur, the atmospheric backscatter component of the adjacency effect can have significant influence on ground measurements (Richter et al. 2006) and should therefore be taken into account. This is in accordance with Guanter et al. (2007) who state that especially at wavelengths above 700 nm the impact of adjacency effects is strong since neighbouring land pixels show distinctly higher reflectance values. Validity of the results of this study is limited by the absence of using an adjacency correction approach. Also, cloud edge detection in analyzing the satellite imagery is still a challenge. Linking to the adjacency effect, the unrealistically high TSM value estimates at the river banks are most likely caused either by vegetation or by the adjacency effect. Also, these could be actual mixed pixels of land and water. These values are partly neglected and cut out by changing the boundaries set for pixel identification, though this approach limits the usability of narrower river segments.

Limitations found by this study using remotely sensed Sentinel-2 satellite data are limitations due to revisit times in combination with non-usable images due to cloud cover in the rainy season. Also uncertainties are introduced by data processing. For more in-depth statistical analysis and for enhancing models performances, more match-ups are needed between satellite imagery and in situ spectral and laboratory measurements, taken within a short timeframe. Match-ups found by this study were low in numbers due to conducting fieldwork in mainly the rainy season. By better timing and more frequent

sampling, this number could have been increased. Also, atmospheric correction issues limit usefulness of remote sensing data. The applied method of skipping atmospheric correction altogether and using uncorrected TOA L1C data only works for estimating TSM concentrations and will not work for estimating other surface water quality parameters, as TSM concentration is not a ratio (of bands). Altogether, the high (10m) resolution delivered by the Sentinel-2 sensor is a great advantage in narrow river monitoring. However, the critical band for analysing TSM concentrations (band 7) is only available in 20 m resolution. It was shown that where the river only consists of 1 pixel, no realistic values are obtained for TSM estimates. However, if 3 or more pixels are present, reasonably well estimates are derived. This opens great potential for monitoring of river surface water quality on a regional and national scale. This study was a first attempt to test the capabilities of the Sentinel-2 satellite mission for narrow river surface water quality estimation, starting with examining TSM concentrations. The followed approach of linking in situ laboratory measurements, above water radiometric measurements and remote sensed satellite data worked very well. The results on performances of atmospheric correction models may be considered preliminary, since only a handful of match-ups of in situ reflectance data is not enough to validate overall performance of atmospheric correction models. It was shown that in situ spectral measurements are not absolutely necessary for establishing a relationship between satellite derived reflectance values and in situ laboratory measurements, but they are however crucial to validate atmospheric correction models.

6

Conclusions

Data analysis presented in this thesis shows that the Brantas river surface water classifies as an extremely turbid water type. The high turbidity levels and corresponding strong reflectance, mask almost all other water quality signatures. TSM laboratory measurements by gravimetry confirm overall high (>100 mg/L) to extremely high (800 mg/L) TSM concentrations.

Single and multiple band models have not only been tested based on linear and polynomial relations, but also on band ratios. Testing the multi-conditional algorithm on the WISP-3 in situ spectral data shows the model's performance can be expressed as $r^2 = 0.79$ with RMSE = 66.5 mg/L and NRMSE = 9.71%. The model shows comparable good results as found by Novoa et al. (2017). Performance of the multi-conditional algorithm while using a combination of linear and polynomial functions is found to be poor when based on S2 L2A data from bands green, red and red edge NIR. Using only the TSM polynomial model recalibrated and based on S2 L1C data from the red edge NIR band (atmospherically uncorrected data) shows good results ($r^2 = 0.75$, RMSE = 64,2 mg/L and NRMSE = 11,3%). When examining the 10 match-ups which are found and compared with the above water reflectance values, it can be concluded that ACOLITE produces the smallest error (RMSE = 5.0 mg/L), followed by C2RCC (RMSE = 11,3 mg/L) and Sen2Cor (RMSE = 42,8 mg/L).

In situ laboratory measurements offer high accuracy, but are time consuming and labor intensive. Thus, it is not feasible to provide a simultaneous water quality database on a regional scale (Duan, Takara, et al. 2013; Duan, He, et al. 2013). When comparing model data to historical measurements, it becomes apparent that the proposed method from this study gives much more specificity than previous measuring methods and point data collection as until now practised by PJT-1, EPA and BBWS. A strong seasonality effect is observed in the data derived from satellite data, which confirms findings from point sampling in situ measurements with the current measuring frequency (but with long periods of no data in between). Data derived with the proposed method helps place in situ point measurements in their context of long-term water quality monitoring. This reinforces the observation that remotely sensed data can enhance the abilities of water resources managers and decision makers to monitor river systems more effectively, as was also shown by Gholizadeh et al. (2016). Using this technique in near future management decisions fits the intention of the Indonesian Government of scaling-up PJT-I to be a nationwide water resources management body to manage national strategic river basins in the future (Subijanto, Ruritan, and Hidayat 2013).

Using Sentinel-2 data, 5 day estimates are achieved with a spatial resolution of 10-20m, depending on which S2 bands are used. In accordance with Kallio (2000), the results of this study show that with applying remote sensing:

1. Spatial and temporal variation of TSM concentration estimations in the Brantas River system can be made visible;
2. An overview of TSM concentration estimation of the entire basin at one moment in time can be achieved;
3. An extensive historical record of TSM concentration estimations can be accessed, enabling trend analysis;
4. Information is provided to prioritize sampling locations and field surveying times.

Restrictions to usability apply due to - among others - river width (usability sharply decreases with river widths < 40m) , cloud coverage, vegetation along river banks, adjacency effect, atmospheric interference and timeframe of match-ups. Although this study shows that capabilities of remote sensing to assess river surface water quality are undeniable, remote sensing should always be used in combination with traditional sampling methods and field surveying.

7

Perspectives

This section gives an overview of research topics which would enhance or better explain the results found in this study. It is relevant to investigate the influence of the adjacency effects from neighbouring land pixels on the river water pixels, along the river bank. This can be done by investigating variance of TSM concentrations over the width of the cross section. For this study, WISP-3 measurements at 25%, 50% and 75% of all cross sections were taken when going out on field trips. So, the data to investigate the adjacency effect is readily available, but falls outside the scope of, and timeframe for this particular study. Also, it is expected that the magnitude of the adjacency effect differs by land cover type of the surrounding pixels, a hypothesis worthwhile investigating. To investigate further what the effect is of different AC models and to see which one performs best for the task at hand, comparison of corrected images from different platforms would be useful (PlanetScope vs Sentinel-2 for example), using additional AC models like iCOR, l2gen and Polymer.

Commonly, DO, BOD₅ and COD are used as a first indicator of the water quality in the Brantas river. These however, are water quality parameters lacking a distinctive optical signal. Nonetheless, concentrations of non optical variables may be correlated with optical variables, such as Chl-a concentrations, TU, TSM, CDOM and SWT, which do affect the reflected radiation. In this context, an indirect relationship between satellite multispectral data and COD, BOD, and DO can be assumed (Jerry C. Ritchie, Zimba, and Everitt 2003; Kallio 2000). An approach could be to first investigate the relationship between DO and TU / TSM or other in the laboratory data. It must be noted that such an empirical relationship has very limited validity in time, space and sensor used. Even if a perfect relationship could be established empirically, one should be able to determine the indirect parameter and the relationship. Literature (Abayazid, El-Adawy, and Others 2019; El Din and Zhang 2017; Arief 2017) shows quite high correlation between optical and non-optical water quality parameters, but often fails to explain these relationships physically. So, if this approach is followed, and an empirical relationship is found, validity greatly depends on whether this relationship can be physically explained. Without physical explanation, the relationship only holds for the one specific moment in time and space.

Modelled TSM concentration time series show a very clear seasonal trend. Further investigations could focus on the difference in the values from same timeslots of the year. Does the water quality change over time (long term changes)? What are maximum and minimum observed values for different seasons? Do peaks always occur at the same time of the year? If patterns can be modelled, something can be done with predictability. What is the observed period? Is the trend changing e.g. as a result of global warming? In samples from more upstream areas of the Brantas river system a peak around ~700 nm is observed, which might indicate an increase of Chl-a concentration that displaces the peak position in the NIR part (Z. Wang et al. 2017). The Brantas might be a good case to investigate these findings. Lastly, results from models derived by this study can serve as input for rainfall run-off and discharge models. By doing so, sediment transport and erosion from upstream catchments can be evaluated and thereby may be a valuable tool in sediment transport monitoring.

References

- Abayazid, Hala O., Ahmed El-Adawy, and Others. 2019. "Assessment of a Non-Optical Water Quality Property Using Space-Based Imagery in Egyptian Coastal Lake." *Journal of Water Resource and Protection* 11 (06): 713.
- Abram, Nerilie J., Nicky M. Wright, Bethany Ellis, Bronwyn C. Dixon, Jennifer B. Wurtzel, Matthew H. England, Caroline C. Ummenhofer, et al. 2020. "Coupling of Indo-Pacific Climate Variability over the Last Millennium." *Nature* 579 (7799): 385–92.
- Aldrian, Edvin, and Yudha Setiawan Djamil. 2008. "Spatio-Temporal Climatic Change of Rainfall in East Java Indonesia." *International Journal of Climatology: A Journal of the Royal Meteorological Society* 28 (4): 435–48.
- Arief, Muchlisin. 2017. "DEVELOPMENT OF DISSOLVED OXYGEN CONCENTRATION EXTRACTION MODEL USING LANDSAT DATA CASE STUDY: RINGGUNG COASTAL WATERS." *International Journal of Remote Sensing and Earth Sciences (IJReSES)*.
<https://doi.org/10.30536/j.ijreses.2015.v12.a2667>.
- Bhatti, A., D. Rundquist, S. Nasu, and M. Takagi. 2008. "Assessing the Potential of Remotely Sensed Data for Water Quality Monitoring of Coastal and Inland Waters." *Res. Bull. Kochi Univ. Technology* 5.
- Brando, V. E., and A. G. Dekker. 2003. "Satellite Hyperspectral Remote Sensing for Estimating Estuarine and Coastal Water Quality." *IEEE Transactions on Geoscience and Remote Sensing: A Publication of the IEEE Geoscience and Remote Sensing Society* 41 (6): 1378–87.
- Brockmann, Carsten, Roland Doerffer, Marco Peters, Stelzer Kerstin, Sabine Embacher, and Ana Ruescas. 2016. *Evolution of the C2RCC Neural Network for Sentinel 2 and 3 for the Retrieval of Ocean Colour Products in Normal and Extreme Optically Complex Waters*. Vol. 740. Living Planet Symposium.
- Bruijns, A. J. 2018. "Water Treatment of Large-Scale Industry and Chances for the Clean Industry HUB in the Downstream Area of the Brantas River Basin, Indonesia." Utrecht University.
- Chen, Zhiqiang, Chuanmin Hu, and Frank Muller-Karger. 2007. "Monitoring Turbidity in Tampa Bay Using MODIS/Aqua 250-M Imagery." *Remote Sensing of Environment* 109 (2): 207–20.
- Curran, P. J., and E. M. M. Novo. 1988. "The Relationship Between Suspended Sediment Concentration and Remotely Sensed Spectral Radiance: A Review." *Journal of Coastal Research* 4 (3): 351–68.
- Dekker, A. G., and S. W. M. Peters. 1993. "The Use of the Thematic Mapper for the Analysis of Eutrophic Lakes: A Case Study in the Netherlands." *International Journal of Remote Sensing* 14 (5): 799–821.
- Diaz, Robert J., and Rutger Rosenberg. 2008. "Spreading Dead Zones and Consequences for Marine Ecosystems." *Science* 321 (5891): 926–29.
- Duan, Weili, Bin He, Kaoru Takara, Pingping Luo, Daniel Nover, Netrananda Sahu, and Yosuke Yamashiki. 2013. "Spatiotemporal Evaluation of Water Quality Incidents in Japan between 1996 and 2007." *Chemosphere* 93 (6): 946–53.
- Duan, Weili, Kaoru Takara, Bin He, Pingping Luo, Daniel Nover, and Yosuke Yamashiki. 2013. "Spatial and Temporal Trends in Estimates of Nutrient and Suspended Sediment Loads in the Ishikari River, Japan, 1985 to 2010." *The Science of the Total Environment* 461-462 (September): 499–508.
- El Din, Essam Sharaf, and Yun Zhang. 2017. "Estimation of Both Optical and Nonoptical Surface Water Quality Parameters Using Landsat 8 OLI Imagery and Statistical Techniques." *Journal of Applied Remote Sensing* 11 (4): 046008.
- Ertsen, Maurits, Daru Setyorini, Christa Nooy, Martin van Beusekom, Floris Boogaard, Prigi Arisandi, and Jan-Willem Knegt. 2018. "Mainstreaming Water Quality in River Basin Management in the Brantas River Basin, Indonesia: Abstract Submitted to the International

- Conference Water Science for Impact." In *International Conference Water Science for Impact*. <https://research.hanze.nl/en/publications/mainstreaming-water-quality-in-river-basin-management-in-the-bran>.
- Espinoza-Villar, Raul, Jean-Michel Martinez, Elisa Armijos, Jhan-Carlo Espinoza, Naziano Filizola, Andre Dos Santos, Bram Willems, Pascal Fraizy, William Santini, and Philippe Vauchel. 2018. "Spatio-Temporal Monitoring of Suspended Sediments in the Solimões River (2000–2014)." *Comptes Rendus Geoscience*. <https://doi.org/10.1016/j.crte.2017.05.001>.
- European Space Agency. n.d. "Sentinel-2 - Missions - Sentinel Online." ESA Sentinel Online. Accessed June 24, 2020. <https://sentinel.esa.int/web/sentinel/missions/sentinel-2>.
- Filipponi, Federico. 2018. "River Color Monitoring Using Optical Satellite Data." *Proceedings: A Conference of the American Medical Informatics Association / ... AMIA Annual Fall Symposium. AMIA Fall Symposium 2* (10): 569.
- Fulazzaky, Mohamad Ali. 2009. "Water Quality Evaluation System to Assess the Brantas River Water." *Water Resources Management* 23 (14): 3019.
- Gao, Bo-Cai, Marcos J. Montes, Curtiss O. Davis, and Alexander F. H. Goetz. 2009. "Atmospheric Correction Algorithms for Hyperspectral Remote Sensing Data of Land and Ocean." *Remote Sensing of Environment* 113 (September): S17–24.
- Gernez, Pierre, Virginie Lafon, Astrid Lerouxel, Cécile Curti, Bertrand Lubac, Sylvain Cerisier, and Laurent Barillé. 2015. "Toward Sentinel-2 High Resolution Remote Sensing of Suspended Particulate Matter in Very Turbid Waters: SPOT4 (Take5) Experiment in the Loire and Gironde Estuaries." *Remote Sensing* 7 (8): 9507–28.
- Gholizadeh, Mohammad Haji, Assefa M. Melesse, and Lakshmi Reddi. 2016. "A Comprehensive Review on Water Quality Parameters Estimation Using Remote Sensing Techniques." *Sensors* 16 (8). <https://doi.org/10.3390/s16081298>.
- Gorelick, Noel, Matt Hancher, Mike Dixon, Simon Ilyushchenko, David Thau, and Rebecca Moore. 2017. "Google Earth Engine: Planetary-Scale Geospatial Analysis for Everyone." *Remote Sensing of Environment* 202 (December): 18–27.
- Guanter, L., M. Del Carmen González-Sanpedro, and J. Moreno. 2007. "A Method for the Atmospheric Correction of ENVISAT/MERIS Data over Land Targets." *International Journal of Remote Sensing*. <https://doi.org/10.1080/01431160600815525>.
- Hagolle, O., M. Huc, D. Villa Pascual, and G. Dedieu. 2010. "A Multi-Temporal Method for Cloud Detection, Applied to FORMOSAT-2, VENUS, LANDSAT and SENTINEL-2 Images." *Remote Sensing of Environment* 114 (8): 1747–55.
- Hellweger, F. L., P. Schlosser, U. Lall, and J. K. Weissel. 2004. "Use of Satellite Imagery for Water Quality Studies in New York Harbor." *Estuarine, Coastal and Shelf Science*. <https://doi.org/10.1016/j.ecss.2004.06.019>.
- Hollstein, André, Karl Segl, Luis Guanter, Maximilian Brell, and Marta Enesco. 2016. "Ready-to-Use Methods for the Detection of Clouds, Cirrus, Snow, Shadow, Water and Clear Sky Pixels in Sentinel-2 MSI Images." *Remote Sensing* 8 (8): 666.
- Jerlov, N. G. 1976. *Marine Optics*. Elsevier.
- Kallio, Kari. 2000. "Remote Sensing as a Tool for Monitoring Lake Water Quality." *Hydrological and Limnological Aspects of Lake Monitoring* 14: 237.
- Kaufman, Yoram J., and Claudia Sendra. 1988. "Algorithm for Automatic Atmospheric Corrections to Visible and near-IR Satellite Imagery." *International Journal of Remote Sensing* 9 (8): 1357–81.
- Kirk, J. T. 1983. "Light and Photosynthesis in Aquatic Ecosystems." *Cambridge Univ. Press. England*.
- Lee, Han. 2015. "General Rainfall Patterns in Indonesia and the Potential Impacts of Local Seas on Rainfall Intensity." *Water*. <https://doi.org/10.3390/w7041751>.
- Liu, Can-de, Bao-Yin He, Mao-Tian Li, and Xian-You Ren. 2006. "Quantitative Modeling of Suspended Sediment in Middle Changjiang River from Modis." *Chinese Geographical Science*

- / Sponsored by Changchun Institute of Geography, Chinese Academy of Sciences 16 (1): 79–82.
- Ma Jianwen, Li Xiaowen, Chen Xue, and Feng Chun. 2006. "Target Adjacency Effect Estimation Using Ground Spectrum Measurement and Landsat-5 Satellite Data." *IEEE Transactions on Geoscience and Remote Sensing: A Publication of the IEEE Geoscience and Remote Sensing Society* 44 (3): 729–35.
- Mangiarotti, S., J-M Martinez, M-P Bonnet, D. C. Buarque, N. Filizola, and P. Mazzega. 2013. "Discharge and Suspended Sediment Flux Estimated along the Mainstream of the Amazon and the Madeira Rivers (from in Situ and MODIS Satellite Data)." *International Journal of Applied Earth Observation and Geoinformation* 21 (April): 341–55.
- Mobley, C. D. 1999. "Estimation of the Remote-Sensing Reflectance from above-Surface Measurements." *Applied Optics* 38 (36): 7442–55.
- Moses, Wesley J., Sindy Sterckx, Marcos J. Montes, Liesbeth De Keukelaere, and Els Knaeps. 2017. "Atmospheric Correction for Inland Waters." *Bio-Optical Modeling and Remote Sensing of Inland Waters*. <https://doi.org/10.1016/b978-0-12-804644-9.00003-3>.
- Muller-Wilm, Uwe, Jerome Louis, Rudolf Richter, Ferran Gascon, and Marc Niezette. 2013. "Sentinel-2 Level 2A Prototype Processor: Architecture, Algorithms and First Results." In *Proceedings of the ESA Living Planet Symposium, Edinburgh, UK*, 9–13.
- Novoa, Stéfani, David Doxaran, Anouck Ody, Quinten Vanhellemont, Virginie Lafon, Bertrand Lubac, and Pierre Gernez. 2017. "Atmospheric Corrections and Multi-Conditional Algorithm for Multi-Sensor Remote Sensing of Suspended Particulate Matter in Low-to-High Turbidity Levels Coastal Waters." *Remote Sensing* 9 (1): 61.
- Onderka, Milan. 2008. "Remote Sensing and Identification of Places Susceptible to Sedimentation in the Danube River." *Available Online: Citeseerx. Ist. Psu. Edu/viewdoc/download*. <http://citeseerx.ist.psu.edu/viewdoc/download?doi=10.1.1.537.9539&rep=rep1&type=pdf>.
- Ouaidrari, Hassan, and Eric F. Vermote. 1999. "Operational Atmospheric Correction of Landsat TM Data." *Remote Sensing of Environment* 70 (1): 4–15.
- Oxford, M. S. 1976. "Remote Sensing of Suspended Sediments in Surface Waters." *Photogrammetric Engineering and Remote Sensing* 42: 1539–45.
- Pereira-Sandoval, Marcela, Ana Ruescas, Patricia Urrego, Antonio Ruiz-Verdú, Jesús Delegido, Carolina Tenjo, Xavier Soria-Perpinyà, Eduardo Vicente, Juan Soria, and José Moreno. 2019. "Evaluation of Atmospheric Correction Algorithms over Spanish Inland Waters for Sentinel-2 Multi Spectral Imagery Data." *Remote Sensing* 11 (12): 1469.
- Peters, S., and M. Laanen. n.d. "How to - Manual Atmospheric Correction of Sentinel-2 Based on a WISP-3 Measurement." Water Insight B.V. the Netherlands.
- . n.d. "WISP-3 User Guide." Water Insight B.V. The Netherlands.
- PJT-I Public Corporation. 2003. "Integrated Water Resources Development and Management in a River Basin Context: The Brantas Basin Experience, a Brantas River Basin Management Agency Report." Third World Water Forum, Kyoto, Japan. Perum Jasa Tirta I.
- . 2005. "Water Allocation In The Brantas River Basin In The Brantas River Basin", Published as Member of Network of Asian River Basin Organizations (NARBO)." Perum Jasa Tirta I.
- Pontius, Robert Gilmore, Olufunmilayo Thontteh, and Hao Chen. 2008. "Components of Information for Multiple Resolution Comparison between Maps That Share a Real Variable." *Environmental and Ecological Statistics* 15 (2): 111–42.
- Rabalais, Nancy N. 2002. "Nitrogen in Aquatic Ecosystems." *Ambio* 31 (2): 102–12.
- Richter, R., M. Bachmann, W. Dorigo, and A. Muller. 2006. "Influence of the Adjacency Effect on Ground Reflectance Measurements." *IEEE Geoscience and Remote Sensing Letters* 3 (4): 565–69.
- Rijkeboer, M. 2000. "Algoritmen Voor Het Bepalen van de Concentratie Chlorofyl-a En Zwevend Stof Met de Optische Teledetectie Methode in Verschillende Optische Watertypen." <https://research.vu.nl/en/publications/algoritmen-voor-het-bepalen-van-de-concentratie->

chlorofyl-a-en-zw.

- Ritchie, J. C., and C. M. Cooper. 1991. "An Algorithm for Using Landsat MSS for Estimating Surface Suspended Sediments." *Water Resources Bulletin* 27: 373–79.
- Ritchie, J. C., J. R. McHenry, F. R. Schiebe, and R. B. Wilson. 1975. "Relationship of Reflected Solar Radiation and the Concentration of Sediment in the Surface Water of Reservoirs." *Remote Sensing of Earth Resources* 1975, 3.
<http://agris.fao.org/agris-search/search.do?recordID=US201302992863>.
- Ritchie, Jerry C., Charles M. Cooper, and Frank R. Schiebe. 1990. "The Relationship of MSS and TM Digital Data with Suspended Sediments, Chlorophyll, and Temperature in Moon Lake, Mississippi." *Remote Sensing of Environment* 33 (2): 137–48.
- Ritchie, Jerry C., Paul V. Zimba, and James H. Everitt. 2003. "Remote Sensing Techniques to Assess Water Quality." *Photogrammetric Engineering & Remote Sensing* 69 (6): 695–704.
- Roosmini, D., M. A. Septiono, N. E. Putri, H. M. Shabrina, I. R. S. Salami, and H. D. Ariesyady. 2018. "River Water Pollution Condition in Upper Part of Brantas River and Bengawan Solo River." *IOP Conference Series: Earth and Environmental Science* 106 (1): 012059.
- Santos, Andre Luis Martinelli Real dos, Andre Luis Martinelli Real dos Santos, Jean Michel Martinez, Naziano Pantoja Filizola, Elisa Armijos, and Luna Gripp Simões Alves. 2018. "Purus River Suspended Sediment Variability and Contributions to the Amazon River from Satellite Data (2000–2015)." *Comptes Rendus Geoscience*.
<https://doi.org/10.1016/j.crte.2017.05.004>.
- "Sen2Cor Configuration and User Manual." 2017. European Space Agency.
- Shafique, Naseer A., Florence Fulk, Bradley C. Autrey, Joseph Flotemersch, and Others. 2003. "Hyperspectral Remote Sensing of Water Quality Parameters for Large Rivers in the Ohio River Basin." In *First Interagency Conference on Research in the Watershed, Benson, AZ*, 216–21. Citeseer.
- Simis, Stefan G. H., and John Olsson. 2013. "Unattended Processing of Shipborne Hyperspectral Reflectance Measurements." *Remote Sensing of Environment* 135 (August): 202–12.
- Sterckx, Sindy, Els Knaeps, Stefan Adriaensen, Ils Reusen, Liesbeth De Keukelaere, Peter Hunter, Claudia Giardino, and Daniel Odermatt. 2015. "OPERA: An Atmospheric Correction for Land and Water." In *Proceedings of the Sentinel-3 for Science Workshop*, 1:3–6.
- Subijanto, Tjoek Walujo, Raymond Valiant Ruritan Harianto, and Fahmi Hidayat. 2013. "Key Success Factors for Capacity Development in the Brantas River Basin Organisations in Indonesia." *Water Policy* 15 (S2): 183–205.
- Sudheer, K. P., Indrajeet Chaubey, and Vijay Garg. 2006. "Lake Water Quality Assessment from Landsat Thematic Mapper Data Using Neural Network: An Approach to Optimal Band Combination selection1." *JAWRA Journal of the American Water Resources Association* 42 (6): 1683–95.
- Suhanti, Indah Yasminum. n.d. "Evaluation on Adult Behavior of Diaper Disposal Into The River in Surabaya and Sidoarjo, East Java." In *4th International Conference on Public Health 2018*, 153–153. Sebelas Maret University.
- Toming, Kaire, Tiit Kutser, Alo Laas, Margot Sepp, Birgot Paavel, and Tiina Nõges. 2016. "First Experiences in Mapping Lake Water Quality Parameters with Sentinel-2 MSI Imagery." *Remote Sensing* 8 (8): 640.
- Tomsett, Christopher, and Julian Leyland. 2019. "Remote Sensing of River Corridors: A Review of Current Trends and Future Directions." *River Research and Applications* 35 (7): 779–803.
- Turner, R. E., N. N. Rabalais, D. Justic, and Q. Dortch. 2003. "Global Patterns of Dissolved N, P and Si in Large Rivers." *Biogeochemistry* 64 (3): 297–317.
- Umar, M., Bruce L. Rhoads, and Jonathan A. Greenberg. 2018. "Use of Multispectral Satellite Remote Sensing to Assess Mixing of Suspended Sediment Downstream of Large River Confluences." *Journal of Hydrology* 556 (January): 325–38.
- Usali, N., and M. H. Ismail. 2010. "Use of Remote Sensing and GIS in Monitoring Water Quality."

- Journal of Sustainable Development in Africa.*
<https://www.academia.edu/download/55602042/7338-22891-1-PB.pdf>.
- Vanhellemont, Quinten, and Kevin Ruddick. 2015. "Advantages of High Quality SWIR Bands for Ocean Colour Processing: Examples from Landsat-8." *Remote Sensing of Environment* 161 (May): 89–106.
- . 2018. "Atmospheric Correction of Metre-Scale Optical Satellite Data for Inland and Coastal Water Applications." *Remote Sensing of Environment* 216 (October): 586–97.
- Wang, F., L. Han, H. -T Kung, and R. B. Van Arsdale. 2006. "Applications of Landsat-5 TM Imagery in Assessing and Mapping Water Quality in Reelfoot Lake, Tennessee." *International Journal of Remote Sensing* 27 (23): 5269–83.
- Wang, Jian-Jun, Xi Xi Lu, Soo Chin Liew, and Yue Zhou. 2009. "Retrieval of Suspended Sediment Concentrations in Large Turbid Rivers Using Landsat ETM : An Example from the Yangtze River, China." *Earth Surface Processes and Landforms*. <https://doi.org/10.1002/esp.1795>.
- Wang, J-J, and X. X. Lu. 2010. "Estimation of Suspended Sediment Concentrations Using Terra MODIS: An Example from the Lower Yangtze River, China." *The Science of the Total Environment* 408 (5): 1131–38.
- Wang, Zuomin, Kensuke Kawamura, Yuji Sakuno, Xinyan Fan, Zhe Gong, and Jihyun Lim. 2017. "Retrieval of Chlorophyll-a and Total Suspended Solids Using Iterative Stepwise Elimination Partial Least Squares (ISE-PLS) Regression Based on Field Hyperspectral Measurements in Irrigation Ponds in Higashihiroshima, Japan." *Remote Sensing*. <https://doi.org/10.3390/rs9030264>.
- Warren, M. A., S. G. H. Simis, V. Martinez-Vicente, K. Poser, M. Bresciani, K. Alikas, E. Spyarakos, C. Giardino, and A. Ansper. 2019. "Assessment of Atmospheric Correction Algorithms for the Sentinel-2A MultiSpectral Imager over Coastal and Inland Waters." *Remote Sensing of Environment* 225 (May): 267–89.
- Willmott, C. J., and K. Matsuura. 2006. "On the Use of Dimensioned Measures of Error to Evaluate the Performance of Spatial Interpolators." *International Journal of Geographical Information Science: IJGIS* 20 (1): 89–102.
- Wu, Guangyu. 2003. "Seasonal Change Detection of Water Quality in Texas Gulf Coast Using MODIS Remote Sensing Data." *UC GIS Summer Assembly*.

Appendix A: Effect of fingerprinting algorithm on WISP-3 in situ spectra

Rrs values of 27 WISP-3 measurements corresponding to analysed lab samples

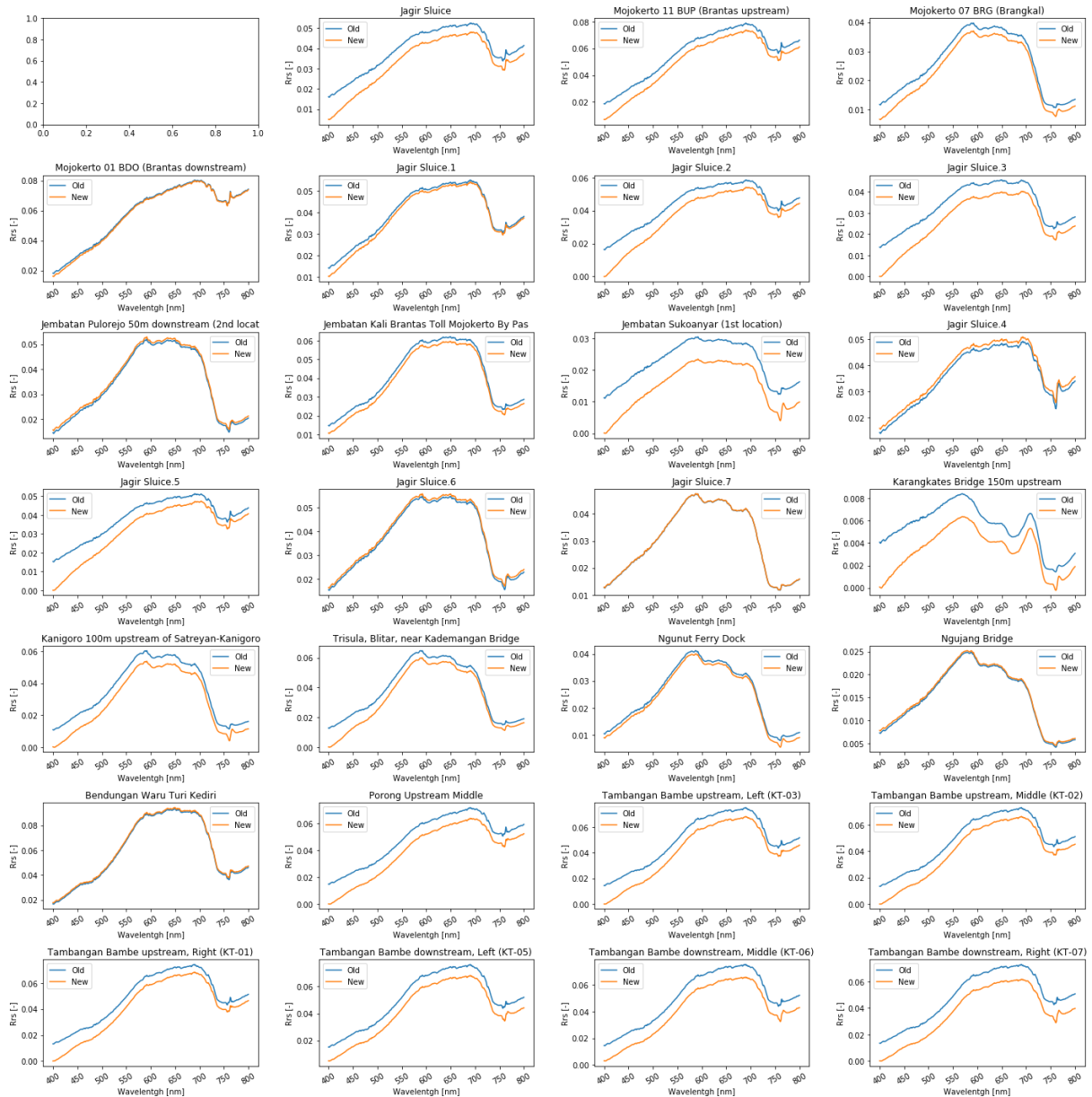


Figure 47: Subplots showing all 27 matched up WISP-3 measurements after recalibration and which are matched to laboratory analysed water samples. Blue lines show the R_{rs} values before fingerprinting (based on a constant sky correction factor), the orange lines show the R_{rs} values after fingerprinting (based on measurement unique sky correction factors). The plots nicely show the overall extremely turbid water type (high reflectance values > 750 nm), but also variation where the reflectance values are high in the blue and red region, but low at higher wavelengths. These samples are taken more upstream in the basin, where water is clearer.

Appendix B: Built-in algorithms WISP-3 compared to laboratory results TSM concentrations

At first, as a first try, known relationships from literature were used– based on data and circumstances from the Brantas region – to relate TSM concentrations and lab results. The same relationship was used to tune the parameters according to data from this research. The resulting models performed quite poorly. I looked into $\log_{10}(\text{Sentinel-2}_{\text{Red Band}})$, $\log_{10}(\frac{\text{Sentinel-2}_{\text{Blue Band}}}{\text{Sentinel-2}_{\text{Red Band}}})$ and $\ln(\frac{\text{Sentinel-2}_{\text{Blue Band}}}{\text{Sentinel-2}_{\text{Green Band}}})$. Based on those results I could say there is a relationship, especially for lower and higher TSM concentrations, but the deviation was great for lab values > 220 mg / L. The same trends could be seen for all linear relationships (single band, band ratios).

Firstly, calculated TSM concentrations according to Rijkeboer (2000) his algorithms were modelled. She developed algorithms for several water types:

- Water type 1: eutrophic small peat pools
- Water Type 3: Dutch canals called ‘boezemwateren’
- Water type 4: eutrophic large peat pools
- Water type 5: silt-rich rivers and silt-rich large shallow lakes
- Water type 6: deep clear lakes and tidal waters

The WISP-3 built-in algorithm is based on water type 6.

The graphs below in figure 48 firstly show how extremely turbid the water can be, with TSM concentrations up to almost 900 mg/L. Results from the Rijkeboer (2000) and WISP-3 algorithm reach their maximum detection limit, resulting in significant underestimation of TSM concentrations.

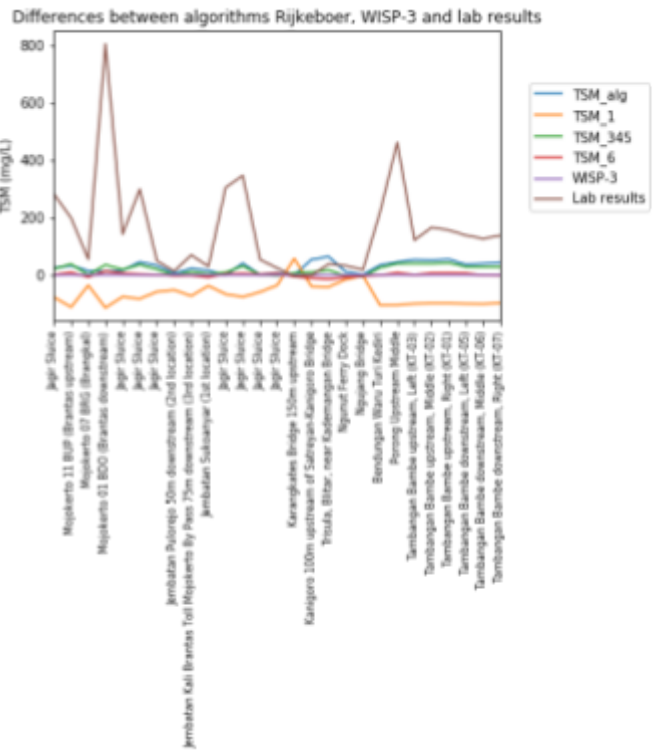
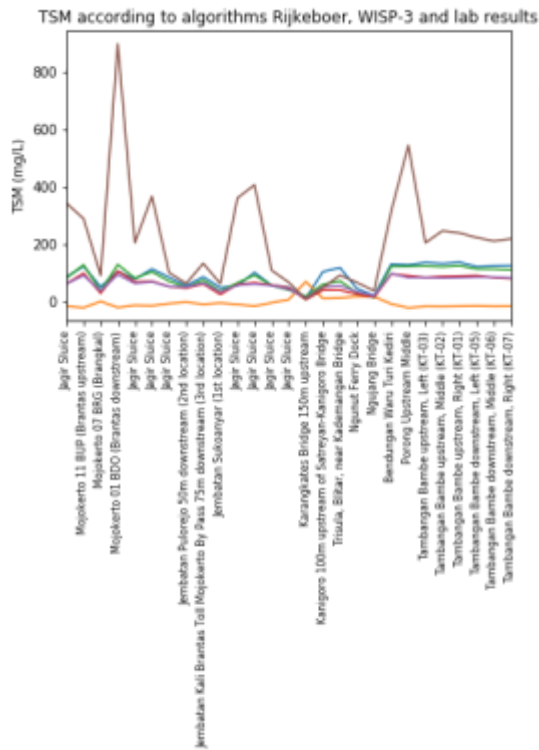


Figure 48: The figure on the left shows TSM concentrations according to lab results and calculated using Rijkeboer (2000) algorithms. Also, the WISP-3 results are shown from the built-in algorithm, which is an adopted version of Rijkeboer’s water type 6 model. The lab results show how extremely high TSM concentrations can get (up to almost 900 mg/L). It is clearly visible that the Rijkeboer and the WISP-3 algorithm reach their maximum detection limit. The figure on the right shows differences from TSM concentrations according to lab results and calculated using Rijkeboer (2000) algorithms.

Appendix C: Comparing results of single and multiple band algorithms based on WISP data and laboratory results

Simple (single) linear regression for all bands WISP and lab results

For extremely turbid waters it makes sense to look at the elevated signal >750 nm, especially around 800 nm. Water absorption decreases between 770 and 860 nm with the lowest absorption coefficient at ~810nm. Therefore, one can notice easily if there is any other parameter present (such as sediment, phytoplankton, dissolved organic matter or benthic plant at the bottom). These parameters will backscatter the light signal and create a higher peak ~810 nm (except the WISP-3 does not extend beyond 800nm).

Linear regression is performed on all 401 bands of the WISP-3 measurements matched with lab results. The goodness-of-fit is assessed from the regression model simply by looking at r^2 values and calculating NRMSE (%). In general, 65% of the samples are used to train the model, and the remaining 35% of samples to test the model. Figure 8 shows r^2 values from linear regression of all 401 WISP-3 bands and lab results, figure 51 and figure 49 show zoomed in details of figure 50.

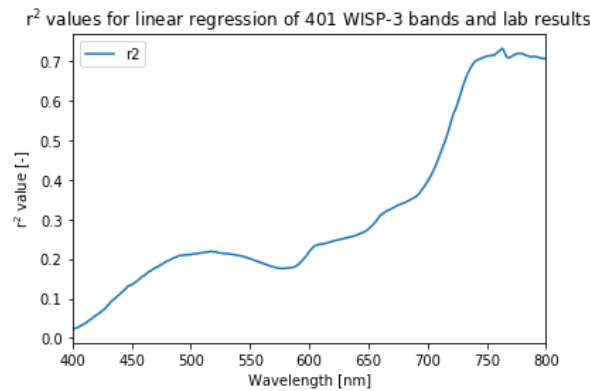


Figure 50: r^2 values after linear regression for all separate 401 bands from the WISP-3 measurements. It shows that reflectance values in the blue and green bands have a low correlation. Correlation increases in the red region and is highest for the bands above 740 nm.

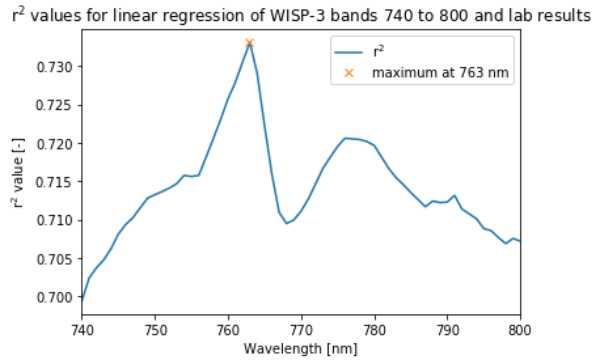


Figure 51: zoomed in detail of figure 50. Absorption by oxygen and ozone in the atmosphere dominates the visible part of the spectrum. The peak at 763 nm is caused by absorption of O_2 . In general, the region around 760 - 770 nm is highly influenced by interference from the atmosphere, there is a lot happening at the same time. Therefore, I will focus on the section beyond the atmospheric absorption dip of 770 nm. At all times, I want to avoid absorption dips which can be seen on all channels.

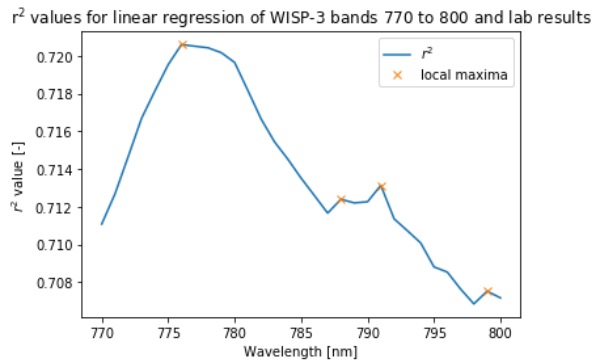


Figure 52: zoomed in part of figure 50 and figure 51, showing r^2 values from linear regression of bands 770 - 800 nm with lab results. The orange x's show the local maxima. Corresponding r^2 values are shown in table 11.

Table 11: WISP-3 bands and their corresponding r^2 values from linear regression with lab results, graphically shown in figure 52.

	Wavelength [nm]	r^2
1	776	0.72
2	791	0.71
3	788	0.71
4	799	0.70

Multiple linear regression for all WISP bands and lab results

To check whether a combination of 2 bands algorithm performs better than a 1 band algorithm, all uniquely possible combinations of two of the 401 WISP-3 bands are tested with multiple linear regression analysis. The resulting r^2 values are plotted and shown in figure 53, ranging from high to low correlation.

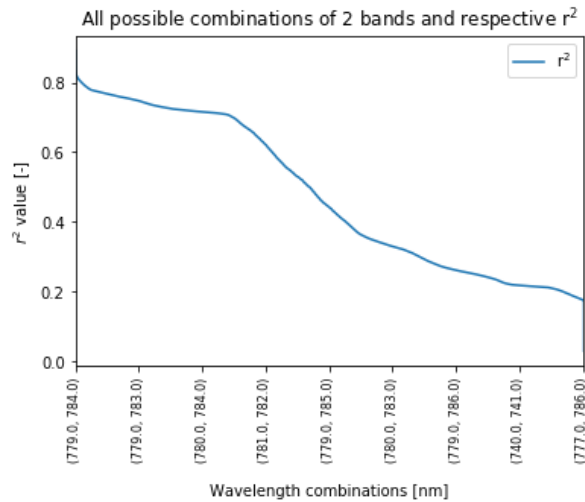


Figure 53: r^2 values from linear regression for all unique combinations of the 401 bands from the WISP-3 measurements. Generally, combinations of higher wavelengths show higher r^2 values.

The combination of the 779 and 784 nm bands result in the highest r^2 value of 0.89. This band combination gives the following algorithm:

$$TSM \left(\frac{mg}{L} \right) = 101200 * R(0-)_{779} - 98800 * R(0-)_{784} + 88.69$$

When combining bands with highest r^2 value resulting from single linear regression, the combination of 776 and 788 nm gives the highest r^2 value (0.81). This results in the following algorithm:

$$TSM \left(\frac{mg}{L} \right) = 37140 * R(0-)_{776} - 34540 * R(0-)_{788} + 53.40$$

TSM algorithms applied to set of 27 matched up measurements corresponding to lab samples Based on WISP-3 bands

Figure 54 shows plots of the TSM concentrations calculated by 1 and 2 WISP-3 band algorithms, plotted against TSM concentrations as calculated by Rijkeboer and from lab analysis. Both models perform relatively well. The 2-band algorithm performs slightly better in predicting the high peaks in TSM concentrations. Figure 55 shows the differences in TSM concentrations between calculated values by the single and multiple WISP-3 band algorithms, the Rijkeboer algorithm and lab results. The 2-band algorithm clearly performs best.

TSM according to single and multiple WISP-3 bands algorithms, Rijkeboer and lab results

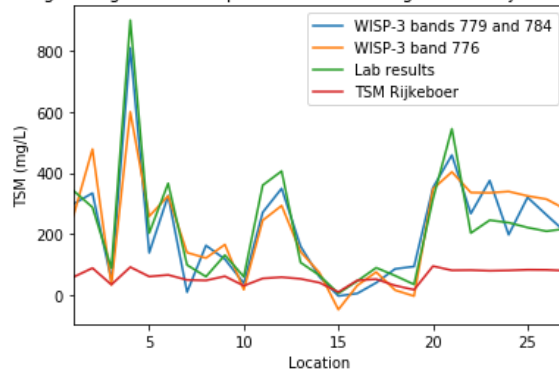


Figure 54: TSM concentrations calculated by 1 and 2 WISP-3 band algorithms, plotted against TSM concentrations as calculated by Rijkeboer and from lab analysis. Both models perform relatively well. The 2-band algorithm performs slightly better in predicting the high peaks in TSM concentrations.

Differences between algorithms single and multiple WISP-3 bands, Rijkeboer and lab results

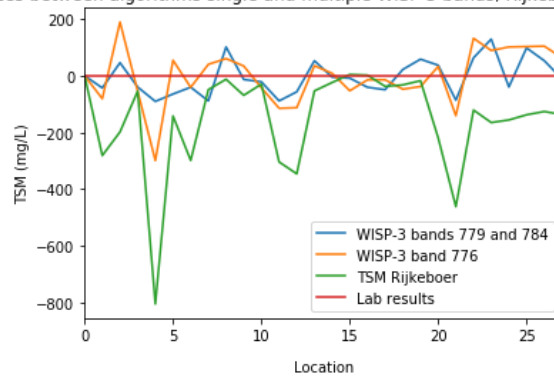


Figure 55: Differences in TSM concentrations between calculated values by the single and multiple WISP-3 band algorithms, the Rijkeboer algorithm on the one hand and the lab results on the other. The 2-band algorithm clearly performs best.

To summarise, table 12 below shows r^2 values for the 2 and 1 WISP-3 band algorithm, Rijkeboer’s water type 6 algorithm and the lab results.

Table 12: r^2 values for the 2 and 1 WISP-3 band algorithm, Rijkeboer’s algorithm and the lab results

	WISP-3 bands 779 and 784	WISP-3 band 776	TSM Rijkeboer	Lab results
r²	0.89	0.72	0.42	1.0

Appendix D: Comparing results of single and multiple band algorithms based on Sentinel-2 simulated data and laboratory results

Simple (single) linear regression for all bands Sentinel-2 bands and lab results

All bands 1-7 from S2 are simulated by averaging high resolution WISP-3 data. When looking at TSM concentrations as measured in laboratories, plotted against Rrs values corresponding to Sentinel-2 bands 1, 2 (blue) and 3 (green), no clear relationship can be detected as can be seen from figure 56.

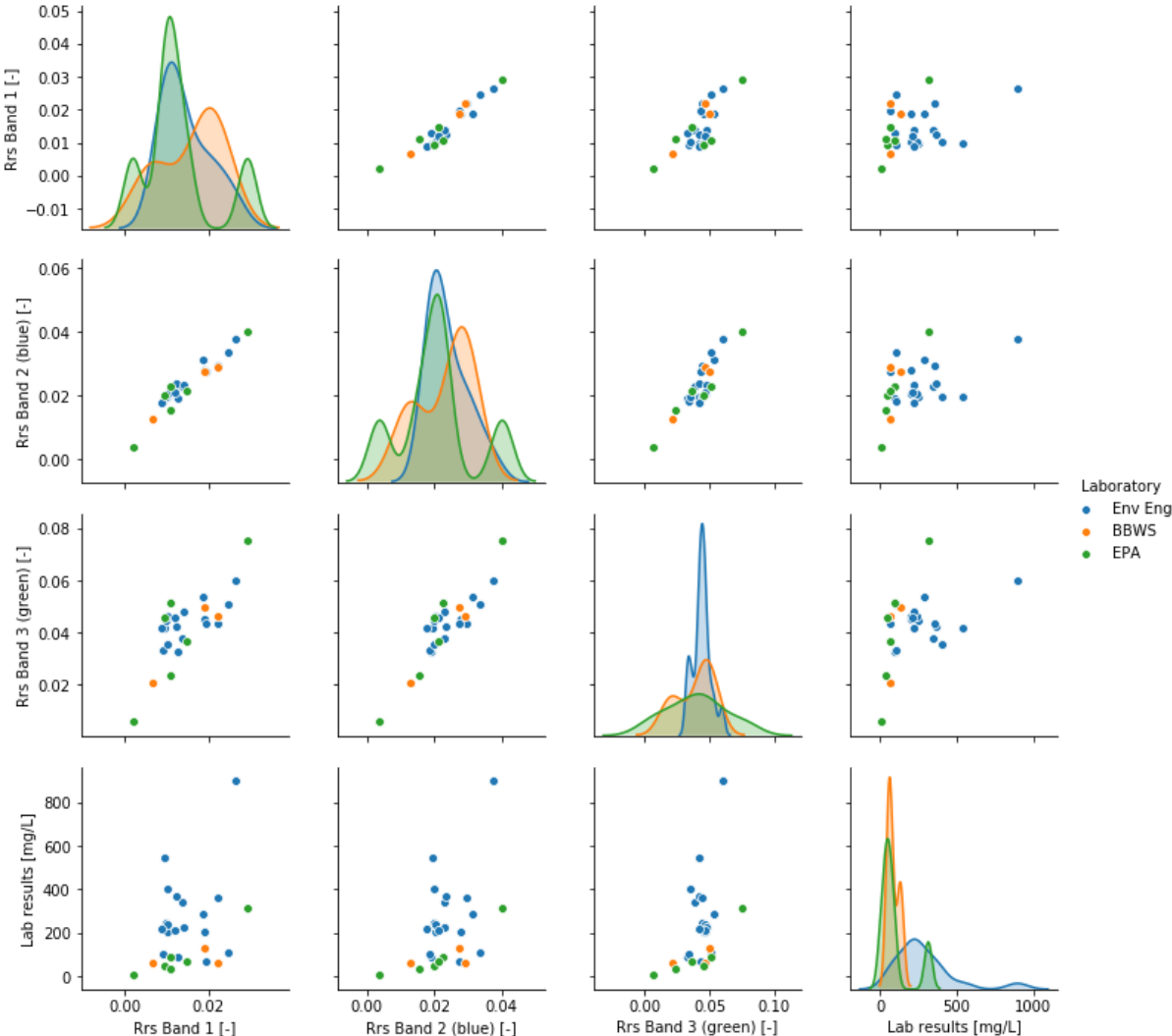


Figure 56: Pair plots showing lab results against Rrs values derived from WISP-3 measurements corresponding to Sentinel-2 bands 1, 2 (blue) and 3 (green). No clear relationship can be detected.

When looking at TSM concentrations as measured in laboratories, plotted against R_{rs} values corresponding to Sentinel-2 bands 4 (red), 5 (central wavelength 704 nm), 6 (central wavelength 741 nm) and 7 (central wavelength 783 nm), a possible linear relationship can be seen, especially for the bands with higher wavelengths. Table 13 below shows r^2 values when linear regression is applied on these relationships.

Table 13: This table show r_2 values when simple linear regression is applied on bands 1 to 7 from the Sentinel-2 mission

	Rrs Band 1	Rrs Band 2 (blue)	Rrs Band 3 (green)	Rrs Band 4 (red)	Rrs Band 5	Rrs Band 6	Rrs Band 7	Lab results [mg/L]
r^2	0.118	0.203	0.19	0.316	0.425	0.692	0.716	1.0

Linear regression with band 7 gives the highest r^2 value. Using Sentinel-2_{Band 7} remote sensing reflectance values from band 7 to predict the laboratory measurements results in the following algorithm:

$$TSM \left(\frac{mg}{L} \right) = 10720 * R_{rs}(Band 7) - 95.50$$

Multiple linear regression for all bands Sentinel-2 bands and lab results

Also, all possible unique combinations of Sentinel-2 bands are tested to predict TSM concentrations. This results in r^2 values from which the top 10 are as shown in table 14 below.

Table 14: This table show r_2 values when multiple linear regression is applied on all unique combinations of 2 of the bands 1 to 7 from the Sentinel-2 mission

Combination	r^2
1 (Band_5, Band_7)	0.78
2 (Band_5, Band_6)	0.77
3 (Band_6, Band_7)	0.77
4 (Band_4_red, Band_7)	0.77
5 (Band_4_red, Band_6)	0.76
6 (Band_3_green, Band_7)	0.73
7 (Band_1, Band_7)	0.72
8 (Band_2_blue, Band_7)	0.72
9 (Band_3_green, Band_6)	0.71
10 (Band_1, Band_6)	0.69

The best performing combination of Band 5 and Band 7 result in the following algorithm:

$$TSM \left(\frac{mg}{L} \right) = 19280 * R_{rs}(Band 7) - 10310 * R_{rs}(Band 5) + 171.33$$

TSM algorithms applied to 27 measurements corresponding to lab samples Based on Sentinel-2 bands

Figure 57 shows plots of the TSM concentrations calculated by algorithms using the Sentinel-2 bands, as well as the 1 as 2 parameter models, plotted against TSM concentrations as calculated by Rijkeboer and from lab analysis. The 2-band algorithms perform slightly better in predicting the high peaks in TSM concentrations. Figure 58 shows TSM concentrations between calculated values by the single and the best performing multiple Sentinel-2 algorithms, as well as the lab results.

Figure 59 shows the differences in TSM concentrations between calculated values by the single and the best performing multiple Sentinel-2 algorithms, the Rijkeboer algorithm and lab results. The 2-band algorithm only performs slightly better.

TSM according to algorithms Sentinel-2 bands, Rijkeboer and lab results

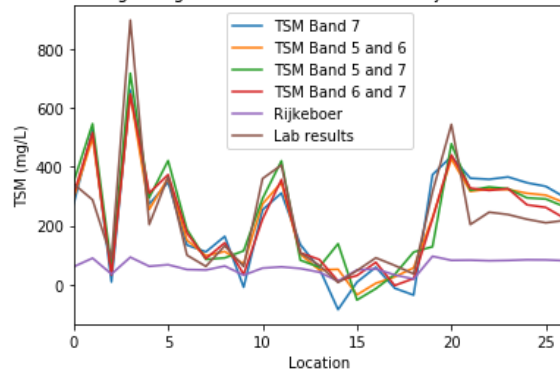


Figure 57: TSM concentrations calculated by 1 and 2 Sentinel-2 band algorithms, plotted against TSM concentrations as calculated by Rijkeboer and from lab analysis. The 2-band algorithm performs slightly better in predicting the high peaks in TSM concentrations.

TSM according to single and multiple band algorithms Sentinel-2 and lab results

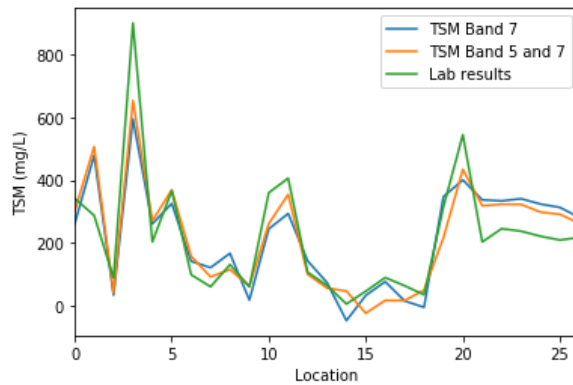


Figure 58: The 1 and 2-band algorithm seem to equally well perform.

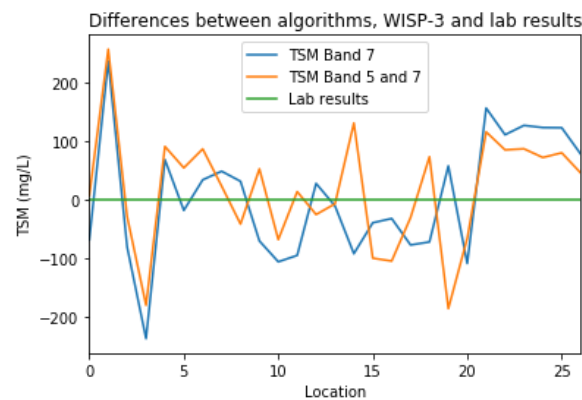


Figure 59: Differences in TSM concentrations between calculated values by the single and multiple Sentinel-2 band algorithms, the Rijkeboer algorithm and lab results. The 2-band algorithm seems to perform slightly better. To summarize, all relevant r^2 values are shown in table 15.

Table 15: r^2 values for the 2 and 1 Sentinel-2 band algorithms, Rijkeboer's algorithm and the lab results

	TSM Band 7	TSM Band 5 and 6	TSM Band 5 and 7	TSM Band 6 and 7	Rijkeboer	Lab results
r^2	0.72	0.77	0.78	0.77	0.42	1.0

Appendix E: Inter-comparison of TSM algorithms based on single and multiple WISP-3 and Sentinel-2 bands

TSM based on single band WISP-3 and Sentinel-2 inter-comparison

To conclude this chapter, the single band WISP-3 and Sentinel-2 are compared, as well as the multiple band algorithms. Figure 60 shows pair plots of single band WISP-3_{776 nm} and Sentinel-2_{Band 7} algorithms compared to lab results. Figure 60 shows graphs depicting the TSM concentrations as calculated by the single band WISP-3_{776 nm} and Sentinel-2_{Band 7} algorithms, compared to lab results. Figure 62 graphically shows the differences calculated from TSM concentrations as calculated by the aforementioned algorithms.

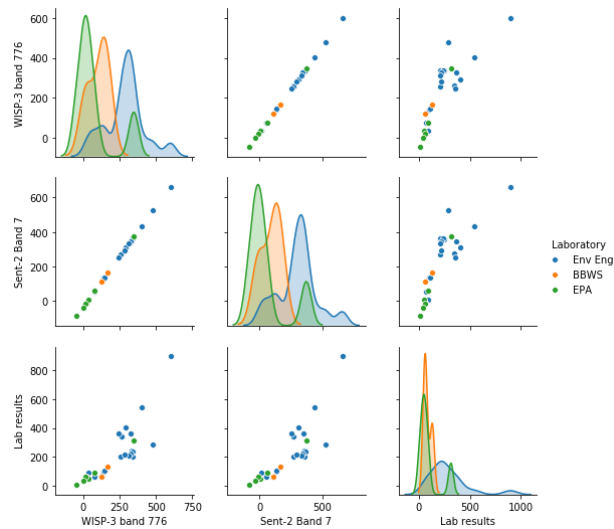


Figure 60: pair plots of single band WISP-3_{776 nm} and Sentinel-2_{Band 7} algorithms compared to lab results

TSM according to single band algorithms based on WISP-3 and Sentinel-2 and lab results

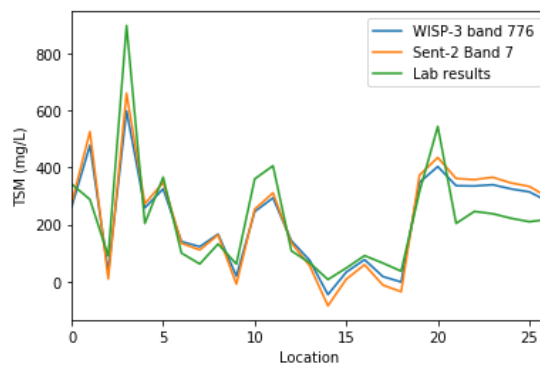


Figure 61: graphs depicting the TSM concentrations as calculated by the single band WISP-3_{776 nm} and Sentinel-2_{Band 7} algorithms, compared to lab results

Differences between single band algorithms based on WISP-3, Sentinel-2 and lab results

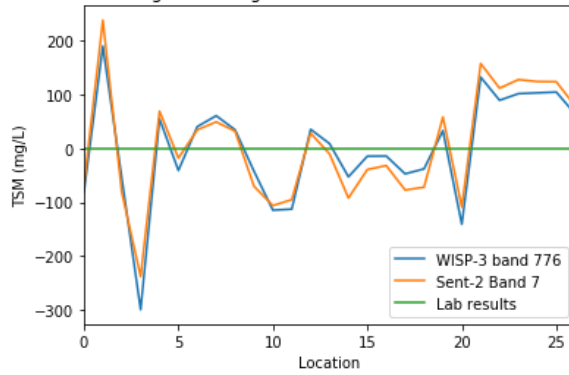


Figure 62: Differences calculated from TSM concentrations as calculated by the single band WISP-3_{776 nm} and Sentinel-2_{Band 7} algorithms, compared to lab results

TSM based on multiple band WISP-3 and Sentinel-2 inter-comparison

Figure 63 shows pair plots of multiple band (WISP-3_{779 nm} + WISP-3_{784 nm}) and (Sentinel-2_{Band 5} + Sentinel-2_{Band 7}) algorithms compared to lab results. Figure 64 shows graphs depicting the TSM concentrations as calculated by these multiple band WISP-3 and Sentinel-2 algorithms, compared to lab results. Figure 65 graphically shows the differences calculated from TSM concentrations as calculated by the aforementioned algorithms.

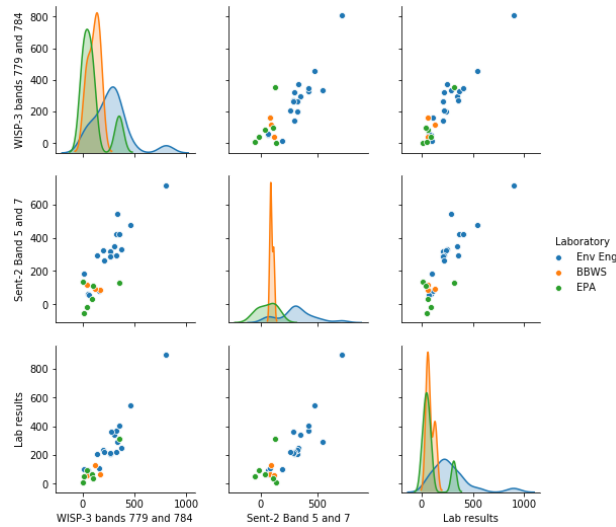


Figure 63: pair plots of multiple band (WISP-3_{779 nm} + WISP-3_{784 nm}) and (Sentinel-2_{Band 5} + Sentinel-2_{Band 7}) algorithms compared to lab results

TSM according to multiple band algorithms based on WISP-3 and Sentinel-2 and lab results

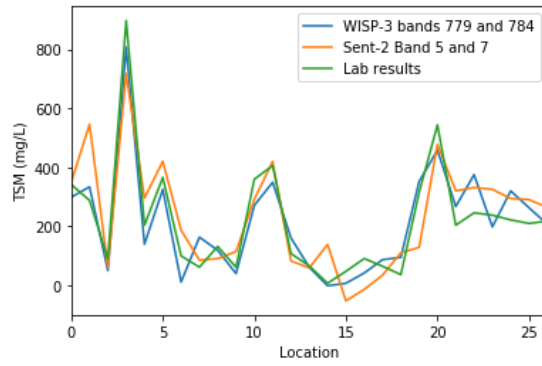


Figure 64: graphs depicting the TSM concentrations as calculated by the multiple band ($WISP-3_{779\text{ nm}} + WISP-3_{784\text{ nm}}$) and ($Sentinel-2_{Band\ 5} + Sentinel-2_{Band\ 7}$) algorithms, compared to lab results

Differences between multiple band algorithms based on WISP-3, Sentinel-2 and lab results

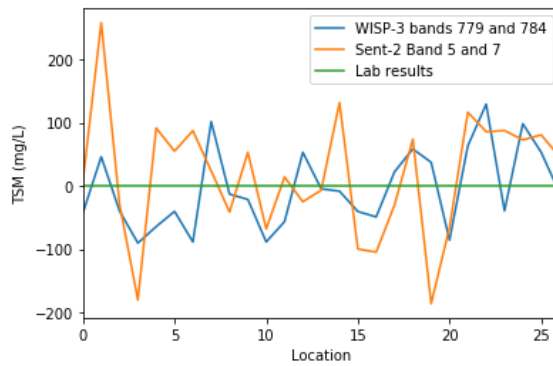
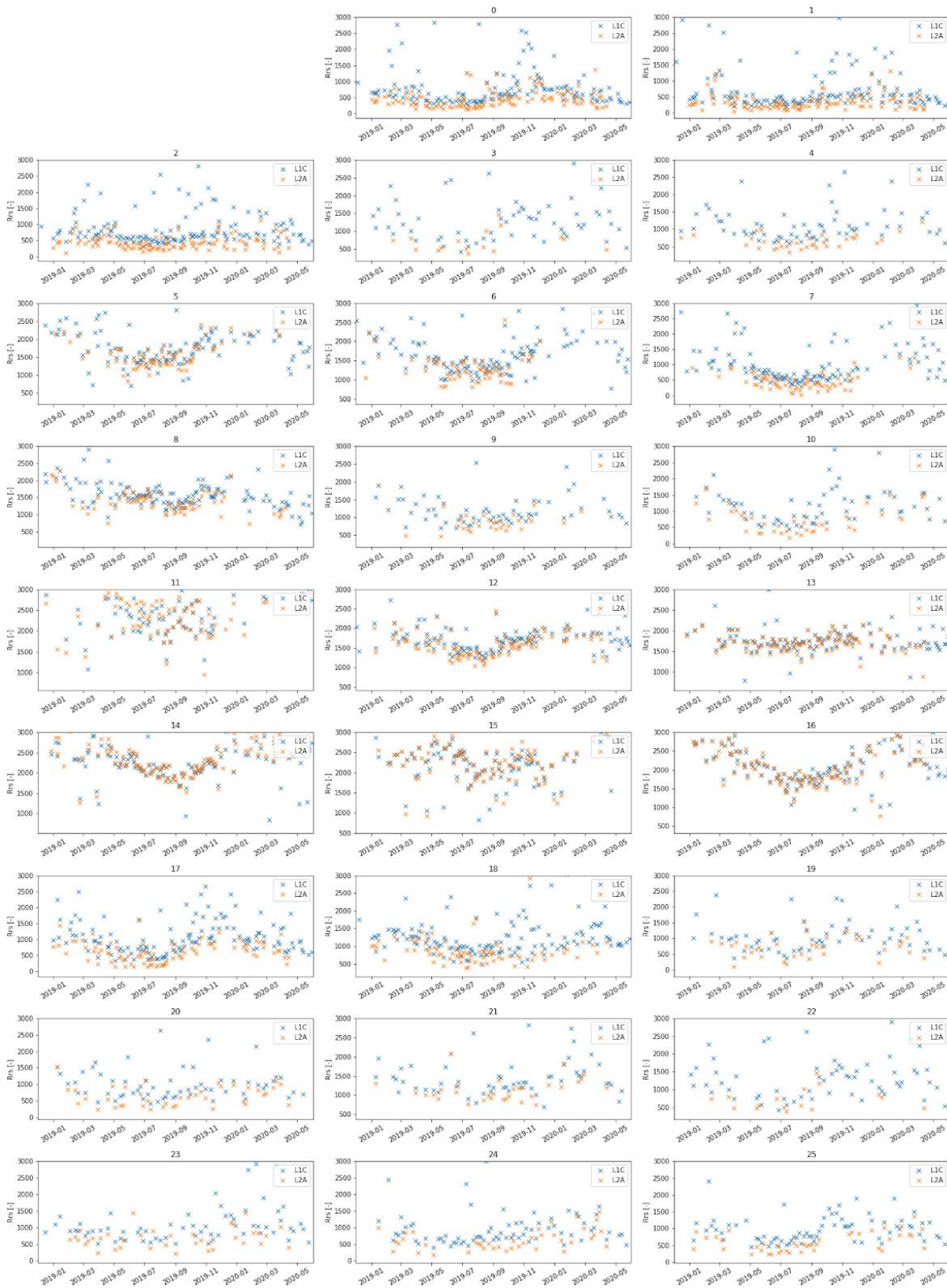
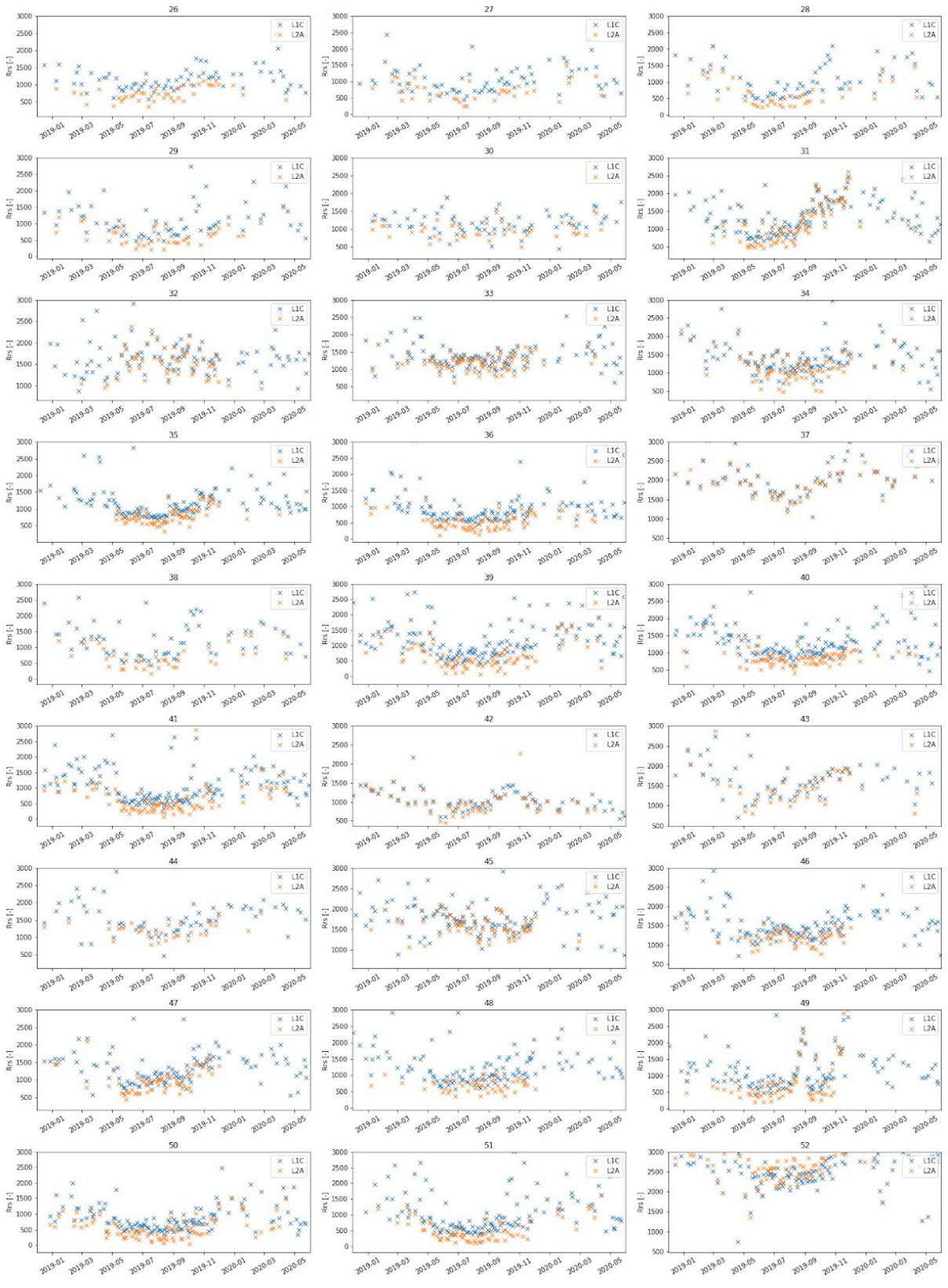


Figure 65: Differences calculated from TSM concentrations as calculated by the multiple band ($WISP-3_{779\text{ nm}} + WISP-3_{784\text{ nm}}$) and ($Sentinel-2_{Band\ 5} + Sentinel-2_{Band\ 7}$) algorithms, compared to lab results

Appendix F: Time series spectral information band 7 Sentinel-2 L1C and L2A compared for 59 locations





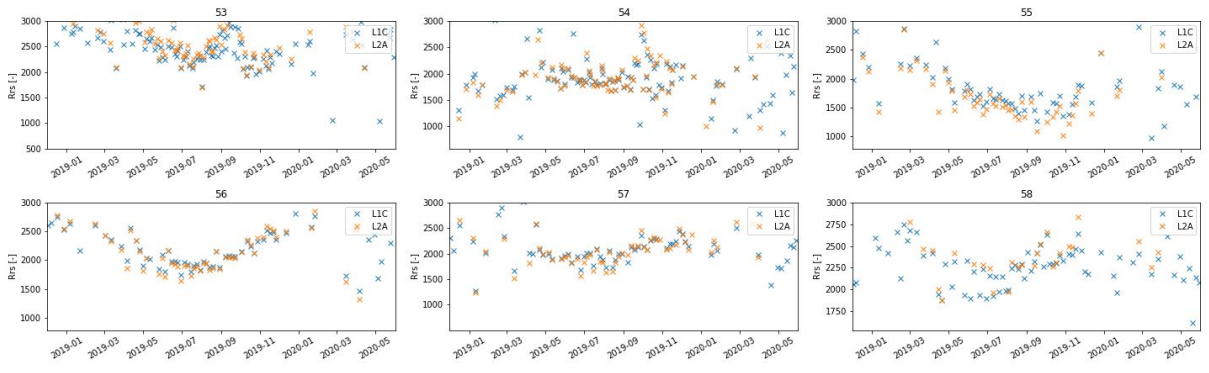


Figure 66: Time series spectral information Sentinel-2 B7 L1C and L2A for 59 locations

Appendix G: Match-ups S2 B7 data with historical TSM values, investigating reason for noise

The historical database of BBWS, EPA and PJT-1 is explored and matched with results from S2. Match-ups between those in situ measurements and satellite imagery - given a positive correlation can be found - can serve as a database to derive parameters for a new model, solely based on satellite data and in situ laboratory measurements.

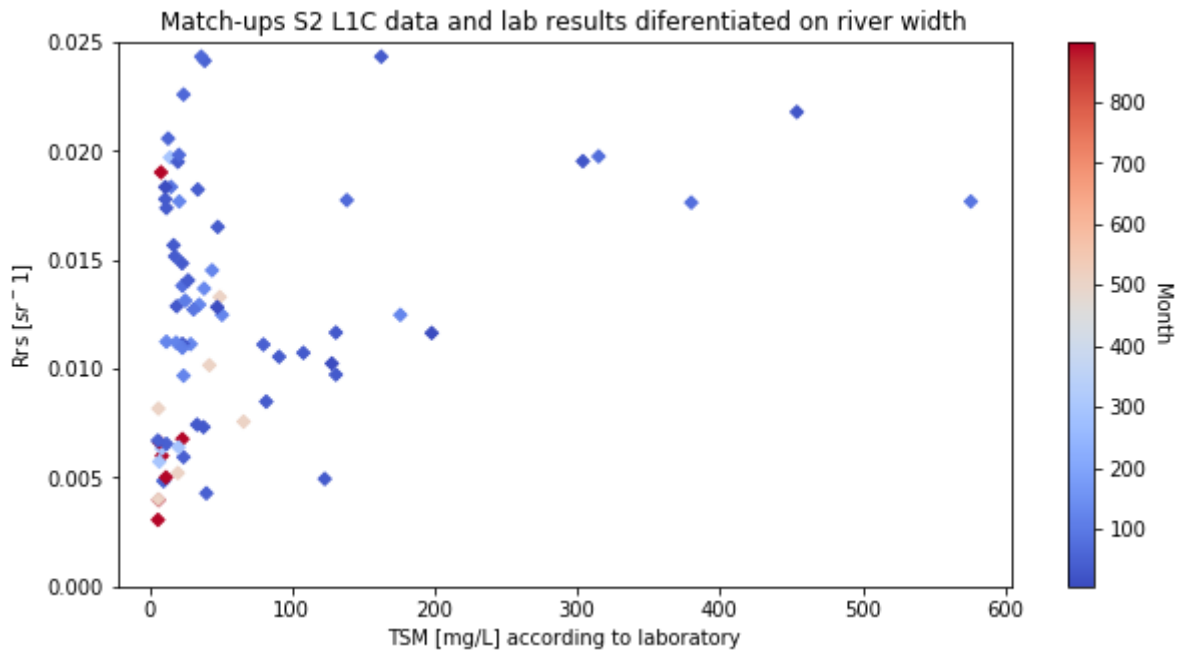


Figure 67: Match-ups between S2 L1C and laboratory results, river width plotted as third variable

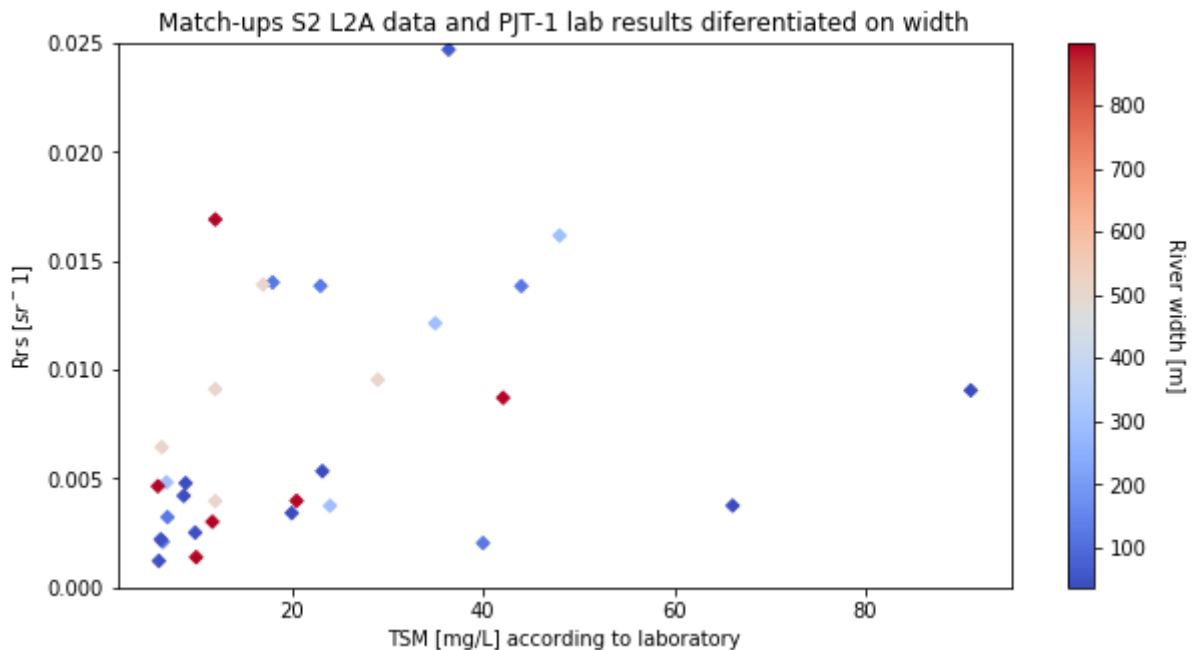
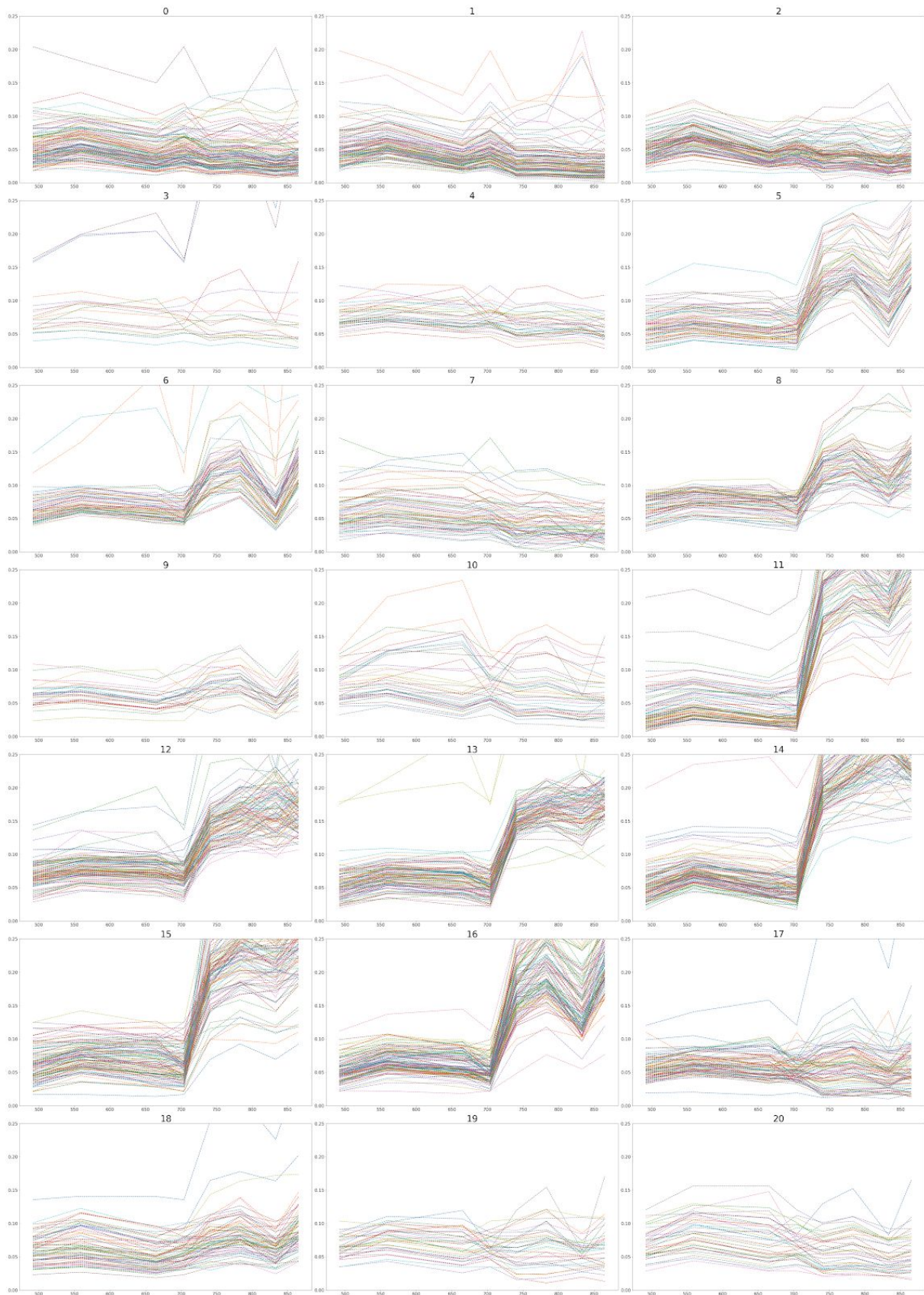
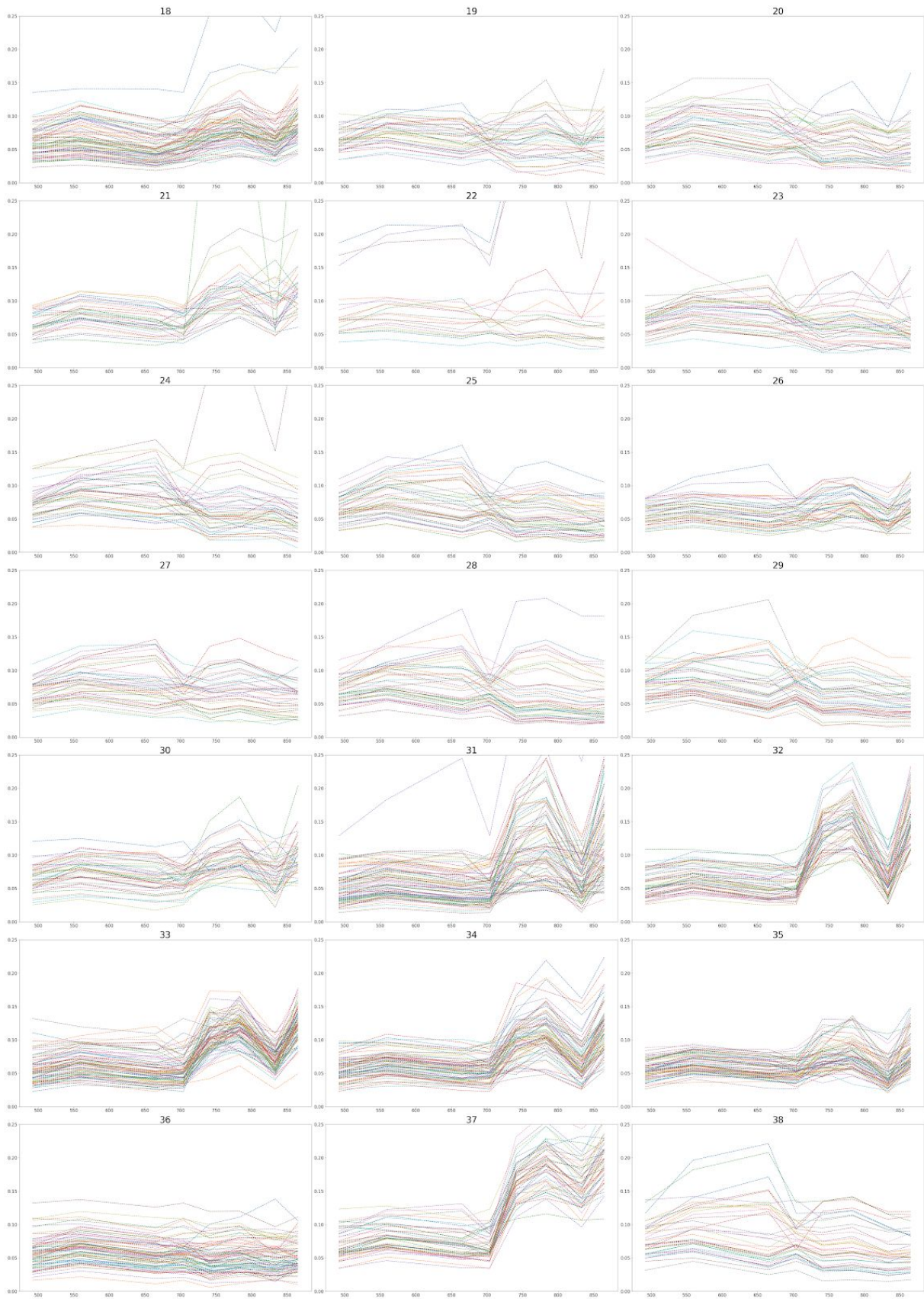


Figure 68: Match-ups between S2 L2A and laboratory results, river width plotted as third variable

Appendix H: Whole spectra (all bands) L2A from S2 satellite imagery from all are measurements for all locations





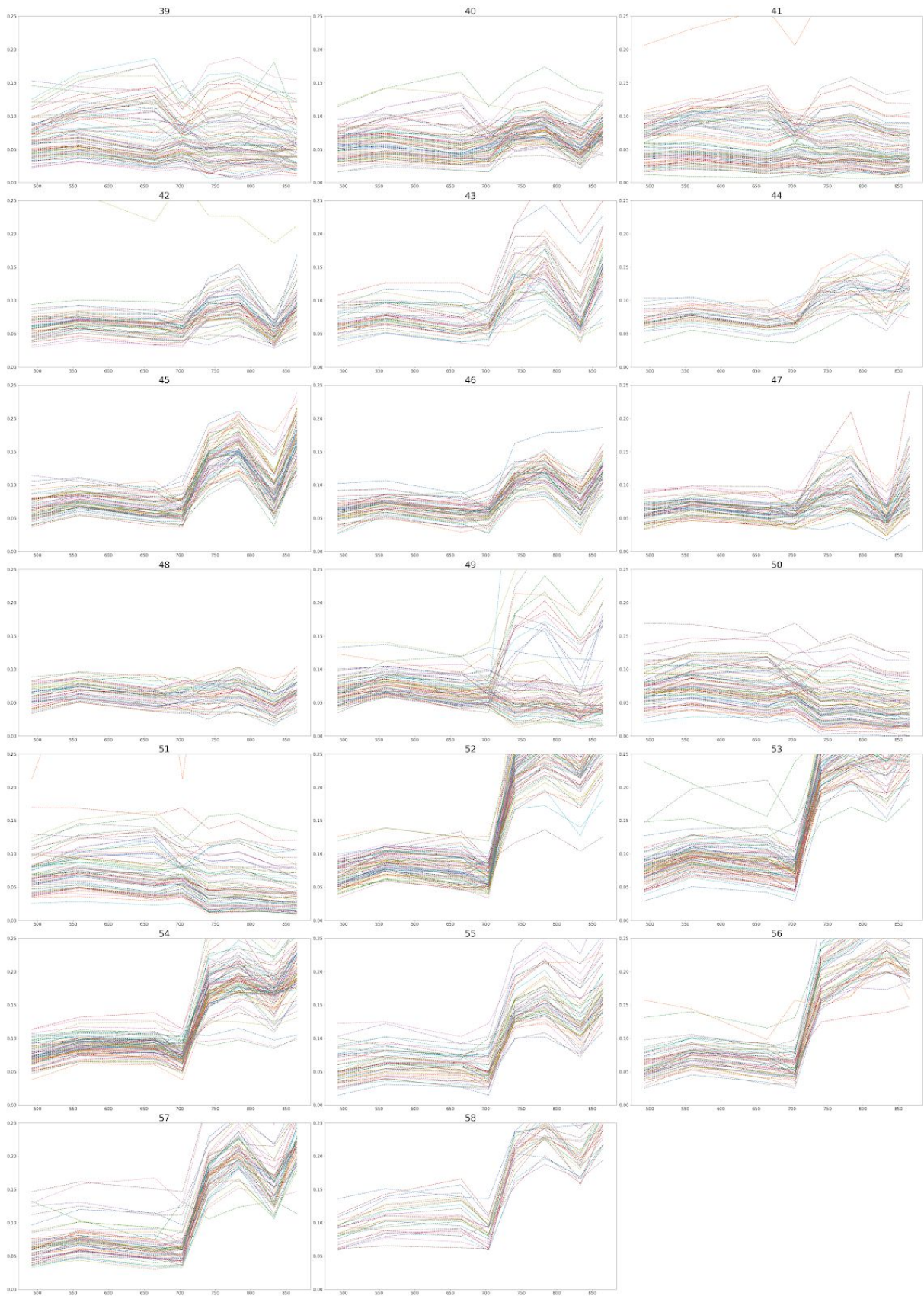


Figure 69: All measurements for all 59 locations plotted for quality checking if reflectance values stem from water pixels, or spurious or land pixels.

Appendix I: Overview of sampling days, region and sampling stations

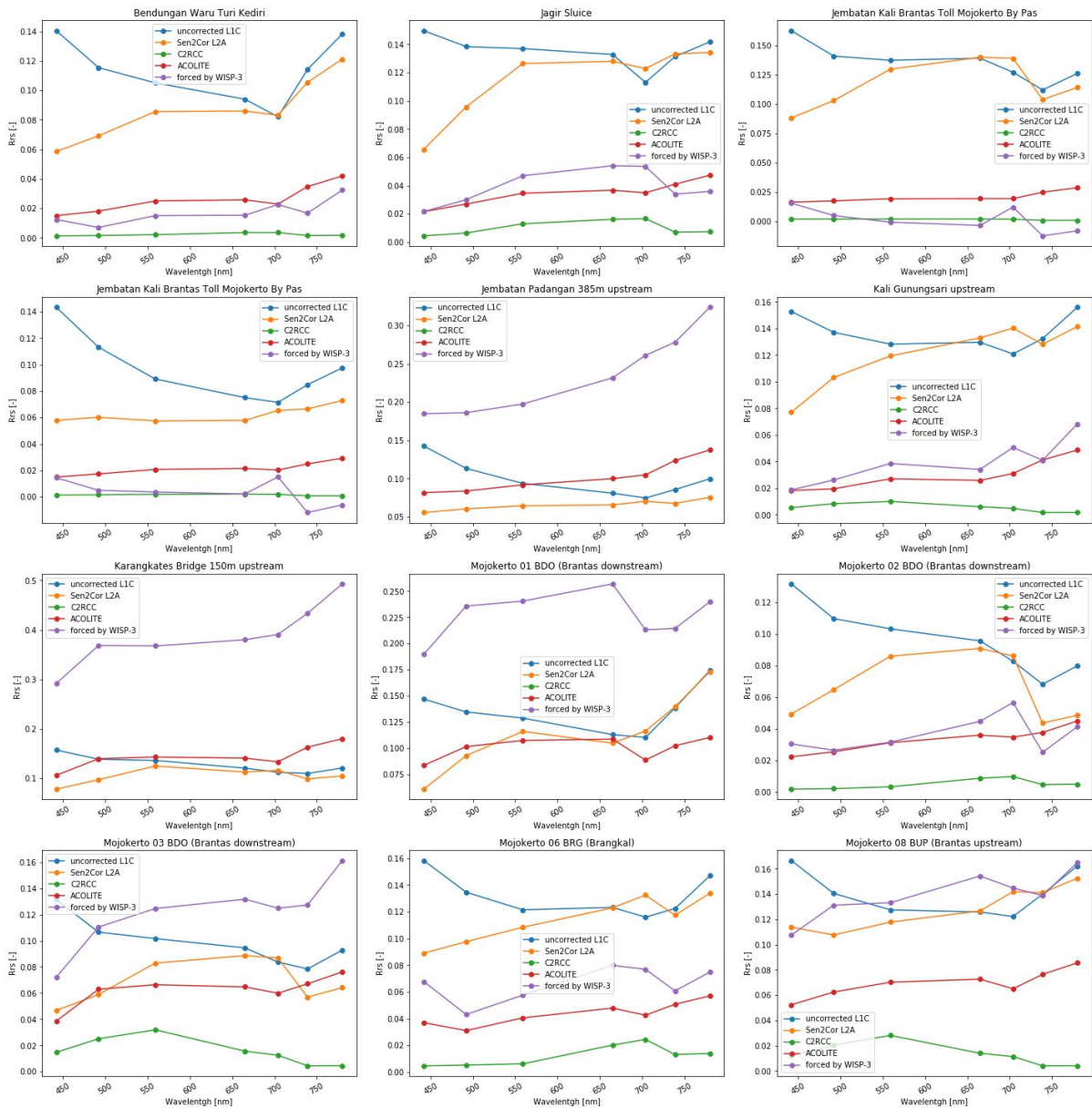
This appendix gives an overview of in situ sampling days, region and sampling stations, dates from which Sentinel-2 images are available and corresponding cloud cover. Only match-ups exist for 1 sample on 28-02-2020 and 9 samples on 24-03-2020 due to high cloud cover percentage during the fieldwork campaign period. So unfortunately extensive (statistical) analysis cannot be performed. Nonetheless the found match-ups provide valuable information which is used by this study.

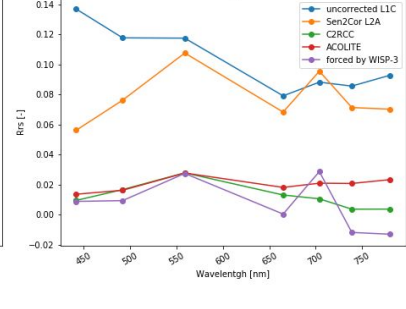
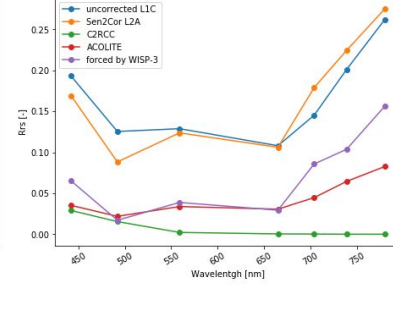
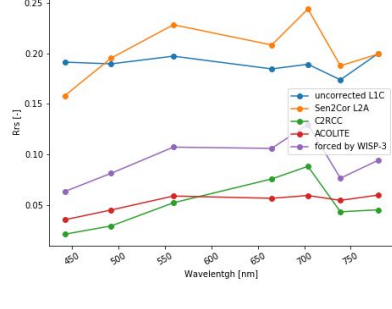
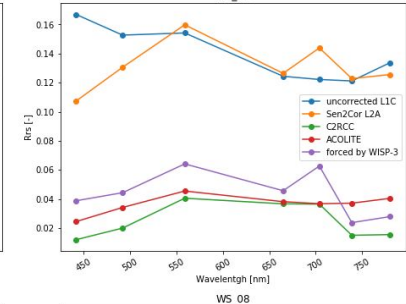
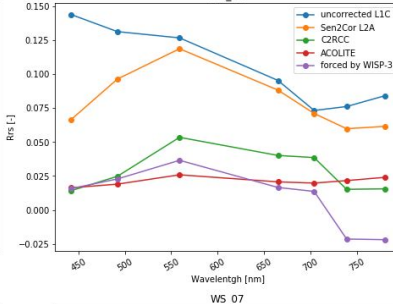
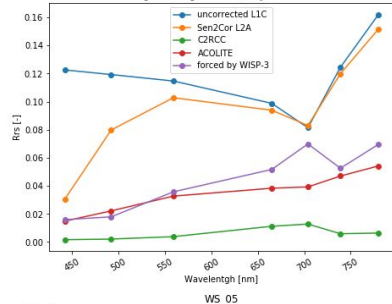
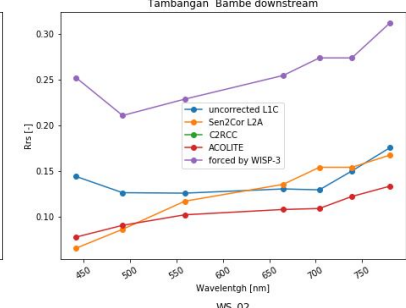
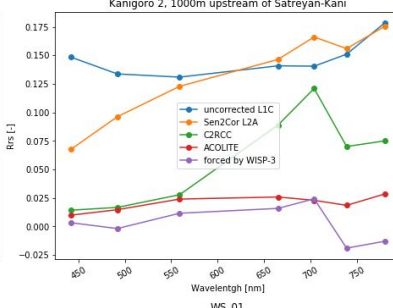
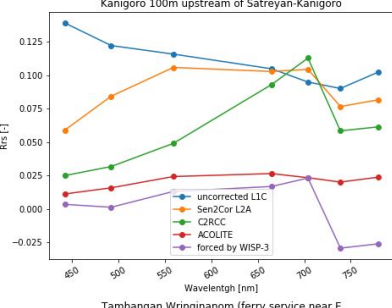
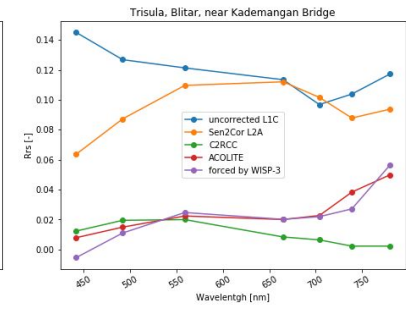
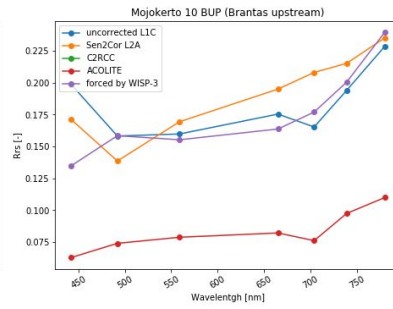
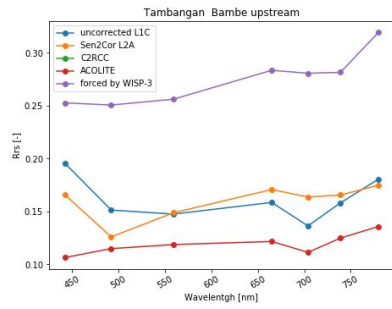
Table 16: *Overview of sampling days, region and sampling stations, dates from which Sentinel-2 images are available and corresponding cloud cover. Only images with cloud cover < 20% are usable which are matched the same day.*

Date	Region	Sample stations	Sent-2 image	Cloud coverage Sent-2 image [%]
30-dec	Surabaya	Tambangan Bambe	30-dec	60.4
2-jan	Porong	Porong Upstream	4-jan	98.0
23-jan	Brantas	Bendungan Waru Turi, Ngujang bridge, Ngunut Ferry Dock, Trisula Blitar, Kanigoro 1, Kanigoro 2	24-jan	34.7
24-jan	Brantas	Karangkates bridge 150 m upstream	24-jan	34.7
16-feb	Kali Jagir	Jagir Sluice	18-feb	69.9
17-feb	Kali Jagir	Jagir Sluice		
19-feb	Kali Jagir	Jagir Sluice		
20-feb	Kali Jagir	Jagir Sluice		
21-feb	Brantas	Jembatan Sukoanyar, Jembatan Pulorejo, Jembatan Kali Brantas Toll Mojokerto By Pass	23-feb	19.7
22-feb	Kali Jagir	Jagir Sluice	23-feb	19.7
23-feb	Kali Jagir	Jagir Sluice	23-feb	19.7
28-feb	Kali Jagir	Jagir Sluice	28-feb	17.1
7-mrt	Brantas	Mojokerto 01 BDO, 07 BRG, 11 BUP	9-mrt	74.7
9-mrt	Kali Jagir	Jagir Sluice	9-mrt	74.7

Appendix J: Comparing results of AC models including forced-by-WISP-3 for 24 locations along the Brantas River (S2 image 28-02-2020)

Rrs values spectra corresponding to uncorrected and AC images





Appendix K: Comparing results of AC models including above water spectral measurements by WISP-3 for 9 locations on Waduk Sutami (S2 image 24-03-2020)

Rrs values spectra corresponding to uncorrected and AC images, 24-03-2020



Appendix L: Overview of 59 investigated locations with water / land pixel indication

#	Sampler and Sample location name	Land / water/ spurious pixel
0	PJT-1 Waduk Sutami hulu	Water
1	PJT-1 Waduk Sutami tengah	Water
2	PJT-1 Waduk Sutami hilir	Water
3	PJT-1 Pakel Tambangan	Water
4	PJT-1 Jembatan Padangan	Water
5	PJT-1 Cangkir Tambangan	Land
6	PJT-1 Karangpilang	Land
7	PJT-1 Ngagel / Jagir Sluice	Water
8	BBWS Jembatan Ngoro (1st location)	Land
9	BBWS Jembatan Pulorejo (2nd location)	Water
10	BBWS Jembatan Tol Mojokerto (3rd location)	Land
11	EPA Arboretum Malang Kota Batu Kec. Bumiaji	Land
12	EPA Jembatan Pendem	Land
13	EPA Jembatan Dinoyo	Land
14	EPA Jembatan Soekarno - Hatta Depan Univ. Brawijaya Malang	Land
15	EPA Jembatan Gadang	Land
16	EPA Jembatan By Pass Kepanjen	Land
17	EPA Jembatan Sengguruh	Spurious
18	EPA Jembatan Kali Pare	Spurious
19	EPA Jembatan Selopuro Blitar	Water
20	EPA Jembatan Glondong / Satreyan Blitar	Water
21	EPA Jembatan Kademangan	Land
22	EPA Tambangan Ngunut 2 Tulungagung	Land
23	EPA Jembatan Ngujang	Water
24	EPA Jembatan Masjid Agung Kediri / Bandar Ngalim	Water
25	EPA Jembatan Meritjan	Water

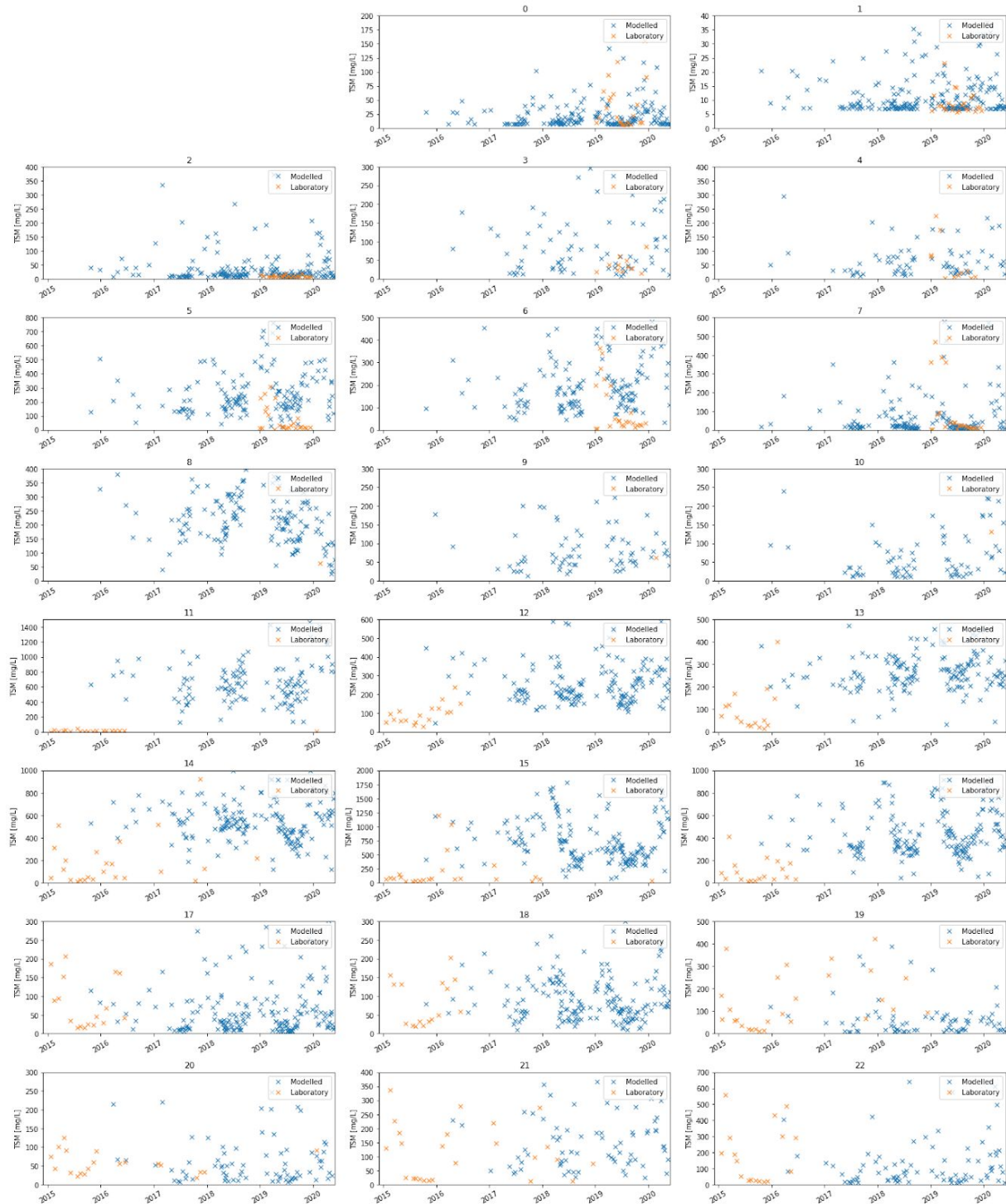
26	EPA Jembatan Papar Kediri	Water
27	EPA Jembatan Kertosono	Water
28	EPA Jembatan Ploso	Water
29	EPA Jembatan Padangan	Water
30	EPA Jembatan Ngembul / Kesamben Blitar	Land
31	EPA Jembatan MERR Surabaya	Land
32	EPA Tambangan Wonorejo Surabaya	Land
33	EPA Jembatan Bungkuk Ngagel	Land
34	EPA Jembatan Sono Kembang	Land
35	EPA Jembatan Pasar Besar	Land
36	EPA Jembatan Petekan	Land
37	EPA Jembatan Jetis IV Mojokerto	Land
38	EPA Jembatan By Pass	Water
39	EPA Jembatan Ngrame II Mojokerto	Land
40	EPA Jembatan Tanjang Rono (dekat PG. Krembung) Mojokerto	Spurious
41	EPA Jembatan Porong	Water
42	EPA Tambangan Tlocor	Water
43	EPA Jembatan Canggü	Water
44	EPA Jembatan Perning	Water
45	EPA Jembatan Legundi	Land
46	EPA Tambangan Cangkir	Land
47	EPA Tambangan Bambe	Land
48	EPA Sebelum Intake PDAM Jemb. Karangpilang	Land
49	EPA Jembatan Karangpilang Baru Sepanjang	Land
50	EPA Bendungan Gunungsari	Water
51	EPA Jembatan Gunungsari	Water
52	EPA Hulu Kali Tengah	Land
53	EPA WWG Kali Tengah	Land

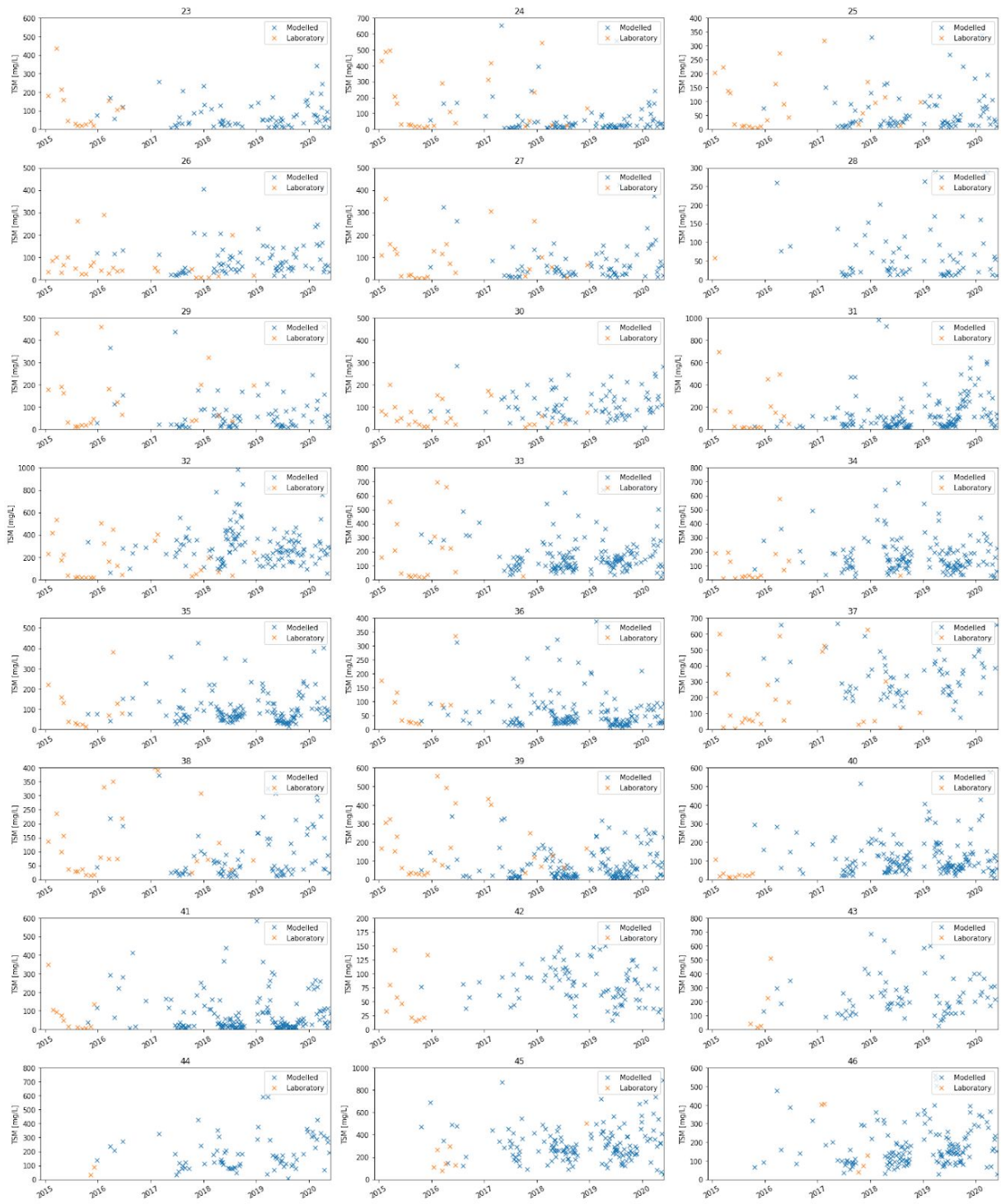
54	EPA Jembatan Bambe	Land
55	EPA Jembatan Lawang	Land
56	EPA Dam Paras Lawang	Land
57	EPA Jembatan Kraton	Land
58	EPA Jembatan Tumpang Purwosari	Land

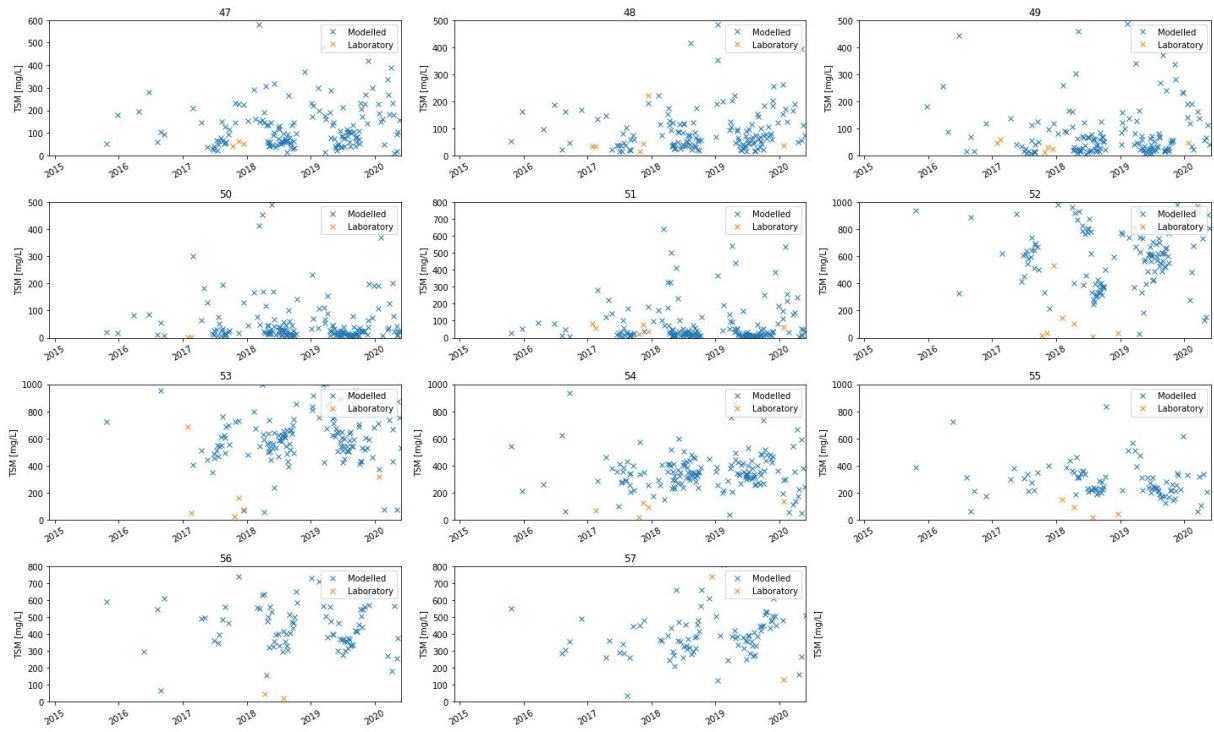
The table above shows the classification of the individual locations as used during S2 image analysis. It turns out that 23 out of 59 (39%) are actual water pixels, 33 (56%) are land pixels and 3 (5%) are spurious pixels. It shows that careful selection of coordinates of sample locations is necessary.

Appendix M: Comparing TSM in situ measurements with modelled values based on S2 L1C B7 for all 59 locations

This appendix should be consulted using [Appendix L](#), since that appendix shows whether pixels are considered to be land or water pixels after examination of individual spectra derived from these locations.







Appendix N: Data management plan

Data Management Plan (DMP)

Editable Form adapted from CESSDA using DMPonline
 Integrated parts from the Delft University Fund DMP Template

1. Overview

Title of the project/study	Estimating Total Suspended Matter in Low to Extremely High Level Turbid River Surface Waters using a WISP-3 Hyperspectral Radiometer and Sentinel-2 (S2) Optical Imagery	
Date of this plan	Last updated Friday, 31 July 2020	
Version of this plan	This is version 3.1. Major changes or updates will increase the main number (i.e. the number before the dot, e.g. 2.0). Intermediate updates with minor changes will increase the secondary number (i.e. the number after the dot, e.g. 1.1).	
Description of the project	<p>This study will be the final work (thesis) of my MSc program Water Management, Civil Engineering. Choosing the Brantas River as case follows from its importance: The Brantas River is East Java's largest river with a watershed area of about 12,000 km² and stretches 320 km from its spring at Mt. Arjuno to the point where it branches into two rivers, the Surabaya River and the Porong River, both of which drain into the Madura Strait. Approximately 30 million people are living in the Brantas River watershed. Through 35 organizations that have a role in water resource development and management of the Brantas River, a long time series with a fast amount of data is available. This study will focus on the Surabaya River. This study will use remotely sensed data validated against in situ data from monitoring databases to identify Total Suspended Solids (TSM) using optical satellite data.</p>	
Project timeline	Research proposal	Oct – Nov 2019
	Literature study	Dec. 2019
	Set-up collaborations	Dec. 2019 – Jan. 2020
	Gather historical data	Jan. – Apr. 2020
	Site visits	Jan. – Mar. 2020
	Sampling with PJT-1, BBWS, EPA	Jan. – Mar. 2020

	Analysis laboratory Env. Eng. Dep. ITS	Dec. – Feb. 2020
	Analysing results, mining satellite data, modelling algorithms	May. – July 2020
	Presenting results	Aug. 2020
Institution leading the collaboration	Technische Universiteit Delft is leading the project, in close cooperation with Ecoton, BBWS Brantas, Jasa Tirta I Public Corporation, WLN Indonesia (PT. WLN), Tauw B.V. and Netherlands Enterprise Agency	
Responsible for the data resulting from this project	Dr.ir. Maurits W. Ertsen Senior lecturer Water Management Resources (m.w.ertsen@tudelft.nl) in the role as project leader of “Fostering inclusive growth, health and equity by mainstreaming water quality in river basin management in the Brantas river basin, Indonesia” (referred to in this document as “the Brantas project”).	
Origin of Data: produced or issued by principle researcher	<ol style="list-style-type: none"> 1. Data produced by principle researcher: <ol style="list-style-type: none"> a. WISP-3 handheld radiometer water leaving reflectance measurements b. Dissolved Oxygen and temperature measurements by a handheld AZ 8403 Portable Digital Dissolved Oxygen DO Tester 2. Laboratory measurements issued for this research and carried out by the laboratory of the Environmental Engineering Department of ITS (Sepuluh Nopember Institute of Technology): <ol style="list-style-type: none"> a. Total Suspended Solids (TSS) b. Dissolved oxygen (DO) c. Chlorophyll-a (Chl-a) d. Turbidity (TU) e. Chemical oxygen demand (COD) f. Biological oxygen demand (BOD) <p>All collected data have a quantitative nature. Collection of new measurements is necessary because no dataset exists of water leaving reflectance values for the Brantas River. Furthermore, these measurements need to be taken at the same time as in situ laboratory examined water samples are taken, to be able to validate and calibrate the proposed algorithms.</p>	
Origin of Data: from existing, external data sources	<ol style="list-style-type: none"> 1. Existing, external data sources: <ol style="list-style-type: none"> a. In situ measurements: 	

	<ul style="list-style-type: none"> i. Perum Jasa Tirta I, Agency for Brantas and Bengawan Solo River Basins (PJT-1) ii. Brantas Water Resources Management (BBWS) iii. Environmental Provincial Agency East Java (EPA) <p>b. Satellite related data:</p> <ul style="list-style-type: none"> i. Sentinel-2 MSI 2A and 2B reflectance values in band 1 to 8A ii. Atmospheric correction algorithms, scripts and data: <ul style="list-style-type: none"> 1. Sen2Cor 2. C2RCC 3. ACOLITE <p>From the Sentinel-2 platform, all images of the Brantas river basin (granule T49MFM) are used from the start of the mission 2015 until now. Most images are analysed online using the Google Earth Engine (GEE). Only resulting reflectance data for specific locations are downloaded and stored for further analysis (.csv files). Top of atmosphere (TOA) images of match-ups with in situ reflectance data are downloaded, archived and analysed, being data from 17-11-2019, 30-12-2019, 28-02-2020 and 08-04-2020. These are left intact in the .jp2 format and are analysed using SNAP and ArcMap. Sen2Cor bottom of atmosphere (BOA) data is specifically downloaded through GEE for appropriate sampling locations. C2RCC and ACOLITE calculations of BOA reflectance values are processed offline on a personal computer. Resulting images (SNAP standard BEAM-DIMAP format and .nc format) are stored, analysed and archived on a local SSD.</p>
Integration of data sources	<p>External datasets holding values of water quality parameters are delivered as excel files, as PDF or hard copy. Laboratory results requested by this study are delivered hard copy or as PDF. Own in situ data is noted hard copy in the field and transferred into excel file format the same day. All data is converted into .csv files in order to be read by the Python Notebook interface.</p> <p>Satellite reflectance values are extracted by either GEE or by using SNAP and stored as .csv files for further analysis using the Python Notebook interface. Files resulting from atmospheric correction using the ACOLITE algorithm (.nc files) are directly read in Python.</p> <p>Raw WISP-3 samples are taken from the devices SD-card and uploaded on WISPweb, a web-based user interface for storing, reading, analysing and downloading WISP-3 data. It</p>

	<p>also provides running algorithms estimating a selection of water quality parameters and a means of adding metadata to the individual measurements. Downloaded data is formatted as .csv files for further analysis using Python.</p> <p>All analysis and producing resulting figures, graphs and tables is done using Python. All relevant scripts are bundled and archived.</p>	
Principal researcher /creator	J.C. Wiggins	
Contact details principal researcher	joris@wiggins.nl , 0031-6-24646303	
ORCID iD	https://orcid.org/0000-0003-4351-8304	
Collaborating researchers	None	
Funding organizations and project's title in the funding contract	1. Delft University Fund	Grant number: 2019-060
		<i>"Water quality monitoring and evaluation using optical satellite data in the delta of the Brantas River, Indonesia"</i>
	2. Lamminga Fonds	Grant number: Lamm-19-41-PV
		<i>"Veldwerk in Surabaya, Indonesië 2019-2020 in het kader van MSc Thesis project Afdeling Water Management"</i>
	3. Sustainable Water Fund (FDW) of the Ministry of Economic Affairs of the Kingdom of the Netherlands	Grant number: NL-KVK-27378529-FDW16046RI
		<i>"Fostering inclusive growth, health and equity by mainstreaming water quality in river basin management in the Brantas River basin, Indonesia"</i>
Data producer	Organizations which have the administrative responsibility for the data: J.C. Wiggins, ITS Env. Eng. Department ITS, PJT-1, BBWS and EPA, ESA (European Space Agency)	
Project data contacts + e-mail address	ITS Env. Eng. Dep. ITS	Edy Pratikno edypratiko27@gmail.com
	PJT-1	Astria Nugrahany astria@jasatirta1.net

	BBWS	BBWS Brantas Water Quality Staff kualitasair.bbwsbrantas@gmail.com
	EPA	Immanuel Kharisma imkh40@gmail.com
	ESA	EOSupport@Copernicus.esa.int
Project data overall contact	J.C. Wiggins, MSc. student of Water Management, faculty of Civil Engineering of the TU Delft	
Data owner(s) and respective roles	J.C. Wiggins	Project owner, data producer, responsible for updating the DMP and making sure that it's followed
	PJT-1, BBWS and EPA, ESA	Stakeholders, data producer and data owners
Costs and Resources	<p>Are there costs you need to consider to buy specific software or hardware?</p> <p>ArcGIS for Desktop software is provided as part of following the Geographic Information Systems (GIS) Specialization offered by UC Davis University of California, USA.</p> <p>the Sentinel Application Platform (SNAP) is a common architecture for all Sentinel Toolboxes is being jointly developed by Brockmann Consult, SkyWatch and C-S. Its use is without costs.</p> <p>Expenses for hardware are limited to costs of USB drives and an external hard drive for back-up of research data.</p> <p>Are there costs you need to consider for storage and backup?</p> <ol style="list-style-type: none"> Dropbox €11,99 monthly plan (all data files, S2 data downloads) Google Drive €4,39 monthly plan (results of GEE scripts and data requests, draft versions of thesis, transcriptions of research interviews and meetings, fieldwork photos) Microsoft OneDrive for free (Python Notebook and Spyder scripts, results of data analysis by Python). All files are also stored locally on a SSD. <p>Are potential expenses and resources for (preparing the data for) archiving covered?</p>	

	<p>No, own personal expense. If need arises, a request for financial help can be delivered to the institution leading the collaboration (TU Delft).</p> <p>What resources will be dedicated to data management ensuring that data will be FAIR?</p> <p>At this moment none, since it is (not yet) decided to make the data publicly available. In preparation of such an event, guidelines of the CESSDA data management expert guide are followed as closely as possible in setting up, using and archiving the data regarding this study.</p>
--	--------------------------------------------------------------------------------------------------------------------------------------------------------------------------------------------------------------------------------------------------------------------------------------------------------------------------------------------------------------------------------------------------------------------------------------------------------------------------------------------------------------------------------------------------------

2. Organizing and documenting your data

Data collection	What type(s) of data will be collected?	
	All collected data have a quantitative nature. Data collected are water quality parameters, water leaving reflectance values and atmospheric conditions.	
	What is the scope, quantity, and format of the material?	
	In situ water sampling (handheld radiometer for reflectance values, TSS, DO, Chl-a, TU, COD, BOD) for this study is done at 20 locations. Historical data is gathered from a total of 58 locations throughout the basin (PJT-1, BBWS and EPA sampling stations). All data is delivered either hard copy, as excel files, as PDF or as .csv file. All data is formatted as .csv file. Satellite and atmospherically corrected data are delivered as .jp2, .geotiff or as .nc file. Pixel values per band are extracted and formatted as .csv file.	
	What is the total amount of data collected (in MB/GB)?	
	Google Drive	1.2 GB
	Dropbox	63.6 GB
	OneDrive	190 MB
	Total	64.99 GB
Data organization	How will you organize your data?	
	Dropbox	all data files fieldwork data (in situ measurements, WISP-3 datasets), S2 data downloads, PlanetScope satellite data downloads, ArcGIS files and databases, acquired databases, project proposal, word

		documents and presentation files midterm and greenlight meeting, intermediate versions of thesis report including lay-out, all letters and official documentation for internship ITS and residence permit Indonesia, all official letters for data requests and set-up collaborations
	Google Drive	results of GEE scripts and GEE data requests, draft versions of thesis, transcriptions of research interviews and meetings, fieldwork photos
	Microsoft OneDrive	Python Notebook and Spyder scripts, results of data analysis by Python
	WISPweb	Online storage of all raw WISP-3 measurements, in a GUI which allows visualization, analysis, metadata updates, calibration and export of subsets of data
<p>Will the data be organized in simple files or more complex databases?</p> <p>Most data are organized in simple files (.csv format) to be readable and writable by Python, Spyder, ArcGIS, GEE and Excel. Datasets of external sources are formatted in the same structure and combined before analysing.</p> <p>What is your process for quality assurance? What are your quality measures? Specific quality standards or quality management models applied:</p>		
<p><i>Quality assessment of Standard Laboratory Operating Procedure</i></p>		
<p>The EPA uses standardized protocols (i.e. SNI, APHA) to measure each water quality variable in their own laboratory. PJT-1 uses its own laboratories in Malang and Mojokerto. The PJT-1 water quality laboratory management is ISO-certified. BBWS collects water samples and has them analysed at the laboratories of PJT-1.</p> <p>Water samples taken by myself were analysed at the laboratory of the Environmental Engineering Department of ITS. These samples were analysed using a gravimetric method following an unknown protocol.</p>		
<p><i>Quality assessment of methods with WISP-3 in-situ measurements</i></p>		
<p>The WISP-3 uses a unique configuration of fibre optics. This approach is validated against other non-handheld or mounted</p>		

	<p>spectroradiometers and laboratory concentrations. The WISP-3 is also calibrated against a NIST traceable light source.</p> <p>The WISP-3 radiometer averages 15 automated samples for each measurement. For this study 3 to 5 manually induced measurements (of 15 samples each) per sampling station were performed, in order to do a quality control check on those sets of measurements. Average values of those sets of measurements are used, except when 1 out of all manually induced measurements was more than 20% off, that measurement was neglected.</p> <p>The reflectance (R0-) is a ratio and should therefore never be lower than 0 or higher than 1. Values higher than 1 are flagged and not used. High reflectance values can be caused by sun glint or mirror-like reflection of the water surface. To validate the estimated TSM concentrations from spectral images derived from the WISP-3 measurements, in situ data from the laboratory are used.</p> <p><i>Quality assessment of Sentinel-2 optical satellite imagery</i></p> <p>A first, simple, quick visual inspection is undertaken by analysing the RGB colour composite image of the remotely sensed data. Thereby, images with sun glint and excessive cloud cover can be easily identified and manually taken out of the dataset. All images are later in the process checked in bulk in GEE and cloud and cloud shadow pixels are flagged and left out of analysis. To check whether selected pixels for analysis are indeed water pixels, spectra are plotted and checked for their signal (distinctive water / land or spurious pixel).</p>
Data type and size	There are no specific requirements for compatibility and comparability of my data. Also, there are no specific standards that I want to implement, e.g. naming conventions or standardized coding structures.
File format	All data is delivered either hard copy, as excel files, as PDF or as .csv file. All data is formatted as .csv file. Satellite and atmospherically corrected data are delivered as .jp2, .geotiff or as .nc file. Pixel values per band are extracted and formatted as .csv file. Resulting graphs and visualizations are saved as .png files.
Folder structure & names	<p>Python scripts are saved in a folder structure following the sequential steps undertaken to get from raw data input to final results of analysis. I.e. the main folder for scripts used for analysis are stored in OneDrive>Brantas>Final_report. This folder holds the following subfolders:</p> <ul style="list-style-type: none"> a) Step 01 Re-calibration b) Step 02 Fingerprinting

	<ul style="list-style-type: none"> c) Step 03 Typical spectra and bio-optical properties d) Step 04 WISP-3 spectra vs lab results e) Step 04.1 Linear green and red bands and polynomial NIR band curve fitting f) Step 05 Bounds selection MCA g) Step 06 Performance of MCA h) Step 07 Timeseries Sent-2 bands i) Step 08 Match-ups Sent-2 and lab results j) Step 09 Applying MCA to recent Sent-data <p>All data which is used as input for scripts is stored in a separate folder, as is all data produced as output stored in a specific folder. These folders have subfolders to sort data per above shown steps in the process.</p> <p>Resulting .png files with plots and visualizations is stored in OneDrive>Brantas>Final_report>visualization. External scripts are saved and run from separate folders, named after the author. For example, the scripts for fingerprinting the WISP-3 spectra and all associated results are stored in OneDrive>Brantas>StefanSimis.</p> <p>Fieldwork data is sorted by source and file type. All original data is stored as such and alterations are done only on copies of the original datasets.</p>
File structure & names	<p>Names of individual scripts are structured as follows: <What is done by the script><What does it use as input><What does it give as output>.ipynb. E.g. <i>"Create files for fingerprinting Input is 27 measurements WISP after re-calibration data output is files for fingerprinting algorithm.ipynb"</i>.</p> <p>Fieldwork data is named after the source and date of sampling.</p>
Documentation	<p>No other separate files accompanying the data will be produced besides this document. At this moment, no database structure is used, besides the above described folder structure.</p>
Metadata	<p>Are the data produced and/or used in the project discoverable with metadata?</p> <p>The WISP-3 data has added, detailed metadata added and stored in WISPweb. The data is available for users of the platform and only when they are granted access.</p> <p>S2 data comes with its own metadata files and formats. They are left as is.</p> <p>What metadata will you use?</p>

	For all ArcMap files (visualization of geoinformation, maps and details of satellite imagery analysis) get added, ArcGIS standard metadata files.
--	---------------------------------------------------------------------------------------------------------------------------------------------------

3. Processing your data

Versioning	<p>How will you version your scripts during the project?</p> <p>Scripts of first try-outs on analysing data are stored in OneDrive>Brantas>archive. After, a sequence of steps was determined, and scripts were sorted following that sequence. A first series is stored in OneDrive>Brantas>after_calibration following the structure as depicted under the "Folder structure & names" part of this plan. The final version of all scripts following this sequence can be found under OneDrive>Brantas>final_report.</p> <p>How can different versions of a data file be separated?</p> <p>The file names are defined in such a way that they reflect what version it is. This is done by adding a date and a version number to the file name. The general convention is followed, being using the date format (YYYY-MM-DD) as the start of the file name, allowing you sorting of files in chronological order. Every time major changes are made to datasets; a new version is stored. Raw data is preserved at all times by creating a copy of raw datasets before any manipulations are done.</p>
Interoperability	<p>Which software will you use?</p> <p>ArcGIS for Desktop (ArcGIS Desktop 10.7.1, ArcGIS Service Pack: 0 (build 0)) is used for all GIS related work. All data is stored in geodatabases, collection of files in a folder on disk that can store, query, and manage both spatial and nonspatial data. Geodatabases can be read by ArcGIS software or accessed and managed using MS Access.</p> <p>SNAP is used for all S2 downloaded data and is ideal for Earth Observation processing and analysis. All data is stored as BEAM-DIMAP format (SNAP-standard) and can be opened with whatever version of SNAP installed.</p> <p>Scripts (javascript) for the GEE web-based user interface environment are stored, accessed and executed online. The latest versions are available for registered users.</p> <p>Python Notebook 6.1.6 is used for data import, analysis and visualization. All scripts are stored as .ipynb.</p> <p>Spyder 3.3.6 is used for reading, adjusting and executing Stefan Simins scripts for fingerprinting (correcting reflectance value measurements for sun glint and measuring angle). Scripts are stored as .py files.</p>
Data quality	<p>How will data quality be evaluated?</p> <p>WISP-3 reflectance measurements are evaluated online using WISPweb. To check if spectral measurements are okay,</p>

	<p>guidelines of the "WISP--3 User Guide" (n.d., Water Insight B.V. The Netherlands), follow these steps:</p> <p>Check R(0) directly after measurement. The reflectance (R0) is a ratio and should therefore never be lower than 0 or higher than 1. Sometimes the reflectance around 400nm is negative. If this occurs only on the leftmost side of the graph and the values are just below zero, the data can still be used. Treat these measurements with care though.</p> <p>Ed, Ld and Lu can be examined in WISPweb. The irradiance (Ed) should always have the highest values of the three separate spectra. The downwelling radiance (Ld) is a fraction of Ed and should therefore be much lower (e.g. a factor 10). However, both measure the sky and the spectral shape should therefore be relatively similar. The downwelling radiance (Lu the 'water' signal) should be much lower than Ld. If not, check if there was a high sediment load (than the spectra might be correct), or if there were factors with a negative influence on the measurement, such as bottom visibility, macrophytes, floating plants or garbage, or wrong measuring angles.</p> <p>What data quality control measures will be used?</p> <p>See under Data organization > Quality assessment of this document.</p>
Responsibilities and resources	<p>Who will be responsible for data management?</p> <p>The principal researcher will be responsible for data capture, data management, metadata production, storage and backup, data archiving and data sharing.</p> <p>What resources will you require to deliver your plan?</p> <p>Time and effort are spent within the timeframe of this thesis project to prepare the data for own use and archiving / preservation. I have sufficient storage and equipment to undertake these tasks.</p>

4. Storing your data and metadata

Type of data	<p>Are you collecting personal data or do your data in any other way require special protection?</p> <p>No personal data is stored. All data is op the general type.</p>
Who needs access	<p>Is it necessary to have remote access to the data? Are you e.g. transmitting data from the field?</p> <p>It is not required to have remote access to the data. All S2 data however is remotely accessed using the GEE.</p> <p>How important is fast access?</p>

	<p>Fast access does not play any significant role. To speed up computational time, as much data processing on S2 data is done using GEE's server power.</p> <p>Is simultaneous and synchronised access by several people required?</p> <p>Simultaneous and synchronised access by several people is not required.</p>
Storage and back-up	<p>How will the data be stored and backed up during the research?</p> <p>Storage and back up will be in three places:</p> <ul style="list-style-type: none"> • On Laptop of principal researcher • On a portable storage device (hard drive) • Divided on online storage platforms Google Drive, Dropbox and OneDrive, as specified under 1. Overview > Costs and Resources. <p>The principal researcher will be responsible for the storage and back up of data. This will be done weekly.</p> <p>If required by the TU Delft, a final version ready for archiving / sharing will be made available through Git(lab)/subversion repository at TU Delft. If so, also all data will be uploaded to the 4TU.Centre for Research Data.</p> <p>How much data are you going to generate and how much storage capacity will you need, including backups?</p> <p>All data combined holds 64.99 GB. This is the size of the data on the online storage platforms combined (working documents). Back-ups on the laptop and portable storage device are equal of size. Only the last version of every back-up is stored.</p> <p>Which media types will you use and how often will you replace them?</p> <p>A laptop (SSD) is used, as well as a portable hard disk and online storage capacity is used.</p> <p>The final version of the MSc thesis will be uploaded to TU Delft's Thesis Repository (http://repository.tudelft.nl).</p>
Required storage	64.99 GB
Storage period	<p>For how long is storage required?</p> <p>The digital version of the MSc thesis is published and offered within an Open Access framework for a not by time defined period.</p>
File formats	<p>Are you certain that your data and files are stored in a format for which there will still be suitable software</p>

	<p>available to access and process the stored information in ten years?</p> <p>Yes, all raw data is stored in .csv file format. Processed data in ArcGIS and SNAP format might get outdated, but it is not likely so.</p>
Security	<p>How will you manage access and security?</p> <p>Both the laptop and external storage device are password protected. The risks are that the computer will be hacked and the external drive stolen. Secondary risk is malfunctioning of either the SSD disk from the laptop or the external hard drive. Malfunctioning of the laptop is minimized by installing a new motherboard just before the start of the study. The laptop has anti-virus and anti-malware software installed which is updated daily. The laptop is not used for other any other purpose than all work associated with this study. The external device is in a locked cabinet. Moreover, the data files stored online are also password protected.</p>
Budget	<p>What is the associated cost of storing and backing up data?</p> <p>See under 1. Overview > Costs and Resources</p>

5. Protecting your data

Type of data	<p>Data can be differentiated into three categories:</p> <ul style="list-style-type: none"> - Critical data: data that enables the identification of an individual - Sensitive data: data that is competition-sensitive or confidential - Standard data: data that is not critical nor sensitive <p>All data collected, used and archived during the course of this study belongs to the standard data category. See under 4. Storing your data and metadata > Security for more details.</p>
Ethical review	<p>Does your project require approval by a local ethics committee?</p> <p>No, this is not required.</p>
Informed consent	<p>Does your research involve human subjects?</p> <p>No, so no informed consent issues are at play.</p>
(sensitive) Personal data /confidential information / protecting participants	<p>Will you process any personal data? Tick all that apply</p> <p>No personal data will be recorded or processed.</p>

Intellectual property rights (IPR)/Copyrights	<p>Are there IPR or copyright issues to consider?</p> <p>Data from PJT-1 was shared for this research under strict regulation. Data of PJT-1 may be used solely for data analysis regarding this study. Data of PJT-1 is not allowed to be made public or shared in any way with third parties.</p> <p>Have you established who owns the copyright in your data? Might there be joint copyright?</p> <p>There is no joint copyright. All original data owners who shared their data, stay copyright owner. All except PJT-1 have allowed me to use and share their data at will.</p> <p>Will permission be needed to collect/reuse the data?</p> <p>Permission is granted by all parties to collect their data. Permission is granted by all parties except PJT-1 to share their data.</p> <p>Will these rights be transferred to another organisation for data archiving?</p> <p>No rights will be transferred to another organisation.</p>
Restrictions	<p>Not all data can be publicly shared - please explain below which data and why cannot be publicly shared</p> <p>See under 5. Protecting your data > Intellectual property rights (IPR)/Copyrights (above).</p>

6. Archiving and publishing your data

Metadata and deposit of data	<p>Metadata Policy</p> <p>Anyone may access the metadata free of charge. The metadata may be re-used in any medium without prior permission for not for-profit purposes and resold commercially provided the OAI Identifier or a link to the original metadata record are given.</p> <p>Will the data you produce and/or used in the project be usable by third parties, in particular after the end of the project?</p> <p>Yes, all data is available via request at the principal researcher, also after the end of the project. If required by TU Delft, the data will be made available via an appropriate online data archive.</p> <p>Which data and associated metadata, documentation and code will be deposited?</p> <p>At first, none. The data however is as much as possible prepared to be deposited in a later stage.</p>
------------------------------	-------------------------------------------------------------------------------------------------------------------------------------------------------------------------------------------------------------------------------------------------------------------------------------------------------------------------------------------------------------------------------------------------------------------------------------------------------------------------------------------------------------------------------------------------------------------------------------------------------------------------------------------------------------------------------------------------------------------------------------------------------------------------------------------------------------------------------------------------------------

	<p>What methods or software tools are needed to access the data?</p> <p>ArcGIS for Desktop, the Sentinel Application Platform (SNAP), Jupyter Notebook and Spyder Python environments as well as the web-based GEE interface.</p> <p>Will the application of a persistent identifier to your data be ensured?</p> <p>If the data will be published, a persistent identifier will be applied.</p>
<p>Deposit timing and duration</p>	<p>When will your data be made available for re-use? Is there an embargo period?</p> <p>The data for re-use will be made available if need be or on request, and in any case after handing in the final version of the MSc thesis. There is no embargo period.</p> <p>How long does the data need to be retained? For how long should the data remain reusable?</p> <p>If the data will be deposited, it will be and the end of the project in an appropriate data depository e.g. through Git(lab)/subversion repository at TU Delft. There is no additional cost. Where possible I will store files in open archival formats (e.g. word files converted to .txt files and excel files converted to .csv.) Where this is not possible, I will include information on software used and by what version number.</p>
<p>Access</p>	<p>Does the data contain anything sensitive?</p> <p>The data does not contain anything sensitive.</p> <p>Can the information in this data collection be linked with anything in another data collection which might lead to participant’s identities being disclosed?</p> <p>No, since no sensitive data is collected and stored, this is not an issue.</p> <p>If ‘restricted access’ is to be chosen who will manage the access to this request?</p> <p>‘Restricted access’ will not be chosen as access type.</p>
<p>Data Policy</p>	<p>Access to Full Data Items is controlled because sharing of collected data from PJT-1 is not allowed. Copies of full data items generally can be reproduced, displayed by and given to third parties in any format or medium for personal research or study, educational, or not-for-profit purposes without prior permission or charge, provided that:</p> <ol style="list-style-type: none"> 1. the authors, title and main bibliographic details are given;

	<p>2. a hyperlink and/or URL are given for the original metadata page;</p> <p>3. the content is not changed in any way.</p> <p>Data items must not be sold commercially in any format or medium without formal permission of the copyright holders. Some full items are individually tagged with different rights permissions and conditions. Mentioning of the TU Delft repository is appreciated but not mandatory.</p> <p>Are any restrictions on data sharing required?</p> <p>No, there are no restrictions on data sharing required.</p>
Data licensing	<p>How will your data be licensed to permit the widest re-use possible?</p> <p>This study aims at complying with the open data pilot. Hence all data produced shall be aimed at open access. The currently installed Data management plan clearly states the open access foundation saying that Free and open access without any restrictions shall be granted to the metadata of the data. Furthermore, it aims to identify unnecessary or obsolete barriers towards open access.</p> <p>Have you considered which kind of licence is appropriate for sharing your data and what, if any, restrictions there might be on re-use?</p> <p>Yes, restriction apply due to requirements of third parties, see under 6. Archiving and publishing your data > Data Policy.</p> <p>If you are purchasing or re-using someone else’s data sources have you considered how that data might be shareable, for example negotiating a new licence with the original supplier?</p> <p>Yes, this was allowed by all parties except PJT-1.</p>

7. Discovering data

Identification of needs	<p>Do you plan to use existing data for your research?</p> <p>Yes, data requests are done to share data from parties which are responsible for water quality and water quantity management (PJT-1, BBWS and EPA).</p> <p>What is the purpose for which you need the data?</p> <p>The data is needed to compute timeseries for several water quality parameters (most importantly TSM, DO, COD and BOD but data exists of in total over 40 different water quality parameters).</p> <p>What do you want to learn from the data?</p>
-------------------------	---------------------------------------------------------------------------------------------------------------------------------------------------------------------------------------------------------------------------------------------------------------------------------------------------------------------------------------------------------------------------------------------------------------------------------------------------------------------------------------------------------------------------------------------------------

	<p>This data can reveal trends (yearly, monthly or seasonally) which are possibly overlooked when zooming in on shorter timeslots.</p> <p>What type of data do you need?</p> <p>Needed data has a quantitative character.</p>
<p>Search for data</p>	<p>Do you know where the data may be located?</p> <p>Yes, the data is kept in own, local data repositories by respective data owners.</p> <p>How do you plan to search for the data?</p> <p>I know where to find the data. I need to organize access, and therefor data requests are posted at all parties in separate letters directed to the head of departments or head of the organization. The letters are translated by Reza Pramana K.E.R.Pramana@tudelft.nl, PhD researcher at TU Delft. Letters are signed by Dr.ir. Maurits W. Ertsen (m.w.ertsen@tudelft.nl), head of the Brantas project.</p>
<p>Gaining access to data</p>	<p>What are the (expected) terms and conditions for data access and use?</p> <p>Since all data requests will be posted at partners of the Brantas project, it is expected that they will grant access to all data asked for, without further costs.</p> <p>What is the (expected) process for gaining access to the data?</p> <ol style="list-style-type: none"> 1. Getting consent of the project leader (Maurits Ertsen) to ask stakeholders for data 2. Write letters and get them translated by Reza Pramana. 3. Send data request to respective head of departments. 4. Wait for approval from respective board of directors. <p>What is the (expected) time-span of the process for gaining access to the data?</p> <p>The expected timeframe is a couple of weeks until 2 months, since it is known that all requests have to be discussed by the respective board of directors.</p> <p>What are the (expected) costs for data access and use?</p> <p>If the data requests are honoured, it is expected to come without further costs.</p>